Arenberg Doctoral School of Science, Engineering & Technology
Faculty of Science
Department of Chemistry
Research group Division of Molecular and Nanomaterials
Celestijnenlaan 200F
3001 Heverlee

KATHOLIEKE UNIVERSITEIT LEUVEN

Arenberg Doctoral School of Science, Engineering & Technology
Faculty of Science
Department of Chemistry

Hong Xu

EXPRESSION OF MOLECULAR CHIRALITY AT THE LIQUID-SOLID INTERFACE

May 2010

K.U.LEUVEN ASSOCIATIE

EXPRESSION OF MOLECULAR CHIRALITY AT THE LIQUID-SOLID INTERFACE

Hong Xu

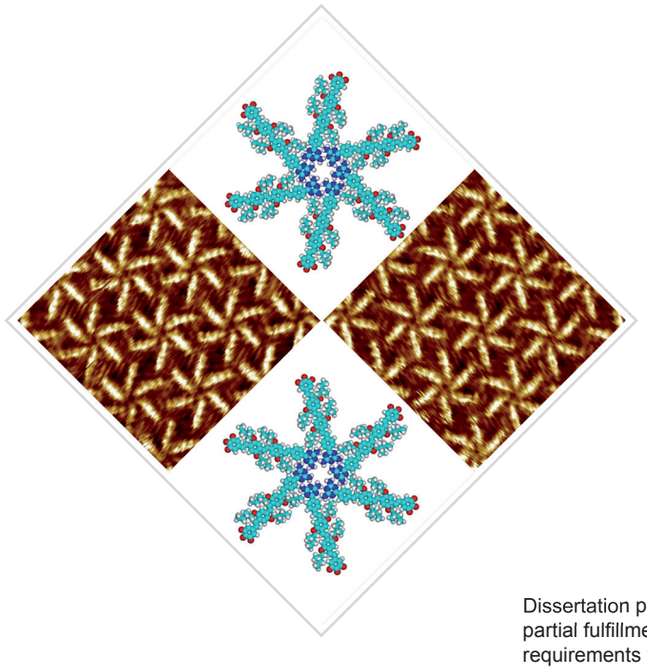

Dissertation presented in partial fulfillment of the requirements for the degree of Doctor of philosophy

May 2010

Arenberg Doctoral School of Science, Engineering & Technology
Faculty of Science
Department of Chemistry

EXPRESSION OF MOLECULAR CHIRALITY AT THE LIQUID-SOLID INTERFACE

Hong Xu

May 2010

Supervisor:
Prof.S. De Feyter

Members of the Examination Committee:
Prof. D. B. Amabilino
Prof. S. De Feyter
Prof. W. Dehaen
Prof. K. –H. Ernst
Prof. M. Van der Auweraer
Prof. T. Verbiest

Dissertation presented in partial fulfillment of the requirements for the degree of Doctor of philosophy.

D/2010/10.705/28
ISBN 978-90-8649-335-7

Preface

Almost five years ago, my application for a PhD position was accepted by Prof. Steven De Feyter. I was excited because I knew that it was the start of a new career. I had the opportunity to obtain new knowledge, new skills and face different challenges every day. As my thesis is finished, I go through my whole PhD study and I want to thank the people who helped me.

First, I would like to acknowledge Prof. Steven De Feyter for being my promoter. Without your guidance and help, I wouldn't have overcome the challenges in the research work. Thank you for answering every question I had.

I also want to thank my promoter Prof. Steven De Feyter, Prof. Mark Van der Auweraer, and the other members of the jury for reading my thesis and providing feedback.

I would like to thank our collaborators: Prof. David B. Amabilino, Dr. Patrizia Iavicoli, Prof. E. W. Meijer, Dr. Albert P. H. J. Schenning, Prof. Ben L. Feringa, Dr. Nathalie Katsonis, Prof. Roberto Lazzaroni, Dr. Andrea Minoia and their co-workers. Thanks for providing me the compounds, theoretical models, discussions and suggestions.

I want to thank my colleagues in the group for their help and support: Jian, Andrey, Shuhei, An, Inge, Krystallia, Guojie, Shengbin, Willem, Jinne, Linh, Yihong, Tibor, Hai, Kunal, Tanya, Min, Zongxia, Yonghai and Elke.

I’m thankful to Carine Jackers and Marino Fumarola and other lab members for their support in the last four years.

I also want to express my thanks to my bachelor promoter Prof. Dr. Xi Zhang and master promoter Prof. Dr. Julius Vancso. They provided me the opportunity for obtaining the necessary knowledge, training and skills of scientific research.

My PhD research was funded by the FP6 Marie Curie Research Training Network CHEXTAN, and FP7 Small Collaborative Project RESOLVE.

Finally, I want to thank my family and friends in my personal life.

My wife Xin always supports me. I would like to share all my happiness and honor with you. Though my parents are thousands kilometers away from me, they do support me in my life.

Thank you!

Abstract

The formation of chiral molecular patterns on a surface is a research area of great interest, because of its impact in various fields and industries, ranging from nanofabrication to pharmacy. For instance, efficient separation of mirror-image molecules, i.e. enantiomers, is a key activity in the pharmaceutical industry. If enantioselective synthesis turns out to be too demanding or expensive, it is in some cases necessary to resolve the enantiomers, for instance if only one of the enantiomers shows the targeted therapeutic activity, or if both enantiomers show a different therapeutic activity but especially, if one of the enantiomers turns out to be harmful. It is believed that surfaces can help in resolving enantiomers.
Motivated by this prospect, in this thesis, a main target was to better understand how chiral and achiral molecules interact with surfaces at the liquid-solid interface. How do molecules interact and organize at the liquid-solid interface? How is molecular chirality transferred and amplified into surface-confined supramolecular structures? Is it possible to separate different enantiomers on the surface?
This thesis mainly focuses on the expression of molecular chirality at the liquid-solid interface. With scanning tunneling microscopy (STM), one can probe the self-assembly process of the target molecules in detail, as long as the substrate is atomically flat, chemically inert, and electrically conducting.
The first aspect is to understand the self-assembly process of the molecular building blocks on the surface. Given that a molecule is chiral, will this chirality be transferred into the self-assembled patterns on a surface? How many of these chiral centers are necessary to transfer molecular chirality? Is there a relation with the size of molecule? To probe these aspects, the self-organization of a number of porphyrin molecules which differ in the number of stereogenic centers was probed at the liquid-solid interface.
Self-assembly is obviously not a static process. At the liquid-solid interface, dynamics play a very important role in the pattern formation. It is not evident though to follow the dynamics of individual molecules at the liquid-solid interface. Often, the dynamics are so fast that only a

time-average picture is obtained. A large chiral hexapod molecule turns out to be an ideal molecular probe to follow and evaluate the influence of conformational and translational dynamics on the ordering and expression of chirality.

An often underestimated factor in self-assembly at the liquid-solid interface is the solvent. Their role is much more than providing a medium where the solute can assemble at the liquid-solid interface. Solvent molecules may also influence the dynamic behavior, the extent of ordering, the pattern structure and potentially also the expression of chirality. Most often, self-assembly at the liquid-solid interface takes place in achiral solvents. Chiral solvents have the potential though to affect in a unique way the self-assembly process. It turns out that carefully designed and selected chiral solvents induce homochirality in case of the self-assembly of achiral molecules on an achiral substrate.

One of the ultimate goals of this thesis is the separation of enantiomers. Is it possible to achieve resolution not by traditional resolution techniques but by relying on the interaction of a racemic mixture with achiral surfaces? As it turns out, a successful strategy is to premix the racemic mixture in presence of a resolving agent, which leads to the selective adsorption of only one diastereomeric complex.

The results in this thesis reveal the role molecular chemical structure and solvent play in (chiral) self-assembly at the liquid-solid interface. Enantioselective adsorption can be achieved, even on an achiral surface, which might turn out to be an efficient approach for the resolution or separation of enantiomers.

Samenvatting

Met zegt van een object dat het chiraal is indien het niet samenvalt met zijn spiegelbeeld. Ook moleculen kunnen chiraal zijn. De chiraliteit van moleculen en de interactie van deze moleculen met oppervlakken vormt een onderzoeksgebied dat een grote interesse wekt omwille van de impact in tal van domeinen zoals de nanotechnologie en farmacie. De scheiding van spiegelbeeldmoleculen, ook enantiomeren genoemd, is een kernactiviteit van de farmaceutische industrie. Wanneer het onmogelijk blijkt om omwille van economische redenen moleculen op een enantioselectieve manier aan te maken, maar waarbij dus een mengsel van spiegbelbeeldisomeren gevormd wordt, is het nodig om die enantiomeren te scheiden. Dit is het geval indien één van beide enantiomeren niet actief is, of erger, indien één van de spiegelbeeldisomeren een ongewenste of schadelijke therapeutische activiteit vertoont. Het uitgangspunt van dit proefschrift is om via de interactie van moleculen met oppervlakken enantiomeren van elkaar te scheiden.

Het hoofddoel van het onderzoek dat in dit proefschrift voorgesteld wordt, is het beter begrijpen van de manier waarop chirale en achirale moleculen interageren met oppervlakken aan het grensvlak tussen een vloeistof en een vaste stof. Hoe interageren moleculen met elkaar en hoe adsorberen ze aan een dergelijk grensvlak? Hoe komt moleculaire chiraliteit tot uiting in de patronen die gevormd worden door de zelfassemblage van die moleculen aan het oppervlak? Is het mogelijk om spiegelbeeldisomeren te scheiden op basis van hun interactie met een dergelijk oppervlak?

Dit proefschrift heeft dus de expressie van moleculaire chiraliteit aan het grensvlak tussen een vloeistof en een vast stof als onderwerp. Met een hoge resolutie microscopietechniek, rastertunnelmicroscopie of ook nog scanning tunneling microscopie (STM) genaamd, kan men het zelfassemblageproces van moleculen aan een oppervlak in detail volgen, indien het oppervlak van het substraat atomair vlak, chemisch inert, en geleidend is.

Een eerste aspect dat bestudeerd werd, is het effect van het aantal chirale centra in een molecule op de expressie van chiraliteit aan een

oppervlak. De resultaten in hoofdstuk 2 tonen aan dat zelfs voor omvangrijke moleculaire systemen de aanwezigheid van één chiraal centrum voldoende kan zijn om met een efficiëntie van 100% chirale oppervlakken te maken: m.a.w. slechts één van de patronen die elkaars spiegelbeeld zijn, wordt gevormd. Het aantal chirale centra heeft een gering effect op de monolaagstructuur.

Zelfassemblage is per definitie een dynamisch proces. Het dynamisch gedrag van moleculen aan een oppervlak is echter niet gemakkelijk in beeld te brengen. De adsorptie van een enantiomeerzuivere moleculaire 'zespoot' aan een grafietoppervlak blijkt echter ideaal om aan het grensvlak tussen een vloeistof en een vast substraat verscheidene dynamische processen te visualiseren zoals veranderingen in moleculaire conformatie, oriëntatie, en beweeglijkheid, (hoofdstuk 3).

In hoofdstuk 4 wordt de invloed van de moleculaire structuur (grootte, vorm, aanwezigheid van specifieke functionele groepen) en de competitie tussen molecuul-molecuul en molecuul-substraat interacties onderzocht op de moleculaire ordening, oriëntatie en expressie van chiraliteit aan een oppervlak. De solventkeuze heeft een grote invloed op het resultaat van het zelfassemblageproces.

De rol van het solvent wordt verder onderzocht in hoofdstuk 5. Hieruit blijkt dat bepaalde chirale solventen een belangrijke invloed uitoefenen op het zelfassemblageproces. In aanwezigheid van een chiraal solvent leidt de adsorptie van een achirale verbinding nagenoeg exclusief tot chirale oppervlakken, m.a.w. slechts één van de twee spiegelbeeldpatronen wordt gevormd. Chirale solventmoleculen blijken dan weer niet in staat om de intrinsieke adsorptie van chirale moleculen te beïnvloeden.

Ten slotte wordt in hoofdstuk 6 beschreven hoe chirale scheiding gerealiseerd kan worden aan het grensvlak tussen een vloeistof en een vaste stof. Een racemisch mengsel van chirale diaminocyclohexanen wordt gescheiden in de enantiomeerzuivere componenten via selectieve adsorptie aan een achiraal oppervlak. Dit wordt gerealiseerd via co-adsorptie met een chiraal resorcinolderivaat als een diastereomeer complex.

List of Abbreviations

1D-One-dimensional
2D-Two-dimensional
2DSD-Two-dimensional structural database
3D-Three-dimensional
A-Achiral
AFM-Atomic force microscopy
Box–Cu-Bis(oxazoline)–copper
CSP-Chiral stationary phase
CCW-Counter clockwise
CD-Circular dichroism
COR-Coronene
CW-Clockwise
DBA-Dehydrobenzo[12]annulene
DTPP-3,5-Di-(4-*n*-tetradecyloxyphenyl)pyrazole
GIXD-Grazing-incidence X-ray diffraction
HOPG-Highly ordered pyrolytic graphite
HPLC- High pressure liquid chromatography
ISA-Isophthalic acids
LEED-Low-energy electron diffraction
MD-Molecular dynamics
MIP-Molecularly imprinted polymers
MWNT-Multi-walled nanotubes
nCB-4'-Alkyl-4-cyanobiphenyl
OPV-Oligo-(p-phenylenevinylene)
PBC-Periodic boundary conditions
PTP-1-Peltier temperature programmer model 1
Rac-Racemic
RAIRS-Reflection adsorption infrared spectroscopy
SEM-Scanning electron microscopy
STM-Scanning tunneling microscopy
T-Diamino triazine
TCB-1,2,4-Trichlorobenzene
TTA-Terephthalic acid

UHV-Ultrahigh vacuum
UT-Ureido triazine
UV-Ultraviolet

Contents

Chapter 1: Introduction

1.1 Nanofabrication

Nanofabrication plays a very important role in nanoscience and nanotechnology. Designing, manipulating, controlling and making nanometer sized structures by using chemical or physical methods becomes an interesting topic. “In nano, the idea is to do something really big and important with objects that are really small and distinct in their properties and behavior from the large objects with which we are all familiar.”[1]

1.2 Top-down and Bottom-up Approaches

Generally, there are two categories of approaches for achieving target nanostructures: top-down and bottom up (Figure 1.1). For top-down approaches, designated structures are sculpted from a larger block of

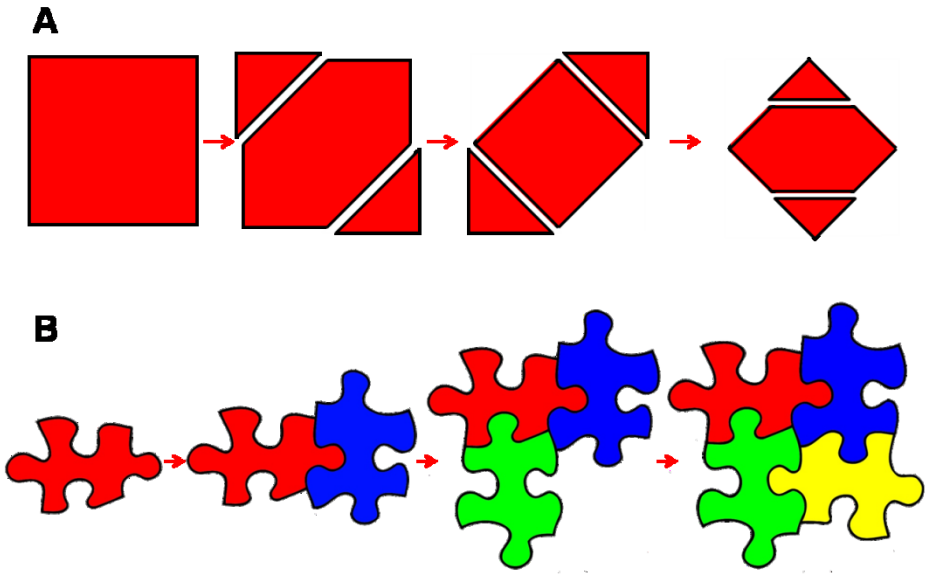

Figure 1.1 *Nanofabrication approaches. A) Top-down, B) Bottom-up.*

matter. The challenges of this approach are the limitations of the structural size, complex facilities, high process cost and low ability of controlling chemical properties of structures created. In contrast to top-down methods, bottom-up approaches start from building blocks which by manipulation or by spontaneous organization form more complex systems. In this latter approach, the building blocks carry the necessary information (size, shape, and functionality) to define the structure and properties of the structures formed.

1.3 Self-assembly

"Self-assembly is the autonomous organization of components into patterns or structures without human intervention. Self-assembling processes are common throughout nature and technology. They involve components from the molecular (crystals) to the planetary (weather systems) scale and many different kinds of interactions."[2]
Self-assembly can be classified as either static or dynamic. In dynamic self-assembly, the interactions responsible for the formation of structures or patterns between components only occur if the system is dissipating energy.[3,4] Static self-assembly involves systems that are at global or local equilibrium and do not dissipate energy.[5,6]
In chemistry and material science, molecular self-assembly is well studied. It is a spontaneous and reversible process. Molecular units organize into ordered structures by non-covalent interactions such as hydrogen bonding, π-π stacking and van der Waals interactions.

1.4 Adsorption on Surfaces[7,8]

Adsorption is the adhesion of molecules of gas, liquid, or dissolved solids to a surface.[9] This process creates a film of the adsorbate on the surface of the adsorbent. The amount adsorbed is determined by several parameters. The most important one is the partial pressure *P* (solid-gas interface)[10,11] or the concentration *c* (liquid-solid interface) of the molecules.[12]

The adsorption process is generally classified as physisorption or chemisorption. For physisorption, the sublimation energy is ca. 20-40 kJ/mol. The adsorbate is able to diffuse on the surface and to rotate. Normally the molecular structure of the surface does not change with the process. The adsorption equilibrium is quickly established and reversible. In chemisorption, typical sublimation energy is ca. 100-400 kJ/mol. There are often specific binding sites. The adsorbate is relatively immobile and usually does not diffuse on the surface. There is often a surface reconstruction. Due to the strong binding, the molecules must overcome an activation energy. Thus the desorption energy is larger than the adsorption energy (Figure 1.2).[13]

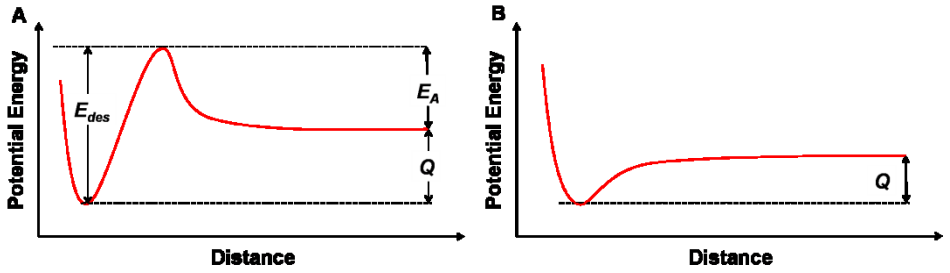

Figure 1.2 *Potential energy profile versus distance for A) Chemisorption and B) Physisorption. E_A – activation energy; Q – adsorption energy and E_{des} – desorption energy.*[7]

In a given system, the differential molar energy of adsorption is defined as:

$$\Delta_{ad} U_m^{dif} = \left.\frac{dU^\sigma}{dN^\sigma}\right|_{T,A} - \left.\frac{dU^f}{dN^\sigma}\right|_{T,A}$$

U^σ is the energy of N^σ moles of molecules adsorbed. U^f is the total internal energy of the free molecules. *T* and *A* indicate the temperature and the total surface area, respectively. Since normally the amount adsorbed is small compared to the total amount of molecules, the equation can be written as:

$$\Delta_{ad} U_m^{dif} = \left.\frac{dU^\sigma}{dN^\sigma}\right|_{T,A} - U_m^f$$

It involves the change of the internal surface energy upon adsorption of an infinitesimal amount of gas at constant temperature and total surface

area. The energy changes with the amount of molecules adsorbed because:

1) Most surfaces are energetically heterogeneous and the binding sites with a high binding energy are occupied first;
2) The first layer has a different binding energy since the adsorption is dominated by the molecule—substrate interactions. For the second layer, the interactions between molecules become more important;
3) If molecules interact with neighboring molecules on the surface, it is energetically more favorable.

The differential molar enthalpy of adsorption and the differential molar entropy of adsorption can be defined similarly as:

$$\Delta_{ad} H_m^{dif} = \left.\frac{dH^\sigma}{dN^\sigma}\right|_{T,\gamma} - H_m^f$$

$$\Delta_{ad} S_m^{dif} = \left.\frac{dS^\sigma}{dN^\sigma}\right|_{T,A} - S_m^f$$

Here $\gamma = N^\sigma / A$. Physisorption of molecules on a surface is enthalpically driven ($\Delta_{ad} H_m^{dif} < 0$) and the adsorbate density will be maximized.

At liquid-solid interfaces, adsorption is an exchange process in which adsorbed molecules replace liquid molecules. At thermodynamic equilibrium the system will in time minimize its total free energy *G*. To minimize the enthalpy *H* by physisorption, the adsorbate density will be maximized. To maximize the entropy *S*, the adsorption of large rigid molecules is more favored since less translational and conformational entropy is lost.[14,15]

1.5 Chirality in Chemistry

Lord Kelvin gave the definition of chirality: I call any geometrical figure, or group of points, chiral, and say it has chirality, if its image in a plane mirror, ideally realized, cannot be brought to coincide by itself. A chiral object and its mirror image are called enantiomorphs. A non-chiral object is called achiral and can be superimposed on its mirror image. Human hands are the most common example of chiral objects: The left hand is a mirror image of the right hand. They are not superimposable, no matter how the two hands are rotated and translated (Figure 1.3).

Figure 1.3 *Human hands. Mirror images which are not be able to be superimposed.*

A molecule which cannot be superimposed on its mirror image is chiral (Figure 1.4). Such a molecule, and its mirror image counterpart, are called enantiomers. A mixture of equal amounts of the two enantiomers is called a racemic mixture. Most often, chiral molecules have point chirality at a single stereogenic center. Diastereomers are stereoisomers that are not enantiomers.[16] Diastereomerism occurs when two or more stereoisomers of a compound have different configurations at one or more (but not all) of the equivalent (related) stereocenters and are not mirror images of each other.[17]

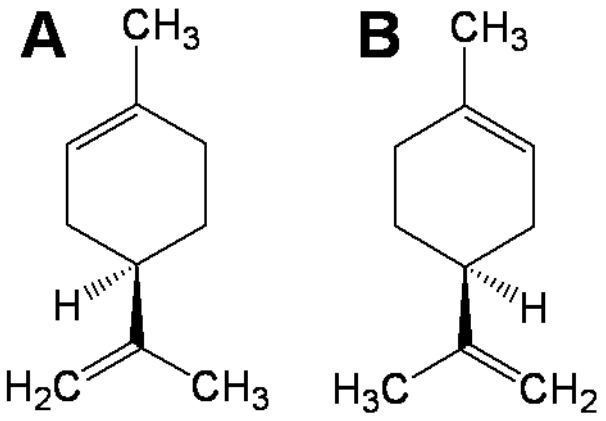

Figure 1.4 *Two chemical structures of mirror-image molecules, i.e. enantiomers, which cannot be superimposed. A) R-(+)-limonene, B) S-(-)-limonene.*

Different enantiomers of a molecule can be either named by configuration (*R/S* system and *D/L* system) or by optical activity ((+)/(-) system). For

molecules that resemble a helix, *M/P* notation is particularly used for expressing right-handed/left-handed helix.[16]

1.6 Chirality at the Nanoscale

Chirality is important in many chemical processes, such as catalysis, crystallization and self-assembly. Understanding and controlling chirality at the nanometer scale is an important development. Enantioselective methods have been investigated and implemented in several technologies. Generally, a mixture of two enantiomers of a compound always condenses in three ways: (1) as a racemic compound in which both enantiomers are present in the same condensate; (2) as a conglomerate in which molecules form condensates comprised of only one enantiomer. However the sample contains equal amounts of enantiomorphic condensates; (3) as a pseudoracemate (racemic solid solution), in which the condensates contain the two enantiomers in a non-ordered arrangement.[18] As an illustration, a few examples covering different areas are presented in the following sections.

1.6.1 The chromatographic separation of enantiomers

In small scale, one important method for the separation of enantiomers is high pressure liquid chromatography (HPLC) using chiral stationary phases (CSPs). However, it shows several limitations mainly regarding the time-consuming development of analytical methods. The application of nanotechnologies to enantioselective process for high throughput and sensitivity has been developed.

Na *et al.* used multi-walled nanotubes (MWNTs), polystyrene, titania and alumina nanoparticles which are modified with a single layer of β-cyclodextrin as a chiral stationary phase, in the enantioseparation of clenbuterol by capillary electrophoresis.[19] In all cases, due to the large surface area platform provided by these nanoparticles, the separation is improved over that obtained using only β-cyclodextrin.

Combining the concept of molecular micelles with that of molecularly imprinted polymers (MIPs), Nilsson and co-workers prepared polymeric

nanoparticles and studied their application in enantioseparation by electrochromatography. Imprinted polymeric micelles were prepared from a surfactant, acting as a monomer, and a cross-linker in the presence of (*S*)-propranolol as a template in a mini-emulsified polymerization environment (Figure 1.5). This environment promoted the peripheral localization of the recognition sites on the imprinted nanoparticles obtained. In contrast to conventional MIP-based separations, the peak corresponding to the template molecule does not show the characteristic tailing.

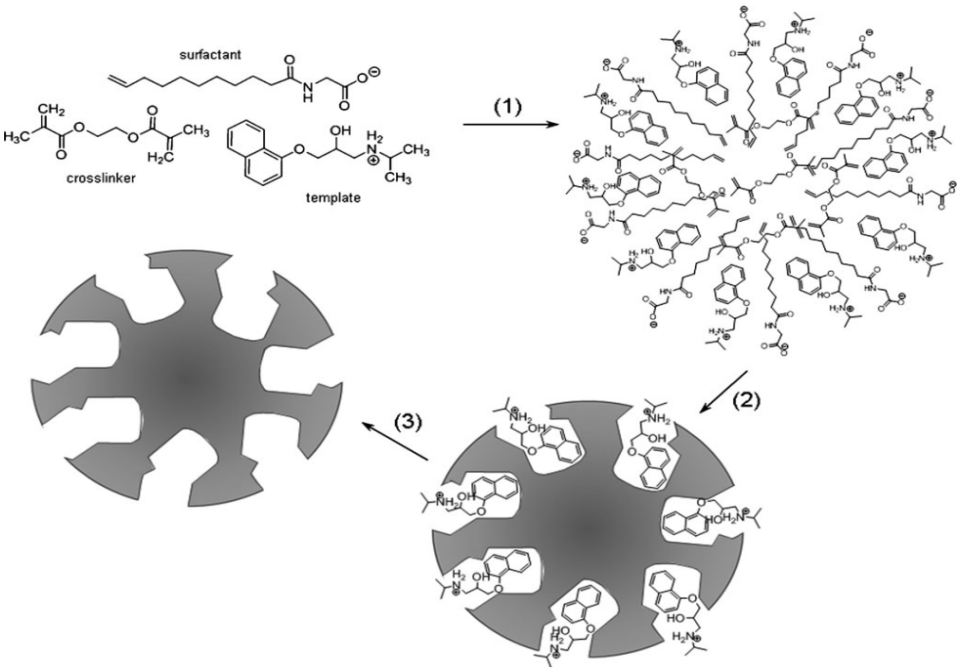

Figure1.5 *Synthesis of MIP molecular micelles. (1) Preassembly of the imprinting complex, (2) cross-linking polymerization, (3) template removal.*[19]

1.6.2 Enantioselective crystallization on nanochiral surfaces

Enantioselective crystallization is another approach to chiral separation. Dressler *et al*. created nanoscale chiral films of (*S*)- or (*R*)-cysteine with a thickness of ca. 10 nm on Au (111) surface and studied chiral interactions between the chiral crystals of glutamic acid and the nanochiral surfaces of

cysteine.[20,21] The crystallization of the pure enantiomer of glutamic acid from supersaturated solutions was studied by X-ray diffraction and scanning electron microscopy (SEM). X-ray diffraction patterns of (*R*)-glutamic acid crystallized on a (*R*)-cysteine nanochiral surface shows two major peaks corresponding to the (020) and (040) planes, indicating a preferential growth of the (*R*)-enantiomer along the [020] direction. On the other hand, (*R*)-glutamic acid does not show preferred orientation when crystallized on the L-surfaces. An equivalent behavior is observed with glutamic acid enantiomers grown on (*S*)-cysteine surfaces. Morphology effects were also observed for the crystallization of rac-glutamic acid crystals grown on nanochiral surfaces of cysteine as show in Figure 1.6. The above data strongly suggests the chiral recognition at the chiral nanostructured surfaces.

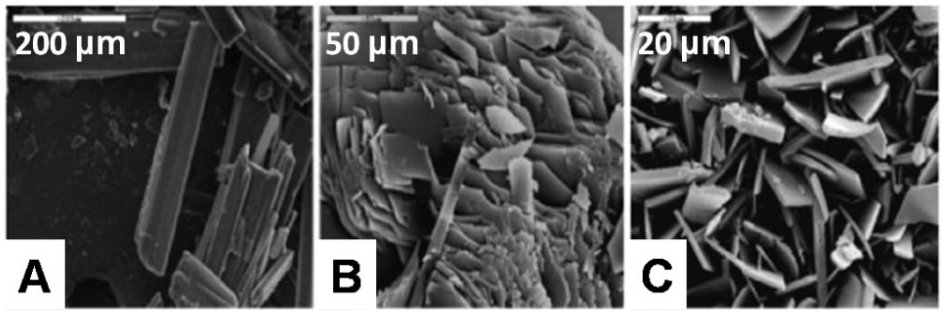

Figure 1.6 *Scanning electron microscopy (SEM) images of rac-glutamic acid crystals. A) crystal morphology of rac-glutamic acid crystallized from solution, B) crystal morphology of rac-glutamic acid crystallized onto a chiral* (*S*)*-cysteine surface (plate like), C) crystal morphology of rac-glutamic acid crystallized onto a chiral* (*R*)*-cysteine surface (rectangular).*[20]

1.6.3 Enantioselective catalysis with chiral complexes immobilized on nanostructured supports

Nanostructured solids with well-controlled surfaces may also act as nanoreactors, hindering or even blocking some of the reaction channels, and hence modifying the stereochemical result of the reaction. Salvatella *et al.*[22] report cyclopropanation reactions catalyzed by C2-symmetric bis(oxazoline)–copper (Box–Cu) complexes immobilized onto laponite

(Figure 1.7). These catalysts were tested in the benchmark cyclopropanation reaction of styrene and ethyl diazoacetate, the selectivity (trans/cis and enantioselectivity) of which changed dramatically in presence of the solid surface. The role of the charged surface nanoenvironment was demonstrated by the effect of the reaction solvent and the dimensionality of the support. The role of proximity of the complex to the support surface was assessed by testing several solvents, with an enhanced stereochemical effect observed with low dielectric constant solvents, a situation that leads to the closer proximity of copper to its counterion, the laponite surface. Thus, when the cyclopropanation reactions were catalysed by the laponite-exchanged PhBox–Cu complex, in hexane or styrene, a complete reversal of the trans/cis diastereoselectivity was observed.

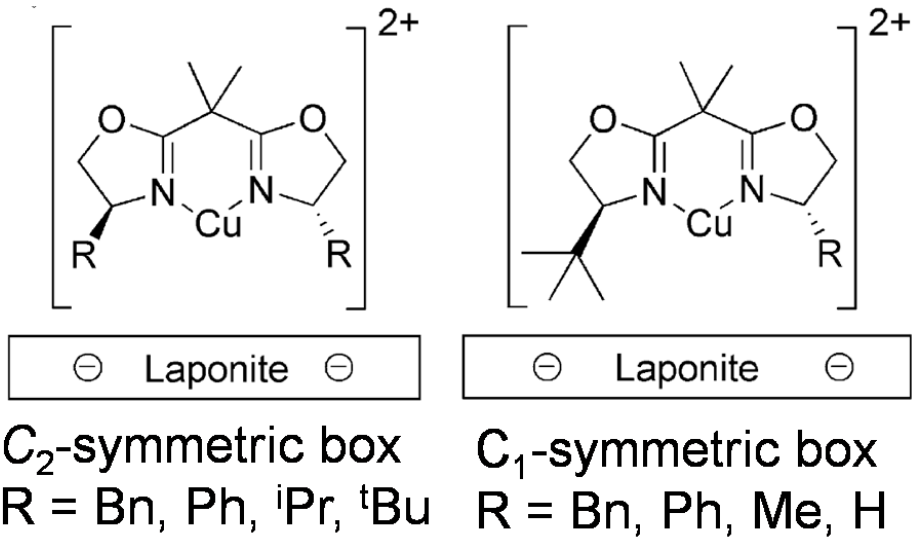

Figure 1.7 *Laponite immobilized bis(oxazoline)–copper* (Box–Cu) *complexes.*[22]

1.7 Chirality of self-assembling molecules at interfaces

Monolayers of molecules can be formed by self-assembly at a variety of

interfaces. There are three most commonly used interfaces: ultrahigh vacuum (UHV)-solid, the air-water and the liquid-solid interface (Figure 1.8). Understanding and inducing amplification of molecular chirality at these interfaces is a topic of intense research activity.

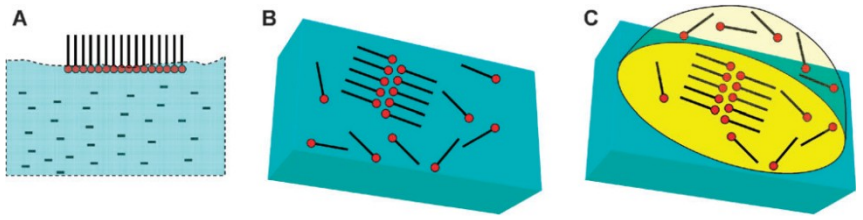

Figure 1.8 *Organization of monolayers of molecules at three types of interface. A) Air–water interface, B) UHV–solid interface, C) Liquid–solid interface.*[23]

At an interface, objects are obviously confined to the surface. Thus chirality is more easily achieved since an interface does not have a center of symmetry and reflection planes can only be maintained normal to the surface. This implies that objects which are inherently achiral in 3D can become chiral on a surface upon their confinement to the interface. This effect is illustrated in Figure 1.9: when confined to the surface, the image on the left cannot be superimposed upon its mirror image on the right.

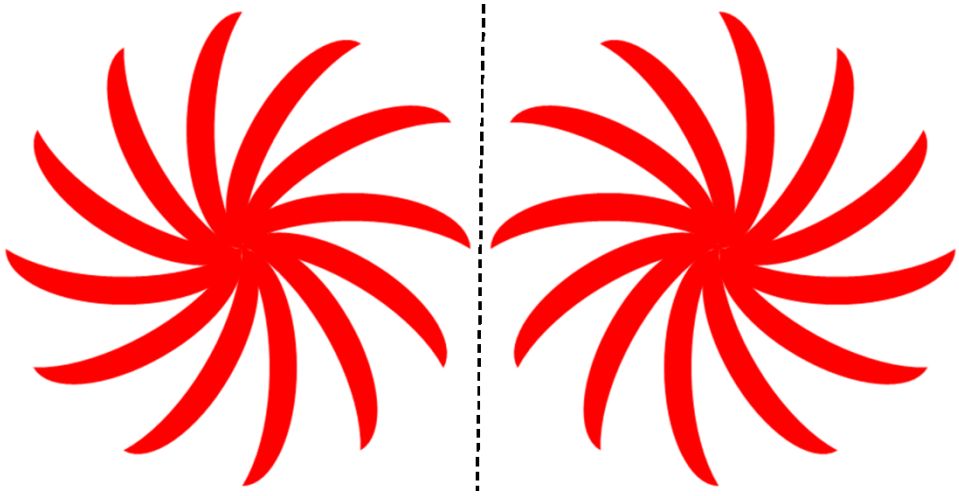

Figure 1.9 *Chirality on a surface.*

Chiral organizations at a surface include both the creation of local chirality

by single adsorption events, referred to as point chirality, and chiral arrangements of individual adsorption motifs, referred to as organizational chirality (Figure 1.10).[24] The expression of chirality on a surface can also be classified as adsorption-induced chirality and molecule induced chirality. A local chiral surface is locally chiral and overall racemic while a surface is globle chiral if it's overall chiral. An initial distinction can already be made between the adsorption of achiral and chiral molecules. When an achiral molecule adsorbs at an achiral surface, an eventually emerging chirality on the surface is adsorption-induced. Such molecules are called prochiral. In that case, the adsorption site symmetry of the molecule locally destroys all surface mirror planes when it breaks the reflection symmetry axes of the surface (Figure 1.10A & B). Mirror image configurations will then always be equal in energy and abundance, meaning that overall the surface will be a racemic mixture. The chirality is strictly only expressed at a local level, and disappears at the global level. The general term for such an adsorption is local point chirality. On the other hand, when a chiral molecule adsorbs on a surface leaving the stereogenic centre intact irrespective of its orientation, a local chiral motif is inevitably formed (Figure 1.10C). In addition, the inherent chirality of the molecule forbids creation of its mirror image and as a result the molecules will be adsorbed in the same chiral fashion at every location on the surface. This is referred to as global point chirality.

However, at the level of a larger organization of molecules, i.e. when a specific 2D organization of molecules destroys the reflection symmetry planes of the underlying surface (organizational chirality). Such an organization can, for example, arise when an adsorbed molecule that displays local point chirality nucleates the growth of a larger enantiomorphous domain via lateral interactions. In the case of achiral molecules, this always leads to the occurrence of equal amounts of mirror image domains at the surface (local organizational chirality, conglomerate) (Figure 1.10D). The highest expression of chirality at an interface occurs when global point chirality also results in an overall chiral organization (global organizational chirality) over the entire surface. This is typically observed for the self-assembly of enantiopure molecules. In this case, the molecule transfers its local chirality to its neighbors resulting in the

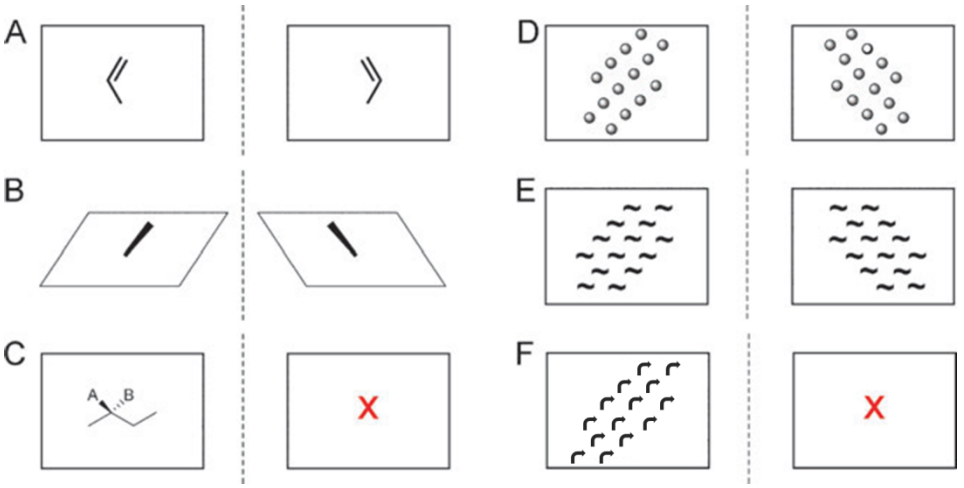

Figure 1.10 *Schematic overview of (A–C) point chirality and (D–F) organizational chirality effects. The dashed lines represent mirrors. A) Achiral molecule adsorbed flat on a surface. An adsorption induced chiral motif is formed - local point chirality. B) Achiral molecule adsorbed tilted on a surface. An adsorption induced chiral motif is formed - local point chirality. In case of A) and B), the alignment of molecules breaks the reflection symmetry axes of the surface. C) Chiral molecule adsorbed on a surface. A molecule induced chiral motif is formed - global point chirality. A mirror image adsorption motif for the same enantiomer is not possible. D) Chiral organization of achiral molecules. Adsorption induced chiral arrangements are formed - local organizational chirality. The ordered domains possess a chiral space group. E) Organization of chiral molecules in which chirality is not expressed into the organization. Adsorption induced chiral arrangements are formed - global point and local organizational chirality. Asymmetric lateral interactions are e.g. mediated by groups that are non-chiral. As a result, also the mirror-image arrangement (in terms of the overall organization) can be observed. F) Highest level of surface chirality in which local and global point chirality are also expressed in global organizational chirality. The chiral molecules (enantiomers) adsorb in a chiral plane group. The mirror-image arrangement is not observed.*[24]

formation of one unique enantiomorphous organization without the occurrence of any mirror image domains (Figure 1.10F). In principle,

however, also chiral molecules, expressing global point chirality, can organize themselves in domains that apparently have mirror image counterparts (local organizational chirality). In that case the interactions between the molecules are generally mediated by groups that are non-chiral and sufficiently remote from the chiral centers, implying that the intrinsic chirality of the molecule is not expressed into the molecular organization of the monolayer (Figure 1.10E).

In what follows, key aspects of the expression of chirality at the different interfaces (UHV-solid, air-water and liquid-solid) will be presented.

1.7.1 UHV-solid interface

A) Chirality in monolayers composed of enantiopure molecules

Raval *et al.* focused on the chiral manifestations caused by organic molecules adsorbed on an achiral metal under ultrahigh vacuum conditions.[25,26] They first reported the self-assembled monolayers formed by enantiopure (*R*,*R*)- and (*S*,*S*)-tartaric acid adsorbed on Cu(110). The monolayers are homochiral and consist of a periodic chiral array composed entirely of the doubly deprotonated the bitartrate species, bonded strongly to the surface via the four oxygen atoms of the carboxylate groups. The molecular model constructed from Reflection Adsorption Infrared Spectroscopy (RAIRS), Low-energy electron diffraction (LEED) and Scanning tunneling microscopy (STM) data (Figure 1.11) shows that chiral 'trimers' of (*R*,*R*)-bitartrate molecules assemble to form long chiral chains aligned along the [1 -1 4] crystallographic direction, thus breaking the mirror symmetry elements of the Cu(110) surface. The chains are propagated across large length-scales and the macroscopic surface organization is non-superimposable on its mirror image. The chiral unit mesh which belongs to the C_2 chiral space group can be described by Matrix notation (1 2, -9 0).[27,28] For (*S*,*S*)-tartaric acid, the monolayer shows the mirror organization and expresses the opposite chirality.

Another key example was demonstrated by Ernst *et al.*[29,30,31] They reported the self-assembly of enantiopure heptahelicene molecules ([7]H,

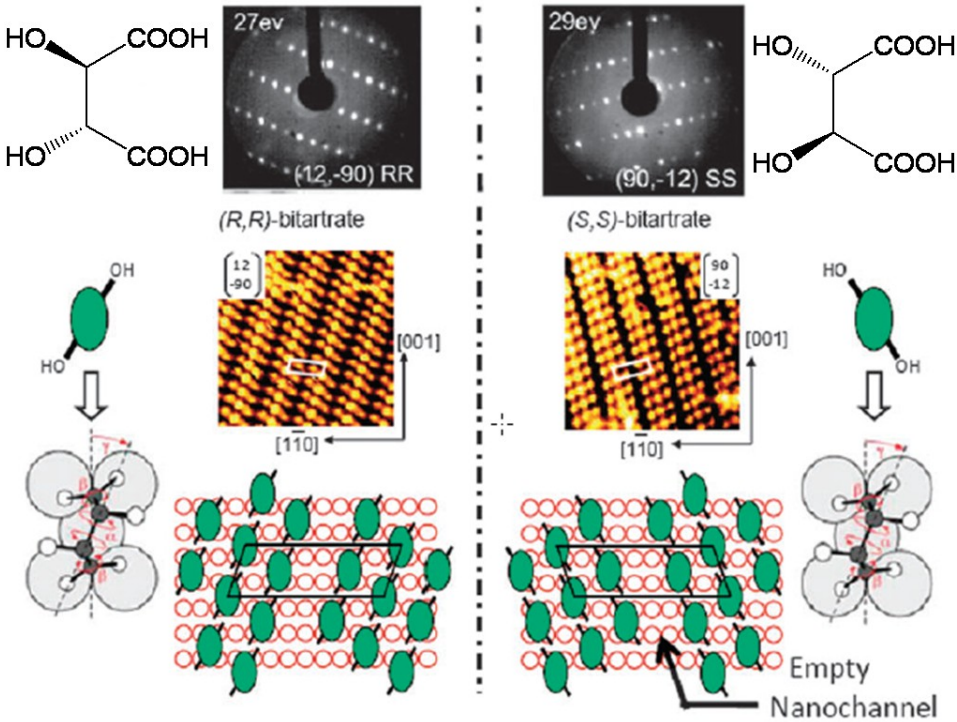

Figure 1.11 *LEED and STM images obtained for the chiral phases of (R,R)-bitartrate and (S,S)-bitartrate on Cu(110) together with models of the chiral domains constructed from STM, LEED and RAIRS data. Note the empty nanochannels that are created within the structure.*[25]

$C_{30}H_{18}$) into a close-packed monomolecular layer on the Cu(111) surface. A long-range ordered structure built-up from clusters containing six molecules and from clusters containing three molecules ('6&3-structure') is observed. The adsorption of the (*P*)-enantiomer of heptahelicene leads to structures which are mirror images of those observed for the (*M*)-heptahelicene (Figure 1.12). Furthermore, the enantiomeric lattices form opposite angles with respect to the [1 -1 0] substrate surface direction. Thus the supramolecular assembly breaks the symmetry of the underlying substrate surface. Molecular chirality is transferred to the surface. The unit cells are not only mirror images of each other, but also the arrangements of molecules within the unit cells are enantiomorphic. This is most clearly seen for the pinwheel-clusters of the 6&3-structures (Figure 1.12 A&B): The pinwheel's wings point either counterclockwise

(CCW), as in the (*M*)-heptahelicene 6&3-structure, or clockwise (CW), as in the (*P*)-heptahelicene 6&3-structure. In the case of the 3-structures (Figure 1.12 C&D), the mirror symmetry is expressed by tilts of the three-molecule cloverleaf units into opposite directions with respect to the molecular lattice vectors.

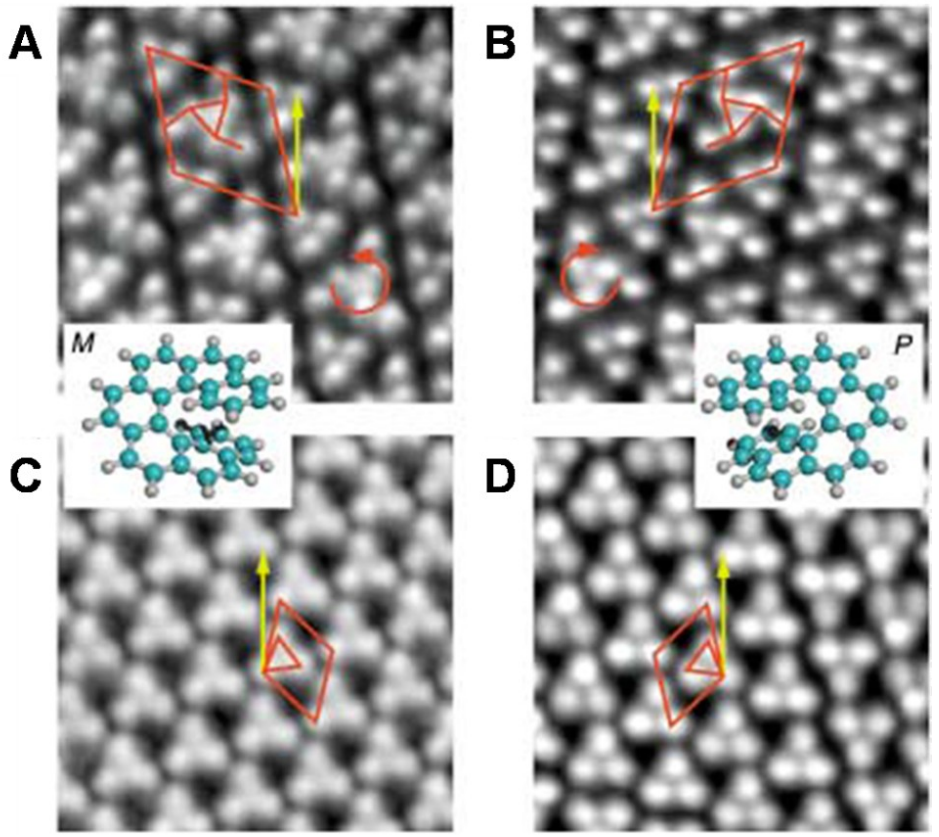

Figure 1.12 *High-resolution STM images of (M)- and (P)-[7]H structures (10 × 10 nm^2). A) (M)-[7]H at θ=0.95, B) (P)-[7]H at θ=0.95, C) (M)-[7]H at θ=1, D) (P)-[7]H at θ=1. The (M)- and (P)-[7]H structures are mirror images of each other. Unit cells and their basic building blocks are outlined by red lines, the [1-1 0] surface direction is indicated by the yellow arrows. θ is percentage of the monolayer saturation coverage.*[30]

B) Racemic mixtures

Since the adsorption of tartaric acid on Cu(110) is one of the best

understood chiral systems on a surface, the racemic mixture of (*R*,*R*)- and (*S*,*S*)-tartaric acid was also investigated.[32] In a 50 : 50 ratio, two types of domains were formed, one associated with enantiopure (*R*,*R*)-tartaric acid and mirror domains associated with pure (*S*,*S*)-tartaric acid (Figure 1.13). Both domains have equal chances to be observed. It indicates that the racemic mixture self-assembled into a racemic conglomerate. This was also proven by low-energy electron diffraction (LEED).

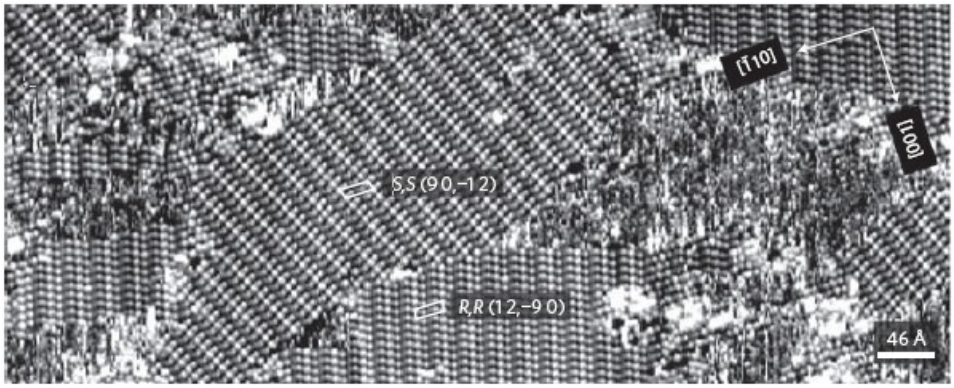

Figure 1.13 *2D organization of racemic (±)-tartaric acid (50:50).*[32] Chiral unit cells are indicated by Matrix notation.

C) Amplification of chirality

The self-assembly of racemic mixture of tartaric acid on a surface often leads to a conglomerate. How to break the symmetry and induce homochirality on surfaces is an interesting topic. Raval *et al.* reported that in a (*R*,*R*)-tartaric acid enriched adlayer with a small enantiomeric excess of 0.2, this small chiral perturbation led to a profound change in the global organization of the monolayer, which only showed the LEED organization associated with enantiopure (*R*,*R*)-tartaric acid.[32] Conversely, when a (*S*,*S*)-tartaric acid enriched adlayer with an enantiomeric excess of -0.2 was created, the system only displayed the chiral mirror LEED organization associated with enantiopure (*S*,*S*)-tartaric acid. STM data (Figure 1.14) provide a direct visualization of the symmetry breaking that occurred in the chiral organization on the surface. The small enantiomeric imbalance leads to single-handed enantiomorphs associated with the majority enantiomer. STM statistics showed a significant deviation

between the enantiomeric composition of the adlayer. A monolayer with a compositional enantiomeric excess of 0.2 resulted in 75% of the organized matter displaying the majority structure within large domains and 25% possessing the minority structure.

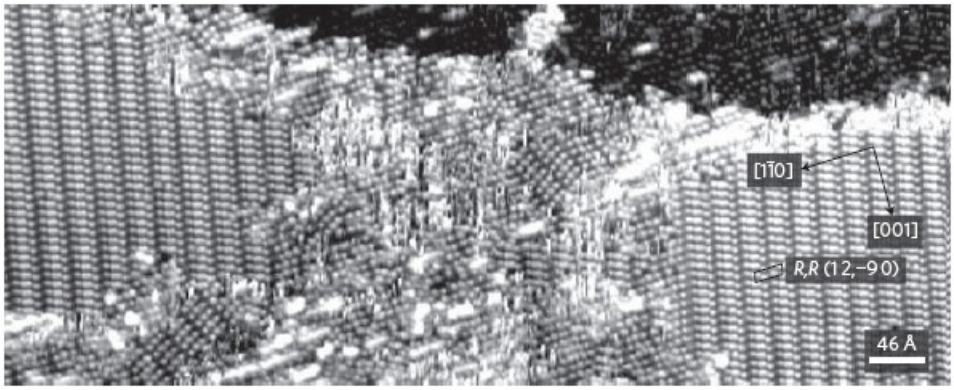

Figure 1.14 *2D organization of an enantiomerically unbalanced adlayer of (R,R)- and (S,S)-tartaric acid on Cu(110) revealed by STM.*[32]

A similar phenomenon is also observed for heptahelicene ([7]H, $C_{30}H_{18}$).[33] The racemic mixture of [7]H leads to two mirror-domains, λ and ρ. Opposite enantiomers form a M-P pair and self-assemble into two types of domains. Though λ- and ρ-domains are homochiral, they were equally being observed and the adsorption of the racemic mixture led to an overall achiral monolayer. In case of an enantiomeric excess, the excess molecules have an influence on the relative alignment of the heterochiral pairs at the domain edge. M–[7]H excess favors formation of λ-domain pairs and P–[7]H excess ρ-domain pairs (Figure 1.15). This chiral bias is amplified by the cooperative interaction among heterochiral pairs, strongly favoring their parallel alignment.

D) Achiral molecules

Achiral molecules can also show chiral packing with the confinement of a surface. Besenbacher *et al.* study the expression of chirality of achiral HtB-HBC molecules upon adsorption on the Cu(110) surface.[34] The chirality is expressed at two different levels: a ±5° rotation of the molecular axis with respect to the close-packed direction of the Cu(110)

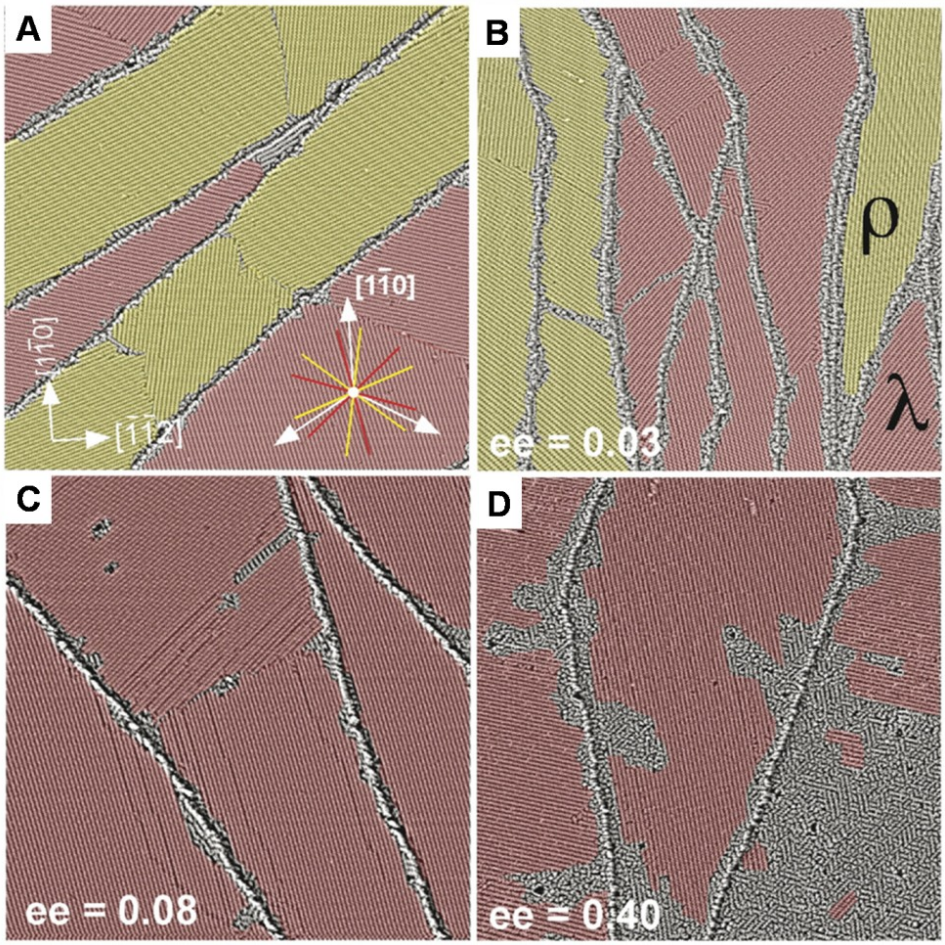

Figure 1.15 *Enantiomeric excess in [7]H layers induces lattice homochirality on the surface. The excess is expelled from the heterochiral domains and forms a solid solution (pseudoracemate) with the racemate (grey area).*[33]

substrate and a chiral close-packed arrangement expected for star-shaped molecules in 2D. Due to the effect of van der Waals interactions forcing the molecules to simultaneously adjust to the atomic template of the substrate geometry and self-assemble in a close-packed geometry, two types of homochiral domains were observed (Figure 1.16).

1.7.2 Air-water interface

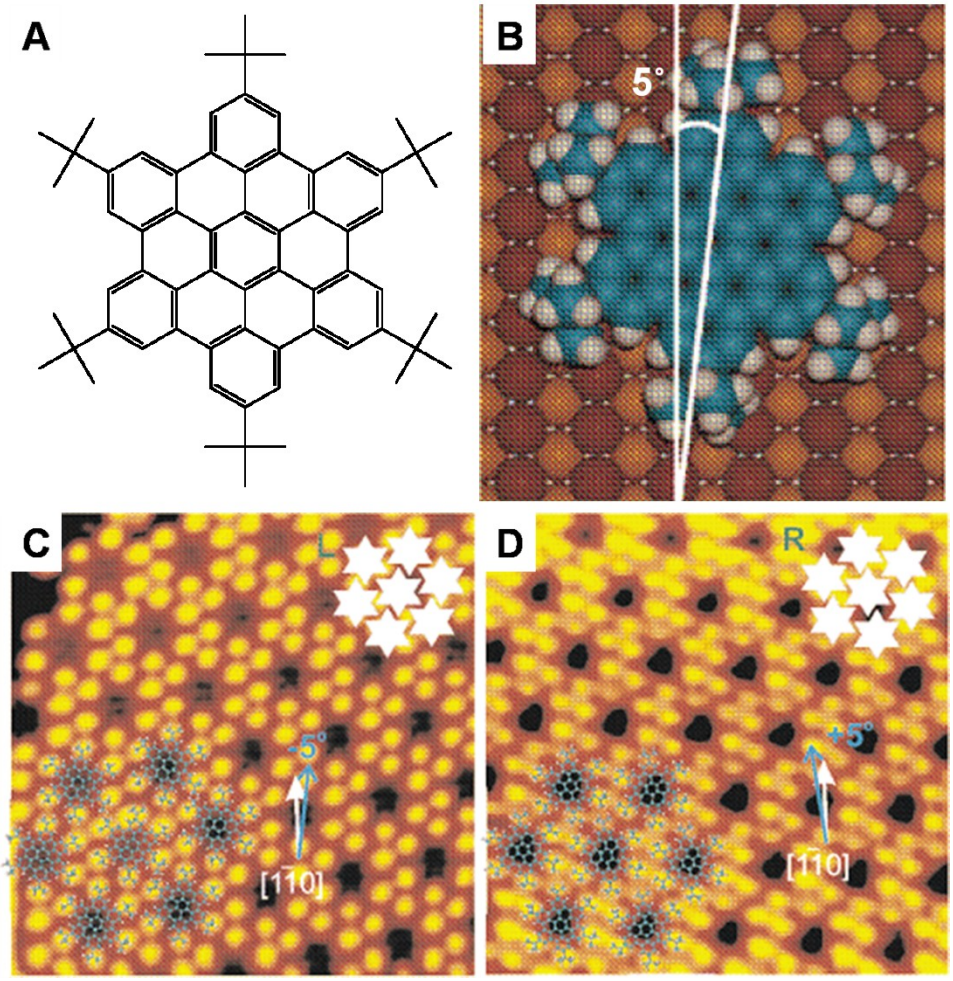

Figure 1.16 *A) Chemical structures of HtB-HBC, B) Ball model of the relaxed conformation of one HtB-HBC molecule adsorbed on Cu(110), showing the 5° rotation of the molecular axis with respect to the close-packed direction of the substrate, C) & D) 10 × 10 nm^2 STM images of the two mirror-symmetric domain orientations for HtB-HBC molecules on Cu(110). Stick models of the HtB-HBC molecules are superimposed on the experimental STM image for eye guidance (lower-left corners). The correspondence with a simple close-packing of star-shaped objects is shown in the upper-right corners, where the handedness of the networks is described. The blue arrows show the ±5° rotation of the molecular axis with respect to the close-packed [1 -1 0] direction of the Cu(110) substrate (white arrow).*[34]

Several enantiopure and racemic long-chain α-amino acids ($C_nH_{2n+1}CH$-$(NH_3^+)CO_2^-$ with n = 12-16, C_n-Gly) self-assemble at the air-water interface and form a monolayer.[35,36] Grazing-incidence X-ray diffraction (GIXD) patterns indicate that the two-dimensional crystallites of racemic C_n-Gly molecules (n=16) are of plane space group *pg* and contain both enantiomeric molecules related to one another by a glide plane perpendicular to the surface of the monolayer, in a herring-bone motif. The crystalline packing arrangement is shown in Figure 1.17A. By contrast, the enantiopure molecules self-assemble in an oblique unit cell of plane group *p*1 in which the molecules are related by translation symmetry (Figure 1.17B & C).

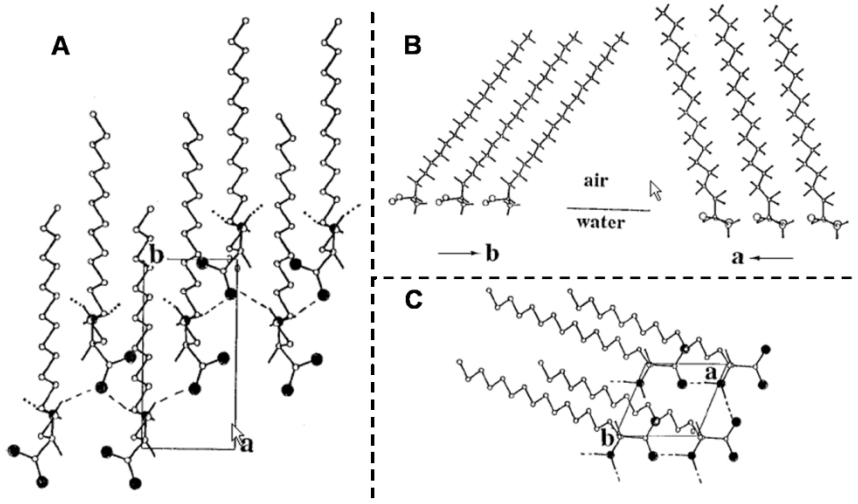

Figure 1.17 *The packing arrangements of A) racemic 2D crystallites of the (R,S) C_{16}-Gly monolayer on water, viewed perpendicular to the layer, B) enantiopure C_{16}-Gly crystallites, viewed parallel, C) enantiopure C_{16}-Gly crystallites, viewed perpendicular. For clarity the nitrogen and oxygen atoms of the head-groups in C) are filled and the hydrogen atoms of n-alkyl chains are omitted.*[35,36]

In order to design racemates that undergo spontaneous segregation into enantiomorphous two-dimensional domains, secondary amide groups were incorporated within the molecules, between the long hydrocarbon chains that provide hydrophobic character and the head-group that orients them toward the water surface. The structure of the monolayer

films of several enantiopure and racemic α-amino acids bearing various alkyl chains $C_nH_{2n+1}CONH(CH_2)_4$-$CH(NH_3^+)CO_2^-$, n=15,17,21 (C_n-Lys) was determined by GIXD. The enantiopure and racemic mixtures of molecules yielded very similar GIXD patterns indicative of the packing into an oblique unit cell with translational symmetry only. The 2D packing arrangement determined from the GIXD measurements is shown in Figure 1.18.[37]

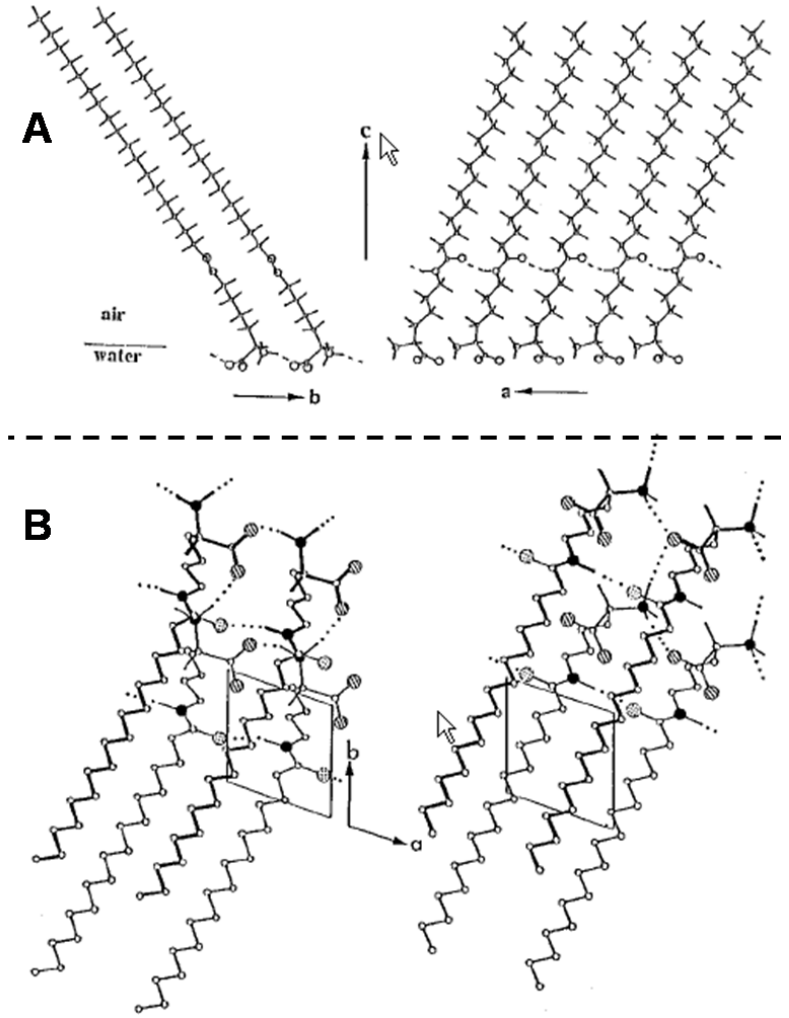

Figure 1.18 *The packing arrangement of the enantiomorphous 2D crystallites self-assembled from either enantiopure or racemic $C_{17}H_{35}CONH(CH_2)_4$-$CH(NH_3^+)CO_2^-$ amphiphiles : A) side view, B) top view.*[37]

1.7.3 Liquid-solid interface

This thesis mainly focuses on the expression of molecular chirality at the liquid-solid interface. Thus, a more detailed introduction on the self-assembly of molecules at the liquid-solid interface, the characterization technique and analysis methods will be given in this part. At a liquid–solid interface, 2D assemblies can be created by depositing a solution of the compound of interest on top of the substrate. Depending on the nature of the solvent, the substrate, and the dissolved molecules, the latter might form an ordered monolayer at the liquid–solid interface. As introduced in section 1.4, the interaction between the substrate and the molecules can be so strong that chemical bonds are formed. In that case the adsorption is referred to as chemisorption. When the interactions remain relatively weak, the process is physisorption (Figure 1.19). The main difference with working under UHV conditions is that the solvent is able to mediate dynamic processes between molecules adsorbed at the surface and molecules dissolved in solution, and as a result, thermodynamic equilibrium can be reached. A related effect of such dynamic processes is the possibility of self-repair of defects present in the

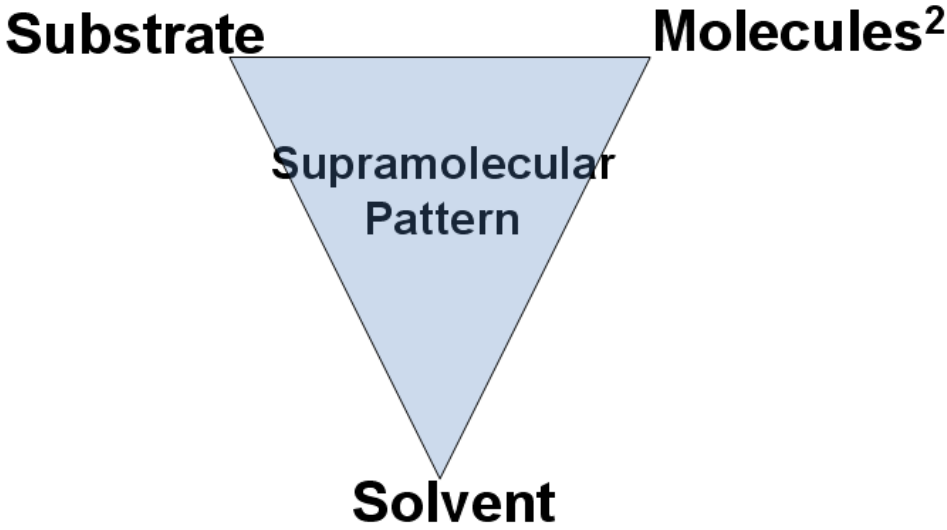

Figure 1.19 *The outcome of the molecular self-assembly process at a liquid-solid interface is the result of a complex interplay between molecule-molecule (molecule^2), molecule-solvent, molecule-substrate, and solvent-substrate interactions.*

self-assembled monolayer structure. An important disadvantage of a liquid environment compared to UHV is the limited temperature range in which processes can be followed, namely the window between the melting and the boiling point of the solvent. On the other hand, for many studies it is considered a huge advantage that liquid–solid interfaces resemble the environment in which many important chemical and biological processes are taking place.

Because the structure of a monolayer at an interface is inherently different from that of molecules in the bulk, and the thickness of the interfacial region is of the order of nanometers or smaller, advanced interface specific methods are needed to study the interface at the microscopic and nanoscopic levels. Superior techniques to characterize interfaces down to the sub-molecular level have been found in the scanning probe microscopy ones. They make use of a sharp tip to probe an atomically flat surface on which molecules can be deposited. With atomic force microscopy (AFM) it is possible to study air–solid or liquid–solid interfaces down to approximately nanometer resolution. This technique also allows the study of multilayers or thicker layers. With STM, though limited to conductive surfaces, even molecules and atoms can be resolved, making it a very powerful technique since it affords the highest spatial resolution one can get of molecules within a monolayer. At the liquid-solid interface (Figure 1.20), the tip is immersed in the solvent layer and therefore generally a non-conducting liquid is used to prevent the interference of the tunneling current with faradaic currents via the metallic tip. In addition, STM has an advantage when it comes to identifying dynamic processes or structural and dynamic phenomena which only involve a small number of molecules or even single molecules.

The choice of the solvent for STM measurements is very important: while dissolving the compound of interest, the solvent molecules should not compete with it for adsorption at the surface, and the solvent should not evaporate too quickly so formation of dry multilayers is prevented. Despite the fact that the effect of the solvent in processes that occur at the liquid-solid interface has not yet been probed systematically at the molecular level yet, its role is anticipated to be crucial in directing the molecular organization at liquid–solid interfaces.

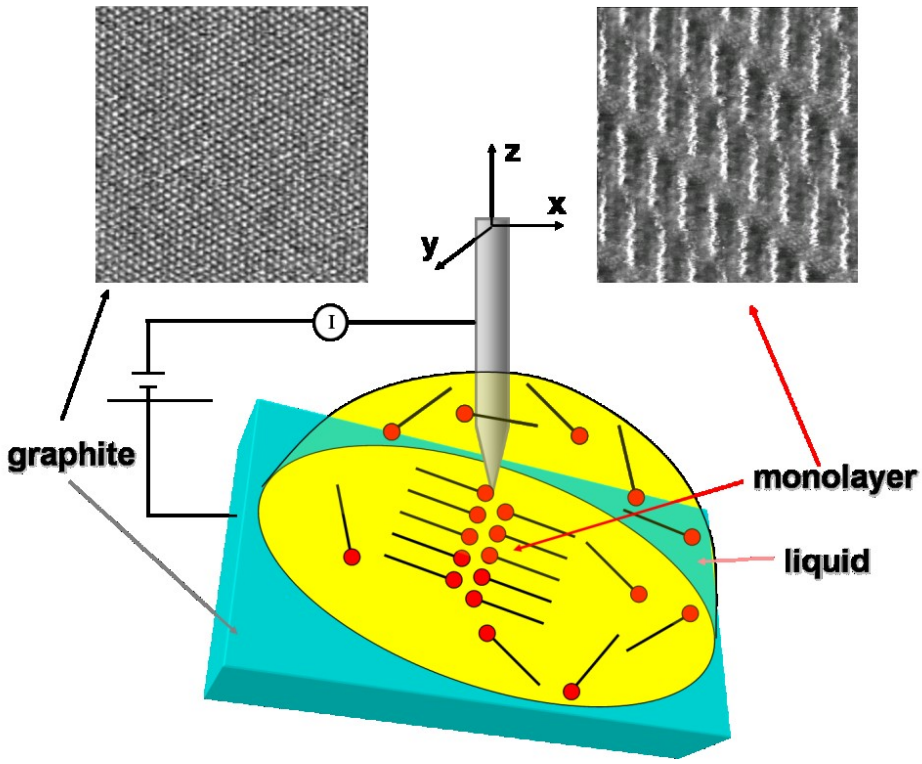

Figure 1.20 *Schematic representation of STM at a liquid–solid interface, in which either a* highly oriented pyrolytic graphite (HOPG) *surface is imaged with atomic resolution (left) or a monolayer of molecules adsorbed at the liquid - HOPG interface (right).*[23]

Though several different substrates can be used for STM, highly oriented pyrolytic graphite (HOPG) is one of the most popular ones. The honeycomb structure of the basal plane of a HOPG surface is depicted in Figure 1.21, including the symmetry directions according to the Weber notation. Those along the equivalent <-1 2 -1 0> directions (yellow vectors) are often called the 'main symmetry directions', whereas the set of equivalent <-1 1 0 0> directions (dashed red vectors), the 'normals', are running perpendicular to them. Normally, HOPG refers to HOPG with an angular spread between the HOPG sheets of less than 1°. If the topmost HOPG layer is rotated by a defined angle with respect to the underlying bulk atomic orientation, the influence of the sublayers may result in a periodic modulation of the surface density of states which appears as an

electronic superlattice with a periodicity (Moiré pattern) dependent on the rotation angle of the HOPG layers (Figure 1.21D).[38,39,40,41]

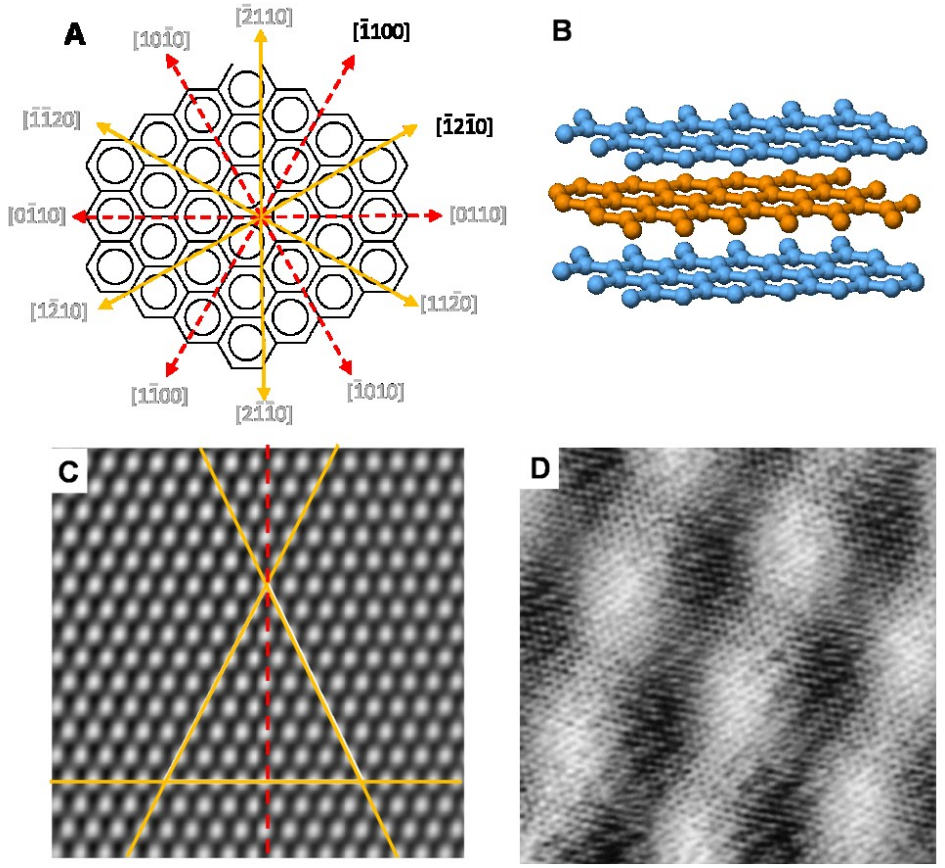

Figure 1.21 *A) Honeycomb lattice of the basal plane of HOPG in which the main symmetry axes are indicated by the yellow vectors and the normals to those by the dashed red vectors. B) side view of HOPG layer stacking C) STM image (4 × 4 nm^2) of a HOPG surface in which the main symmetry axes are indicated by yellow lines and one of the normals by the dashed red line. D) STM image (10.4 × 10.4 nm^2) of Moiré patterns of HOPG. The atomic corrugation of HOPG as well as the super-structure with a periodicity of 4.0±0.1 nm are visible. The orientation angle of the superperiodic lattice relative to the atomic lattice is measured from this image to be 28±1°.*[38]

While in the area of 3D crystallography the molecular ordering can be

classified into 230 space groups, the data of 876 known systems organized in 2D monolayers at the liquid–solid interface and characterized at the (sub)molecular level by STM were compiled in a so-called Two-dimensional structural database (2DSD) and classified into the 17 plane groups of which five are chiral: *p*1, *p*2, *p*3, *p*4, and *p*6 (Figure 1.22).[42] Evaluation of the data revealed that a large majority of molecules, both achiral and chiral, 'crystallized' into plane groups that allow the densest packing of the molecules and maximize intermolecular interactions. At an interface, inversion centers are normally incompatible with a monolayer because of the non-centrosymmetry which is inherent to the presence of an interface. In two dimensions, twofold rotations provide the closest packing, while mirror planes hinder close packing. Therefore, the propensity of twofold rotations in packing motifs on a surface, lacking mirror planes, leads to a preference for chiral crystal formation on a surface (local and global organizational chirality). Indeed, *p*2 and *p*1 are the most abundant space groups and they are chiral: mirror-related, non-superimposable domains can be formed on the surface. This effect is

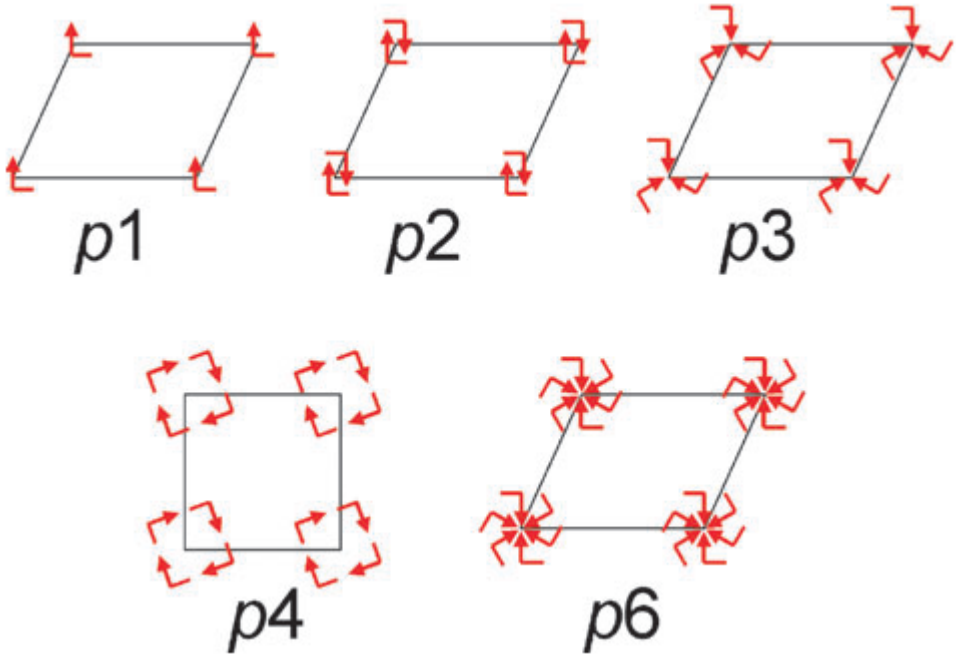

Figure 1.22 *Schematic representations of the 5 chiral plane groups in the Two-Dimensional Structural Database. Each of the arrows indicates an asymmetric unit, and unit cells are denoted by the black lines.*[42]

reflected in the observation that 79% of the monolayer arrangements in the 2DSD are chiral, despite the fact that most of the molecules involved are achiral. So, in those cases where STM imaging is of sufficient quality, the formation and observation of local and global organizational chirality is often obvious, simply by evaluating the symmetry of the unit cell.

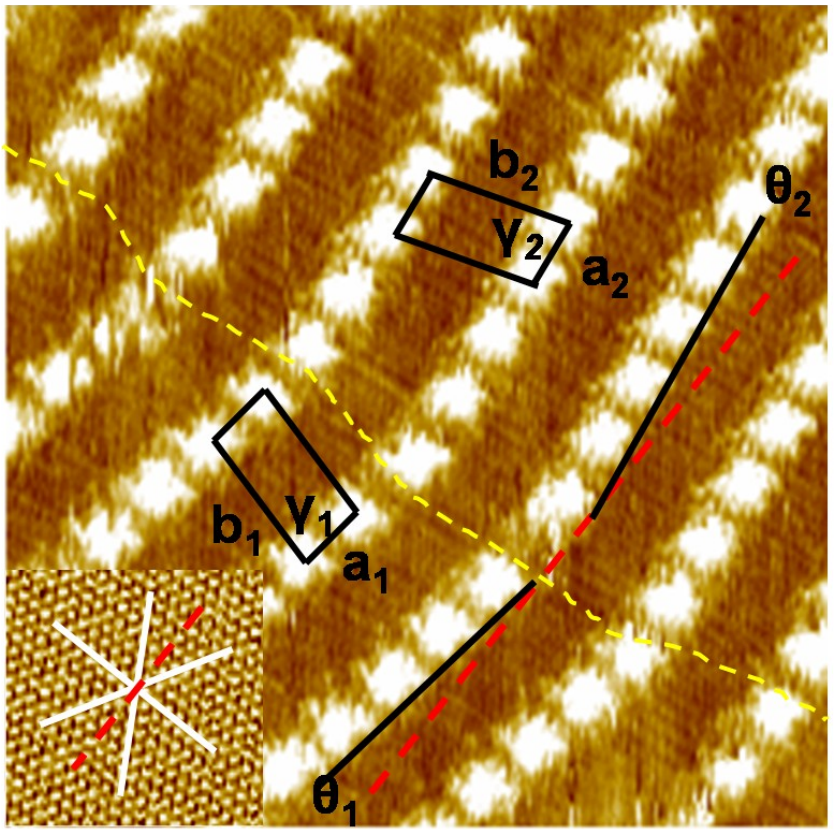

Figure 1.23 *STM image of 5,10,15,20-tetrakis (4-octadecylamidephenyl) porphyrin monolayers self-assembled at a 1-heptanol - HOPG interface (for chemicals structure, see Figure 2.1). The oblique unit cells are indicated in black. Dashed yellow line shows the domain boundary. Solid black line is aligned with the short unit cell vector of the monolayer. The inset shows the STM image at the same location of the sample in which the underlying HOPG surface is imaged by changing the tunneling parameters. The angle θ is defined by the angle between the short unit cell vector of the monolayer and one of the symmetry axes of the HOPG surface (indicated by the dashed red line).*

To illustrate how the relation between monolayer and substrate can be determined, a simple example of a molecule that self-assembles at the liquid–solid interface in rows is considered (Figure 1.23). In many cases, molecular rows do not match the direction of one of the main symmetry axes or the axes that run normal to them. In general, the orientation of a (domain within a) monolayer is determined by evaluating the angle θ between one of the unit cell vectors of the monolayer and one of the symmetry axes of the substrate or the normal (reference axis). For practical reasons, often that particular major symmetry axis, or its normal, which defines the smallest angle with the unit cell vector, is selected. When the selected vector does not run parallel with respect to one of these axes, it can be rotated clockwise (CW, positive angle) or counterclockwise (CCW, negative angle) with respect to the reference axis. Studies on many monolayers have revealed that achiral systems generally form both positive (unit cell vector rotated CW) and negative (unit cell vector rotated CCW) domains, whereas enantiomerically pure molecules typically self-assemble in one of both types of domains. Obviously, this kind of analysis only makes sense if the orientation of the monolayers with respect to the substrate underneath is not random, a condition which is often fulfilled for physisorbed systems at the liquid–solid interface.

A) Chirality in monolayers composed of enantiopure molecules

Many reports have appeared on the self-assembly of enantiopure molecules, especially at the liquid–solid interface. Examples include terephthalic acid.[43] and carboxylic acid derivatives,[44,45] 4-phenylene-vinylene oligomers,[46,47,48,49] monodendrons[50,51] and many others. In almost all of these systems, the enantiomers form enantiomorphous monolayers (global point and global organizational chirality).

Figure 1.24B & C show STM images of physisorbed monolayer structures of respectively the (*S*)-enantiomer and (*R*)-enantiomer of a chiral terephthalic acid derivative, 2,5-bis[10-(2-methylbutoxy)decyloxy] terephthalic acid (TTA), which has two identical stereogenic centers.[43] The monolayers are characterized by two different spacings between

adjacent rows of (*R*,*R*)-TTA or (*S*,*S*)-TTA terephthalic acid groups. For both enantiomers, the width of the broader lamellae (ΔL_1 = 2.54 ± 0.05 nm) corresponds to the dimension of fully extended alkoxy chains, which are lying flat on the HOPG surface and almost parallel to a HOPG main symmetry axis. The width of the narrow lamellae (ΔL_2=1.9 ± 0.1 nm) indicates that the terminal 2-methylbutoxy groups are bent away from the surface, while the decyloxy groups are lying flat on the HOPG surface adopting an all anti-conformation. For this system, monolayer chirality is expressed in several ways. In regions of the monolayer where the alkoxy chains are fully extended, the unit cells for the (*S*,*S*)- and (*R*,*R*)-enantiomers are clearly chiral (plane group *p*2). Moreover, the STM images exhibit a clear modulation of the contrast along the lamellae. This superstructure (Moiré pattern) is attributed to the incommensurability of the monolayer with the underlying HOPG lattice. The unit cells of this contrast modulation, indicated in red, are mirror images for the enantiomers, which means that each enantiomer forms its characteristic enantiomorphous monolayer structure. This enantiomorphism is also expressed by the orientation of the lamella axes with respect to the HOPG lattice: the angle θ between a lamella axis and the normal of the HOPG main symmetry axis (i.e. one of the symmetry-equivalent <-1 1 0 0> directions), which is (nearly) perpendicular to the alkoxy chains, takes a value of respectively -3.7 ± 0.3° and +3.7 ± 0.3° for the (*S*,*S*)-enantiomer and (*R*,*R*)-enantiomer. In addition to the effect of chirality on the surface ordering of these monolayers outlined above, monolayer images reveal elongated discontinuous features (most clearly seen in the upper and lower quarter of Figure 1.24B), both in narrow and wide lamellae. In the narrow lamellae, the position of those features can be assigned to the location of the 2-methylbutoxy groups, which are pointing away from the HOPG surface. The discontinuous fuzzy character of the observed features is due to the mobility of the non-adsorbed chain ends and the interaction with the STM tip during the scanning process. However, these streaky features are also observed in the wide lamellae, and are attributed to the interaction between the scanning tip and the protruding methyl unit on the chiral carbon atom, which allows the visualization of the location of stereogenic centers in a direct way. Further support for this hypothesis was provided by the observation that an increase of the bias

voltage which results in a slight retraction of the tip only leads to the disappearance of the spots correlated with the stereogenic centers, while the spots related to the 2-methylbutoxy groups are still visible.

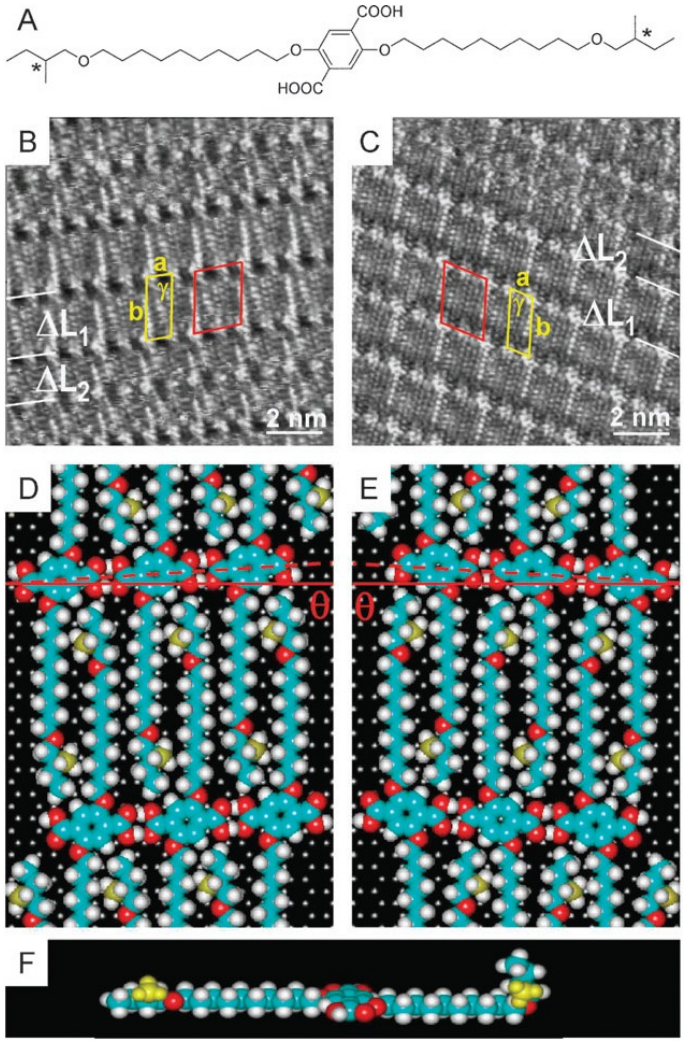

Figure1.24 *A) Molecular structure of the TTA derivatives. B) & D) STM image and molecular arrangement of (S,S)-TTA at the liquid - HOPG interface. C) & E) Idem, of (R,R)-TTA. Both enantiomers form mirror image type patterns; the monolayer unit cells (for the fully extended alkyl chains (ΔL_1)) are indicated in yellow. The red unit cells refer to the epitaxy with the HOPG surface. F) Alkyl chains are not always extended: the 2-methylbutoxy group is often raised up from the HOPG surface (ΔL_2).*[43]

Among the many enantiomerically pure systems which have been investigated, some contain multiple chiral centers, such as the oligo(*p*-phenylene vinylenes) (Figure 1.25). [46,47,48,49] They all carry (*S*)-2-methyl butoxy groups along the backbone. In the first type, oligo(*p*-phenylene vinylenes) which are at both termini functionalized with three dodecyl chains (**3**, Figure 1.25A), self-assemble in highly organized 2D crystals on HOPG by spontaneous self-assembly. They form stacks and the bright features correspond to the conjugated backbones, of which one is indicated by a white oval. Alkyl chains are interdigitated. In the second and the third type, the molecules are functionalized by hydrogen bonding groups such as ureido-s-triazine (**4,** Figure 1.25B) or 2,5-diamino-triazine groups (**5,** Figure 1.25C). The ureido-s-triazine derivatized oligo(*p*-phenylene vinylenes) show linear dimerization via self-complementary hydrogen bonding, as expected. The molecules are indeed stacked in parallel, though not equidistant rows. The fact that the conjugated backbones forming a dimer are slightly shifted is in line with the hydrogen bonding pattern formed. In contrast, the 2,5-diamino-triazine derivatized oligo(*p*-phenylene vinylenes) show cyclic hexamer formation. Both **3** and **4** self-assemble according to the *p*2 symmetry group, while **5** according to the *p*6 plane group. The domains formed by these compounds are again enantiomorphous too: mirror-image related patterns were never observed, except of course for their mirror-image enantiomers.

Polymorphism is a phenomenon that is quite normal in 3D crystals but is less explored in self-assembled monolayers. Physisorbed monolayer films of a chiral terephthalic acid derivative have been imaged on HOPG at the solution - substrate interface using STM. [52] The molecule comprises a non-chiral aromatic moiety and a chiral handle. It is found to form several 2D polymorphs, all corresponding to the plane group *p*2 (Figure 1.26). The STM images are characterized by rather large bright spots corresponding to the location of aromatic terephthalic acid groups, which are aligned in rows and define the lamella axis. The rows of smaller spots perpendicular to the lamella axis reflect the orientation of the extended eicosyloxy groups. The 2-octyloxy groups at the other side of the terephthalic acid row appear with a different contrast, indicating a non-optimal packing and increased dynamics on the STM timescale.

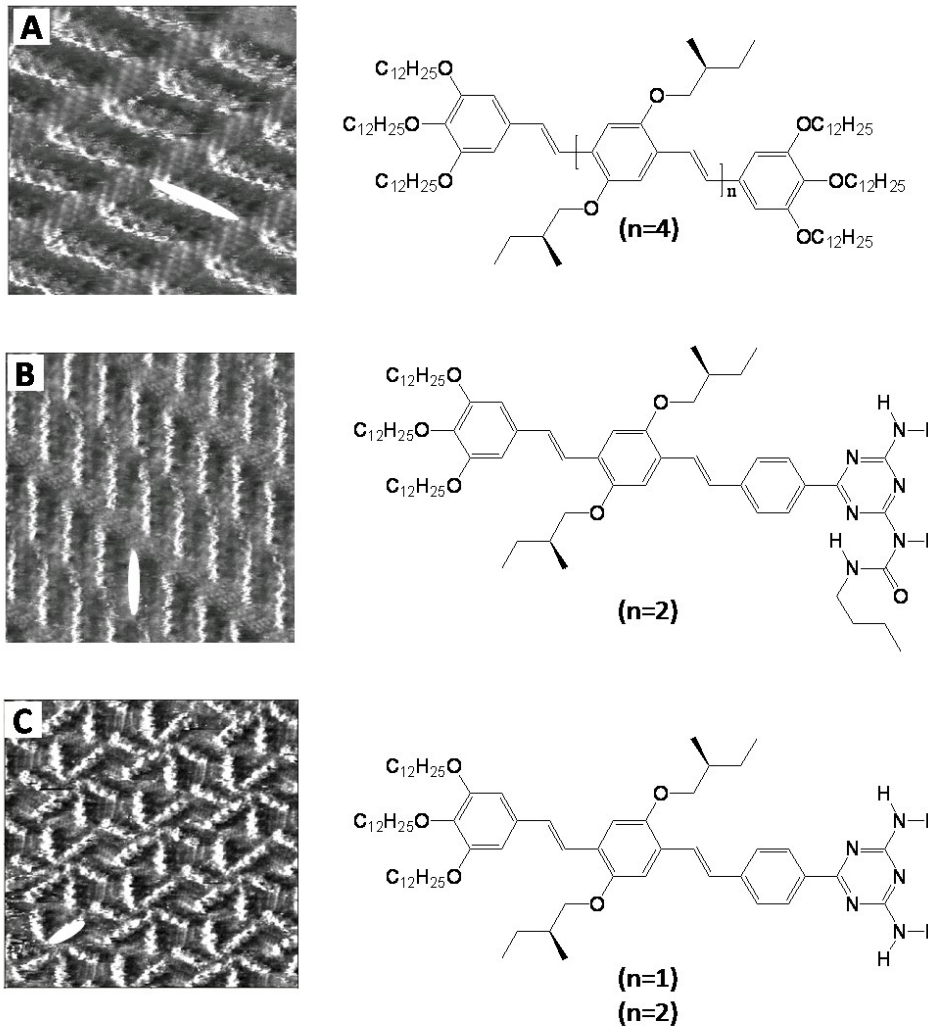

Figure 1.25 *STM images and chemical structures of A)* ***3*** *(n=4) at the 1,2,4-trichlorobenzene – HOPG interface. Image size: 10.7 × 10.7 nm^2. B)* ***4*** *(n=2) at the 1,2,4-trichlorobenzene – HOPG interface. Image size: 12.1 × 12.1 nm^2 and C)* ***5*** *(n=1) at the 1-phenyloctane – HOPG interface. Image size: 18.4 × 18.4 nm^2. Hydrogen bonding has a strong effect on the supramolecular architecture. The white ovals indicate a conjugated backbone.*[46,47,48,49]

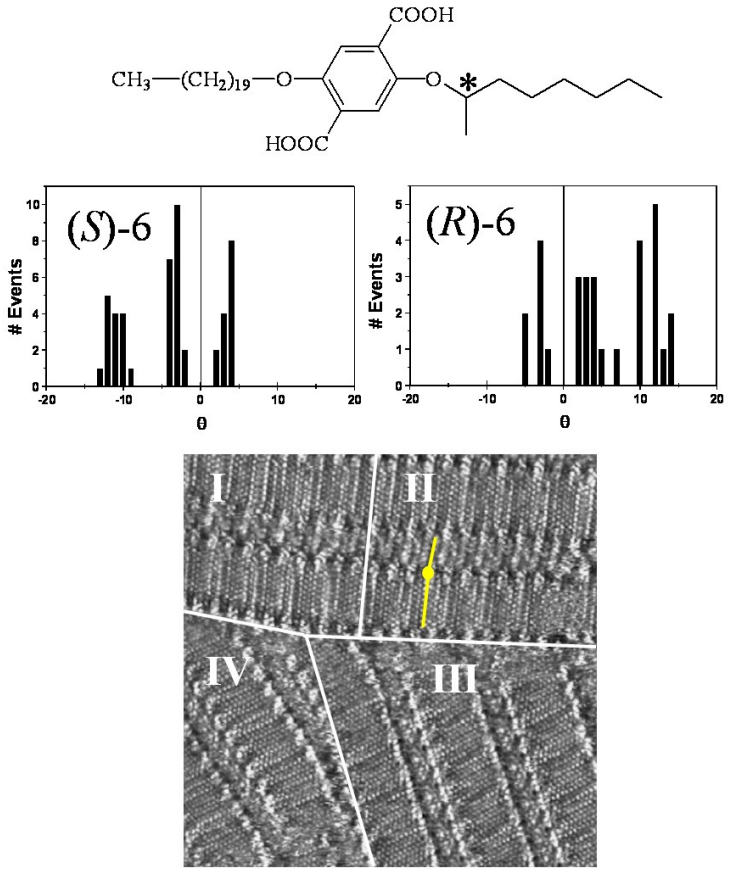

Figure 1.26 *Top: Chemical structure of* ***6****. Center: Histograms reflecting the number of observations as a function of the value of the angle between a row of terephthalic acid groups and the substrate's appropriate symmetry axis (reference axis). Left: (S)-enantiomer. Right: (R)-enantiomer. Bottom: STM image containing several domain boundaries of (S)-****6*** *physisorbed at the 1-phenyloctane – HOPG interface. 20 × 20 nm*^{2}*. The white lines define the several domain areas. These domains are polymorphous and are characterized by different values for the angle between a row of terephthalic acid groups and the substrate's appropriate symmetry axis. The value of this angle in the domains I, II, III and IV is +3.5°, -3.5°, +4.5° and -11°, respectively. The orientation of the 2-octyloxy groups can only be distinguished in the upper two domains. They appear to be rotated a few degrees clockwise with respect to the normal on the lamella axis.*[52]

They are slightly clockwise rotated with respect to the long axis of the eicosyloxy groups. A simplified model is indicated in yellow. This molecule self-assembles in polymorphous patterns (see STM image). As the eicosyloxy groups are oriented parallel to a HOPG main symmetry axis the lamella structure can be characterized unequivocally in terms of its relation with the underlying HOPG substrate. These data are summarized for both enantiomers in the histograms in Figure 1.26. The angle between the terephthalic acid rows and the appropriate substrate symmetry axis has been determined and the characteristic angles for (*S*)-enantiomer are approximately -3° and -12° and +3°. Similarly, for (*R*)-enantiomer the images were analyzed in the same way and depending on the domain, this angle takes the values -3°, +3° or +12°. In agreement with symmetry considerations, the similar absolute value of the row to HOPG symmetry axis angle for both positive and negative domains must be fortuitous and for the same enantiomer, domains with positive and negative values cannot be truly enantiomorphous. Such domains which form apparently mirror images are diastereomeric and are different 2D polymorphs. Polymorphism and quasi-enantiomorphism have also been reported for some liquid-crystalline compounds at their interface with HOPG.

B) Racemic mixtures

Racemic mixtures of chiral molecules can self-assemble quite differently in 2D on a substrate than in 3D in a crystal. In 3D, achiral molecules tend to crystallize in achiral space groups, and the unit cells of racemates generally contain both enantiomers, since these crystals are more densely packed and more stable. However, when restricted to 2D, molecules from a racemate tend to self-assemble into conglomerates, i.e. the enantiomers self-assemble in mirror-image domains, actually physically separating the enantiomers from each other. In this case, each domain contains probably one of the two enantiomers. Most STM studies of self-assembled monolayers at a liquid–solid interface appear to support conglomerate formation, although recent results challenge the generality of this concept.

When a racemate self-assembles on a substrate at the liquid – solid interface, generally an organization of the molecules in what are believed

racemic conglomerates is observed. This was first demonstrated by Walba *et al*., who studied the self-assembly of enantiomerically pure (99%) and racemic biphenylbenzoates (Figure 1.27A) at the liquid–solid interface.[53] Whereas enantiomorphous monolayers were formed from the enantiomerically pure compounds, the racemic mixture gives co-existing mirror image-related domains (Figure 1.27B & C). The latter were indistinguishable from the domains formed by the pure enantiomers, which provides strong, though not definite evidence for racemic conglomerate formation.

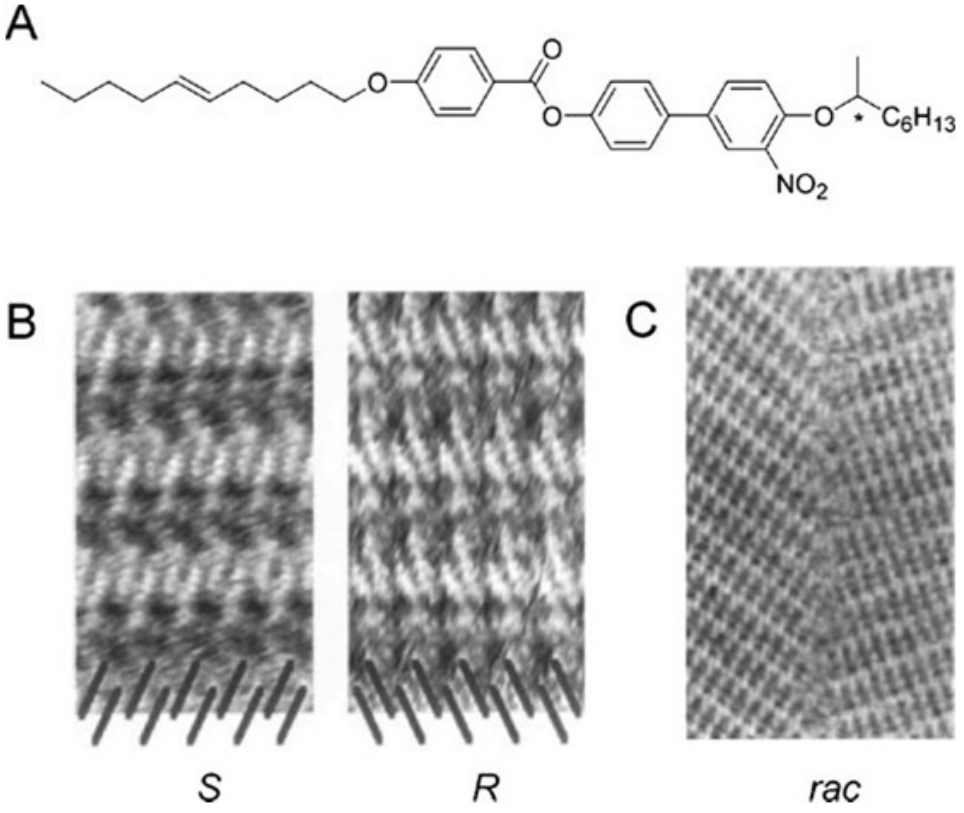

Figure 1.27 *A) Molecular structure of the biphenylbenzoate derivatives, B) STM images (8 × 15 nm^2) of enantiomorphous domains of the (S)-enantiomer (left) and the (R)-enantiomer (right). C) STM image (27 × 38 nm^2) of co-existing mirror image-related domains of the racemate.*[53]

Only in a very few case, has 2D pseudoracemate formation been observed. In a pseudoracemate, a 1:1 ratio of both enantiomers of a chiral

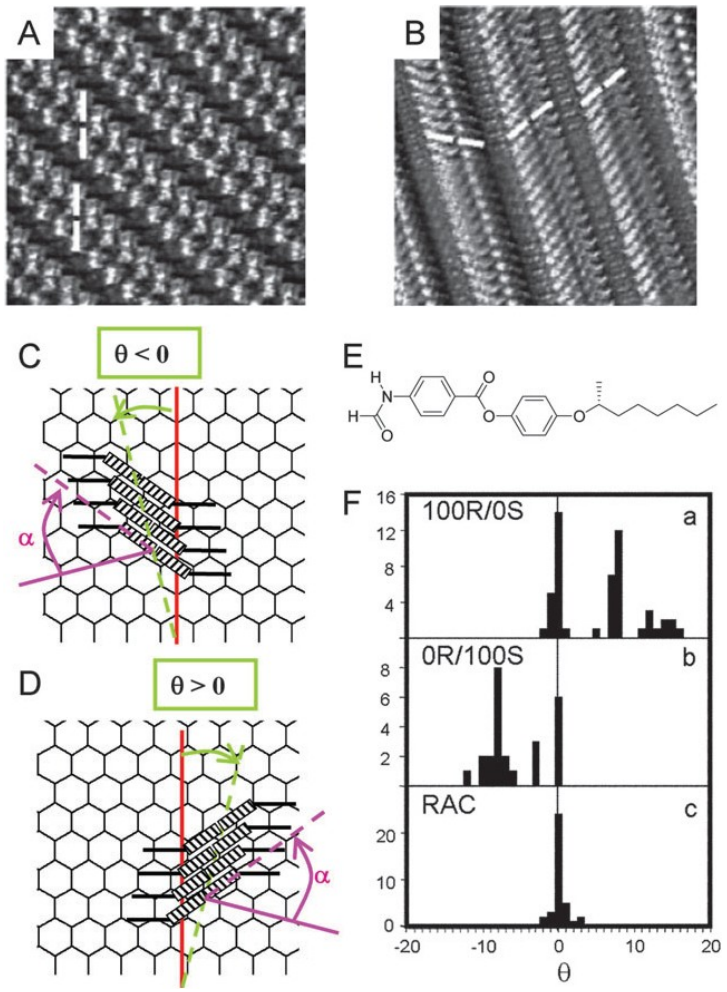

Figure 1.28 *A) STM image (12 × 12 nm^2) of the (R)-enantiomer of the phenyl benzoate derivative monolayers at the 1-heptanol – HOPG interface, B) STM image (13.6 × 13.6 nm^2) of the racemate monolayers at the same interface, C) & D) Schematic representations of the orientation of 'dimers' of the phenyl benzoates on HOPG. (C: (S)-enantiomer; D: (R)-enantiomer. The normal of the HOPG main symmetry axis (HOPG reference axis) is indicated in red. The dashed green line represents a lamella axis. θ: angle between the reference axis and the lamella axis; α is defined as the angle between the normal on the lamella axis and the dimer, E) Molecular structure of the phenyl benzoate, F) Histograms of the angle θ observed for physisorbed monolayers of (a) the (R)-enantiomer, (b) the (S)-enantiomer and (c) the racemate.*[54,55]

compound is organized in disordered arrays within one homogeneous crystal phase. The formamide-functionalized phenyl benzoates, shown in Figure 1.28E, self-assemble as hydrogen-bonded dimers into lamellar arrays at the interface of HOPG and a variety of liquids.[54,55] While the pure enantiomers of the compound self-assemble in 2D enantiomorphous domains, characterized by the angle a between the phenyl benzoate moieties and the normal on the lamella axis (Figure 1.28A), the racemate forms a very distinct monolayer structure in which this angle randomly varies between adjacent lamellae (Figure 1.28B). In addition to the expression of chirality at the level of monolayer structure, the pure enantiomers generally express chirality at the level of the orientation of the monolayer with respect to the underlying HOPG lattice, as observed by the direction of the lamella axis of the monolayer with respect to the symmetry axes of HOPG (angle θ in Figure 1.28C & D). In the histograms in Figure 1.248, the distributions of angles θ observed for the pure enantiomers and the racemate are plotted. In all of the cases, the distribution is random; although the (*R*)-enantiomers show a strong tendency to form domains with $\theta > 0^\circ$ and the (*S*)-enantiomers domains with $\theta < 0^\circ$, they still form a substantial fraction of domains for which θ is close to zero. In contrast to the enantiopure molecules, the racemate exclusively forms domains in which the angle θ is close to zero. Hence, the patterns formed by the racemate are not a mere reflection of the adsorbate layers formed by the pure enantiomers, and no racemic conglomerate formation takes place.

C) Achiral molecules

Not only chiral, but also achiral molecules are able to self-assemble into chiral domains. Certain achiral molecules are described as prochiral—one desymmetrising step away from chirality—if they become asymmetric when they are constrained to a surface. Other molecules remain achiral upon their deposition at a surface, but nevertheless can form chiral structures. This is not a consequence of just molecular asymmetry, but the result of intermolecular and molecule–substrate interactions.[56] For instance, 4'-alkyl-4-cyanobiphenyl (nCB) derivatives, liquid crystal molecules which are well-known from the pioneering STM studies of

organic molecules on a surface carried out by Foster and Frommer, are key examples of molecules which are inherently achiral.[57] However, because their alkyl chains make an angle with the biphenyl axis upon their adsorption on HOPG, the symmetry of the molecule is broken and a chiral pattern is formed.

Similar to chiral molecules, prochiral molecules have a strong tendency to form conglomerates. The packing of one (2D) stereoisomer with copies of itself is thermodynamically more favorable (or kinetically faster) than packing with other molecules.

An elegant system in which the stereochemical morphology of monolayers formed from alkylated prochiral molecules on a HOPG surface switches from a racemate to a conglomerate by the elongation of the side chains with one methylene unit, has been reported by Zimmt *et al*.[58] Two 1,5-bis-(3'-thiaalkyl)anthracene derivatives (Figure 1.29A), having linear alkyl chains containing either 11 or 12 carbon atoms, were adsorbed at the 1-phenyloctane – HOPG interface. STM images of the monolayers formed by the two compounds revealed a striking difference in organization. For the compound with the C_{11}-alkyl chains, the orientation of the anthracene moieties alternates from row to row, leading to a racemic monolayer with *pg* plane group symmetry (Figure 1.29C). In contrast, for the compound with the C*12*-alkyl chains, the orientation of the anthracene moieties is constant within a given domain, which reflects the formation of a conglomerate monolayer with *p*2 plane group symmetry (Figure 1.29B). Isolated mirror image enantiomers have identical energy, while pairs of interacting isomers are diastereomeric and have distinct energies. For both compounds, the chirality on a surface of the anthracene moieties within the same row is identical and apparently of the lowest energy. The difference between both compounds is expressed in the difference in their relative orientation in adjacent rows. The organization of the molecules within the monolayer is determined both by molecule–molecule and molecule–substrate interactions. Alkyl chains tend to align along one of the main symmetry axes of HOPG, and methylene groups of adjacent chains align in registry in order to maximize intermolecular van der Waals interactions. The different stereomorphologies are proposed to arise from a different relative orientation of the CH_2–CH_3 and the C-aryl–C1' bonds within the same

side chain. For the compound with C_{11}-chains, both bonds are parallel while for the compound with C_{12}-chains, these bonds make an angle of about 110˚ within the same chain. Optimization of the van der Waals interactions between the chains, in combination with their all-trans conformation, then leads to the difference in orientation of the anthracene moieties in adjacent rows. By making use of the principles of crystal engineering, the controlled formation of conglomerates and racemates on a surface could be extended, by using anthracene derivatives with one or two oxygen atoms in each alkyl chain. The location and orientation of the ether dipoles in the alkyl chains determine the monolayer morphology and overrule the odd–even effect.

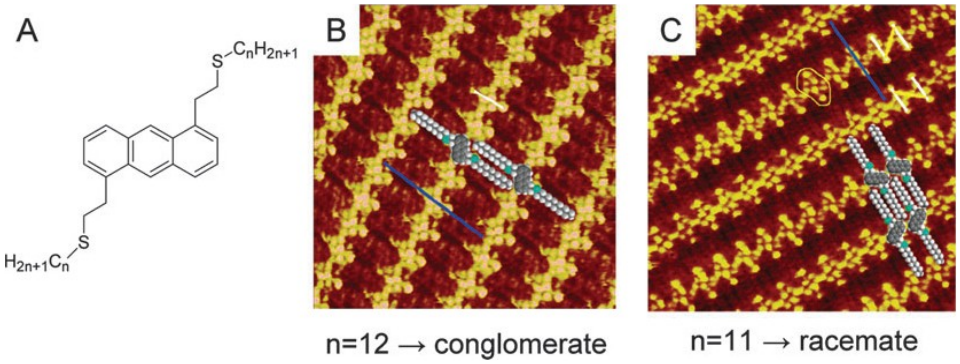

Figure 1.29 *A) Molecular structure of the anthracene derivatives, B) STM image (11 × 11 nm^2) of a monolayer of the compound with C_{12}-alkyl chains at the 1-phenyloctane – HOPG interface; In adjacent rows the anthracene moieties are oriented in a parallel fashion and a conglomerate is the result, C) STM image (12 × 12 nm^2) of a monolayer of the compound with C_{11}-alkyl chains; in adjacent rows the anthracene moieties are oriented in a twisted fashion, giving a racemate.*[58]

D) Multicomponent structures

In a few studies, monolayers have been constructed in which achiral and chiral molecules are mixed. These molecules can be very similar, like in the case of hexadecanoic acid which was self-assembled with an equal amount of racemic 2-bromohexadecanoic acid at the 1-phenyloctane – HOPG interface. Alternatively, the adsorption of chiral molecules into enantiomorphous domains can have a distinct influence on the

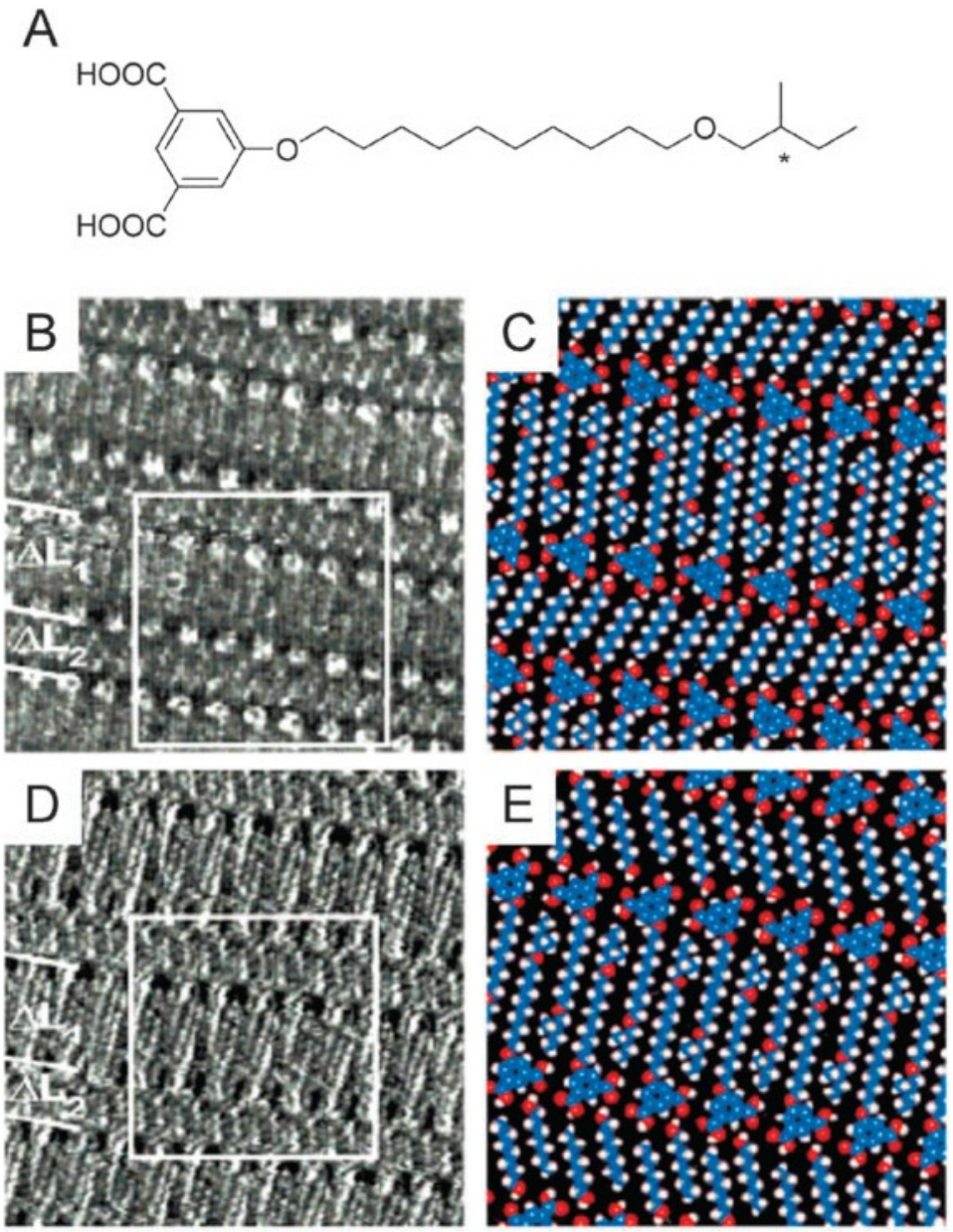

Figure 1.30 *A) Molecular structure of the chiral isophthalic acids (ISAs), B) & C) STM image and molecular model of the monolayer of (S)-ISA and 1-octanol on HOPG, D) & E) Idem, of (R)-ISA. ΔL_1 and ΔL_2 indicate lamellae composed of ISA and 1-octanol molecules, respectively.*[59]

co-adsorption of achiral molecules. A typical example of such an effect

was observed in the case of the co-assembly of alcohols in monolayers of the chiral isophthalic acids (ISAs) depicted in Figure 1.30A.[59] At the interface of HOPG and 1-octanol, each of the enantiomers of this molecule self-assembles into enantiomorphous domains of lamellar arrays (Figure 1.30B & D). Arrays of solvent molecules are co-adsorbed, and their orientation within the lamellae depends on the enantiomeric character of the domain: for (*S*)-ISA, they are rotated clockwise with respect to the lamella normal, while for (*R*)-ISA monolayers they are rotated counterclockwise (Figure 1.30C & E).

Sometimes the addition of a second component even induces clear chirality in a monolayer. At the 1-phenyloctane – HOPG interface, the enantiomers of 16-methyloctadecanoic acid self-assemble into lamellar patterns in which chirality hardly can be recognized, probably because the chiral carbon atom is not adsorbed.[60] When 4,4'-bipyridine was co-adsorbed in a 1:2 ratio with respect to the carboxylic acid, a supramolecular complex was formed via hydrogen bonding and as a result a clear expression of chirality became apparent in the STM image. Adding bipyridine to (*R*,*S*)-16-methyloctadecanoic acid results in an identical pattern exhibiting a mirror-image related organization and indicating the occurrence of spontaneous resolution (Figure 1.31).

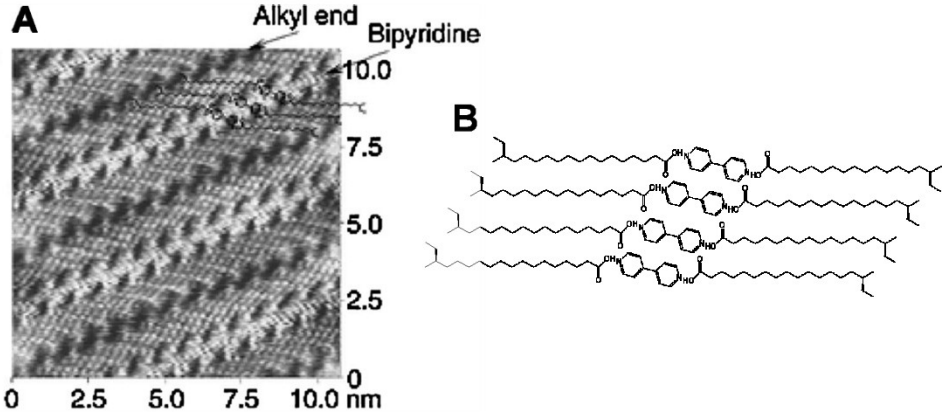

Figure 1.31 *A) STM image of (R,S)-16-methyloctadecanoic acid in the presence of 4,4'-bipyridine. B) Structural drawing of one of the mirror-image related domains.*[60]

Chirality in monolayers of multicomponent systems can also be observed

when none of the components are chiral or prochiral. Two- and three-component self-assembled structures based on coronene (COR), isophthalic acid (ISA) and dehydrobenzo[12]annulene (DBA) derivatives have been reported.[61] While neat ISA forms zig-zag structures at a1-octanoic acid - HOPG interface, the addition of COR induces a structural reformation in which it templates the organization of ISA molecules in cyclic hexamers around its aromatic core (Figure 1.32A). In the STM images of this bicomponent system, it can be seen that chirality is only expressed at the highest level of the hierarchical self-assembly process, which is at the level of 2D pattern formation: the relative shift of the heteroclusters in the 2D lattice, thereby maximizing molecular density and intermolecular interactions, leads to the emergence of chiral domains (Figure 1.32B & C). Analysis of the relative orientation of these mirror image domains with respect to the HOPG lattice underneath revealed that their unit cells were rotated either CW or CCW with respect to the main symmetry axes of the surface, which means that, in addition to at the level of monolayer symmetry, chirality is also expressed at the level of monolayer–substrate interactions. Upon the addition of a third component, DBA, a molecule which is capable of forming nanoporous structures at a liquid–solid interface (depending on its concentration), the bicomponent clusters of ISA and COR became trapped in a nanoporous network formed by the DBA molecules (Figure 1.32D). As a result of different modes of interdigitation of the alkyl chains of the DBA host network, which generates chiral pores (Figure 1.32E), this three-component system also forms domains with different chirality, and also in this case chirality is expressed at the level of the monolayer–substrate interactions.

E) Solvent effects

Also solvent can have an influence on the expression of chirality in a monolayer, for example by tuning the intermolecular interactions between the adsorbed molecules. When solutions of the achiral molecule 3,5-di-(4-*n*-tetradecyloxyphenyl)pyrazole (DTPP) were dropcast onto a HOPG surface, STM studies of the resulting monolayers revealed that the nature of the solvent had a dramatic effect on the molecular ordering.[62] Whereas the use of toluene resulted in the observation of achiral domains

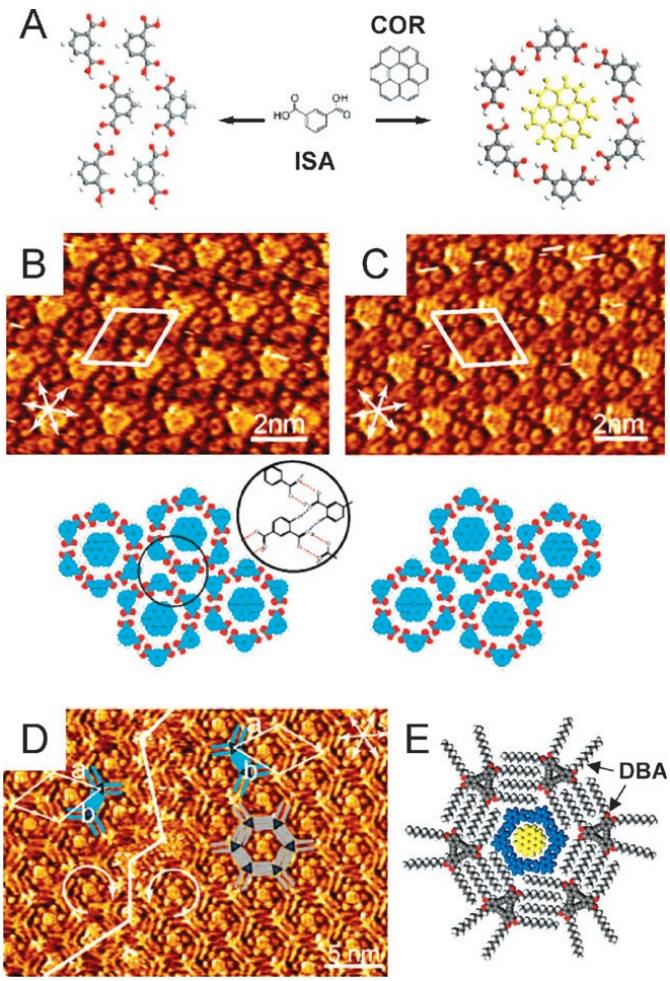

Figure 1.32 *A) Preferred arrangement of ISA molecules at a 1-octanoic acid - HOPG interface (left) and its conversion into a bicomponent structure in which a COR molecules template six ISA molecules into a cyclic hexamer arrangement (right). B) & C) STM images of mirror image domains of monolayers of the bicomponent COR–ISA$_6$ structures, with unit cells and HOPG main symmetry axes indicated in white; below the STM images, molecular models of the molecular arrangements are depicted. D) STM image of the monolayer composed of the three-component assembly of COR, ISA and DBA; the border between two chiral domains is indicated. E) Molecular model of one chiral form of the three-component assembly, in which the chiral nature of the pore can be clearly recognized.*[61]

of molecules with a rod-like shape, the use of a 1:3 mixture of toluene and chloroform revealed the presence of chiral mirror-image domains of molecules which had adopted a bent-core-like shape. The difference in monolayer structure can be explained by the weaker self-association between the DTPP molecules in the toluene–chloroform solvent mixture when compared to pure toluene, and by the difference in solvation which also has an impact on the adsorption–desorption equilibrium of the molecules. Both factors can have a profound influence on the conformation of the molecule (rod-like or bent-core-like) and thus on the expression of chirality on a surface.

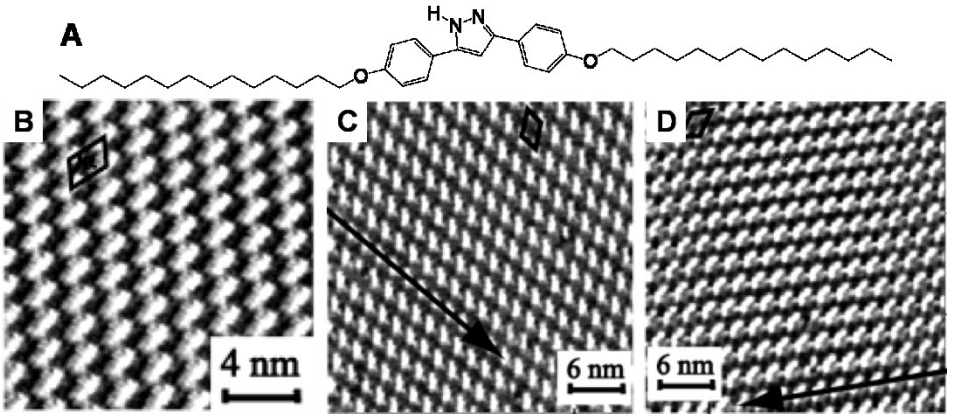

Figure 1.33 *A) Molecular structure of 3,5-di-(4-n-tetradecyloxyphenyl)-pyrazole (DTPP), B) STM image of self-assembled monolayer of DTTP dissolved in toluene adsorbed on the HOPG surface, C) & D) STM image of DTTP dissolved in 1:3 solvent mixtures of benzene and chloroform adsorbed on the HOPG surface showing left-handed and right-handed oriented lamellae.*[62]

1.8 Objectives

Expression of molecular chirality at interfaces is no doubt an interesting topic. Much progress has already been achieved both under ultra-high vacuum conditions and at the liquid-solid interface. Many challenges are still ahead of us though. As far as the liquid-interface is concerned, a systematic investigation on how molecular chirality is transferred to the monolayer level is to be provided yet.

Scanning tunneling microscopy is used for probing the self-assembly process of molecules and digging out details of the ordering and chiral expression of the monolayers. HOPG, as one of the most popular substrates, provides a perfect environment for revealing the expression of chirality in detail.

In an attempt to gain a more general understanding of chiral expression at the liquid-solid interface, a number of aspects have been investigated in detail.

1) It is known that the confinement of molecules on a surface helps to express chirality. An intriguing question is how 'chiral' a molecule needs to be in order to achieve a successful expression of molecular chirality. Therefore, the effect of the number of identical chiral centers per molecule on the expression of chirality on a surface has been investigated. Porphyrin molecules with a different number of stereogenic centers are designed, synthesized and investigated to reveal the relation between the influence of the stereogenic centers on the 2D patterns.

2) How is it possible to follow the dynamic events associated with (chiral) monolayer formation? At the liquid-solid interface, this is normally not possible to study with scanning tunneling microscopy because such dynamics are too fast. Because of its huge size and appropriate structure, a molecular multivalent hexapod shows interesting chirality and dynamics phenomena. Both conformational and translational dynamics could be observed.

3) What is the influence of chemical structure and its environment on the expression of molecule chirality at the liquid-solid interface? Being a versatile building block and marker in STM experiments, oligo(*p*-phenylenevinylene) derivatives are used for exploring the effect of chemical structure and solvent on the degree of ordering, monolayer structure and expression of chirality at the liquid-solid interface.

4) The role solvent plays in self-assembly at the liquid-solid interface cannot be underestimated. Typically, the self-assembly process takes place at the interface between an achiral liquid and the achiral substrate. Under such conditions, achiral molecules very often form chiral patterns. Those surfaces are not globally chiral though as an equal amount of mirror-image domains is formed. A potentially promising approach to induce global chirality for achiral solutes is the use of chiral solvents.

5) A final objective is the enantioselective adsorption of only one enantiomer from a racemic mixture on an achiral substrate, by adding an appropriate resolving agent. If successful and if the process might be upscaled, it would complement the already known approaches and techniques to separate enantiomers.

1.9 References

1 Ozin, G. A. and Arsenault, A. C. *Naochemistry-A Chemical Approach to Nanomaterials* **2005**.

2 Whitesides, G. M. and Grzybowski, B. *Science* **2002**, *295*, 2418.

3 Jakubith, S.; Rotermund, H. H.; Engel, W.; von Oertzen, A. and Ertl, G. *Phys. Rev. Lett.* **1990***, 65*, 3013.

4 Hess, B. *Naturwissenschaften* 2000*, 87*, 199.

5 Desiraju, G. R. *Crystal Engineering: The Design of Organic Solids* (Elsevier) **1989**.

6 Isaacs, L.; Chin, D. N.; Bowden, N.; Xia, Y. and Whitesides, G. M. in *Supramolecular Technology* (WILEY-VCH), **1999**, 1.

7 Butt, H. –J.; Graf, K. And Kappl, M. *Physics and Chemistry of Interfaces* (Wiley-VCH), **2003**, 177.

8 Christmann K. *Introduction to Surface Physical Chemistry (Topics in Physical Chemistry)* (Springer-Verlag), **1991**.

9 Brandt, R. K.; Hughes, M. R.; Bourget, L. P.; Truszkowska, K. and Greenler, R. G. *Surf. Sci.* **1993**, *286*, 15.

10 Lyklema, J. F*undamentals of Interface and Colloid Science II: Solid-Liquid Interfaces* (Academic Press), **1991**.

11 Dabrowski, A. *Adv. Colloid Interface Sci.* **2001**, *93*, 135.

12 Henderson, M. A. *Surf. Sci. Rep.* **2002**, *46*, 1.

13 Nuzzo, R. G.; Zegarski, B. R. and Dubois, L. H. J. Am. Chem. Soc. 1987, 109, 733.

14 Jäckel, F. *Self-Assembly and Electronic Properties of Conjugated Molecules: Towards Mono-Molecular Electronics* (PhD thesis, Humboldt-Universität zu Berlin), **2005**, 20.

15 Samorí, P. and Rabe, J. P. *J. Phys. Condens. Matter* **2002**, *14*, 9955,

16 McNaught, A. D. and Wilkinson A. *Compendium of Chemical Terminology* **1997**.

17 Garrett, R. H. and Grisham. C. M. *Biochemistry* (Saunders College Publishing), **1995**.

18 Pérez-García, L. and Amabilino, D. B. *Chem. Soc. Rev.*, **2002**, *31*,

342.
19 Priego-Capote, F.; Ye, L.; Shakil, S.; Shamsi, S. A. and Nilsson, S. *Anal. Chem.* **2008**, *80*, 2881.
20 Dressler, D. H. and Mastai, Y. *Chirality* **2007**, *19*, 358.
21 Dressler, D. H. and Mastai, Y. *J. Colloid Interface Sci.* **2007**, *310*, 653.
22 Fernández, A. I.; Fraile, J. M.; García, J. I.; Herrerías, C. I.; Mayoral, J. A. and Salvatella, L. *Catal. Commun.* **2001**, *2*, 165.
23 Elemans, J. A. A. W.; De Cat, I.; Xu, H. and De Feyter, S. *Chem. Soc. Rev.* **2009**, *38*, 722.
24 Barlow, S. M. and Raval, R. *Surf. Sci. Rep.* **2003**, *50*, 201.
25 Ortega Lorenzo, M.; Haq, S.; Bertrams, T.; Murray, P.; Raval, R. and Baddeley, C. J. *J. Phys. Chem. B* **1999**, *103*, 10661.
26 Ortega Lorenzo, M.; Baddeley, C. J.; Muryn, C. and Raval, R. *Nature*, **2000**, *404*, 376.
27 Hooks, D. E.; Fritz, T. and Ward, M. D. *Adv. Mater.* **2001**, *13*, 227.
28 Tilley, R. J. D. Crystals and Crystal Structures (WILEY-VCH), 2006.
29 Ernst, K. –H.; Böhringer, M.; McFadden, C. F.; Hug, P.; Müller, U. and Ellerbeck, U. *Nanotechnology* **1999**, *10*, 355.
30 Ernst, K. –H.; Kuster, Y.; Fasel, R.; Müller, M. and Ellerbeck, U. *Chirality* **2001**, *13*, 675.
31 Fasel, R.; Parschau, M. and Ernst, K. –H. *Angew. Chem. Int. Ed.* **2003**, *42*, 5178.
32 Haq, S.; Liu, N.; Humblot, V.; Jansen, A. P. J. and Raval, R. *Nat. Chem.* **2009**, *1*, 409.
33 Fasel, R; Parschau, M. and Ernst, K. –H. *Nature* **2006**, *439*, 449.
34 Schöck, M.; Otero, R.; Stojkovic, S.; Hümmelink, F.; Gourdon, A.; Lægsgaard, E.; Stensgaard, I.; Joachim, C. and Besenbacher, F. *J. Phys. Chem. B* **2006**, *110*, 12835.
35 Weissbuch, I.; Berfeld, M.; Bouwman, W. G.; Kjaer, K.; Als-Nielsen, J.; Lahav, M. and Leiserowitz L. *J. Am. Chem. Soc.* **1997**, *119*, 933.
36 Nassoy, P.; Goldmann, M.; Bouloussa, O. and Rondelez, F. *Phys. Rev. Lett.* **1995**, *75*, 457.
37 Weissbuch, I.; Rubinstein, I.; Weygand, M. J.; Kjaer, K.; Leiserowitz, L. and Lahav, M. *Helv. Chim. Acta* **2003**, *86*, 3867.
38 Bernhardt, T. M.; Kaiser, B. and Rademann, K. *Surf. Sci.* **1998**, *408*, 86.
39 Ouseph, P. J. *Appl. Surf. Sci.* **2000**, 165. 38.
40 Kuwabara, M.; Ciarke, D. R. and Smith, D. A. *Appl. Phys. Lett.* **1990**, *56*, 2396.
41 Rong, Z. –Y. And Kuiper, P. Phys. Rev. B 1993, 48, 17427.

42 Plass, K. E.; Grzesiak, A. L. and Matzger, A. J. *Acc. Chem. Res.* **2007**, *40*, 287.

43 De Feyter, S.; Gesquière, A.; Meiners, C.; Sieffert, M.; Müllen, K. and De Schryver, F. C. *Langmuir* **1999**, *15*, 2817.

44 Yablon, D. G.; Guo, J. S.; Knapp, D.; Fang H. B. and Flynn, G. W. *J. Phys. Chem. B*, **2001**, *105*, 4313.

45 Giancarlo, L. C. and Flynn, G. W. *Acc. Chem. Res.* **2000,** *33*, 491.

46 Gesquière, A.; Jonkheijm, P.; Schenning, A. P. H. J.; Mena-Osteritz, E.; Bäuerle, P.; De Feyter, S.; De Schryver, F. C. and Meijer, E. W. *J. Mater. Chem.*, **2003**, *13*, 2164.

47 Gesquière, A.; Jonkheijm, P.; Hoeben, F. J. M.; Schenning, A. P. H. J.; De Feyter, S.; De Schryver, F. C. and Meijer, E. W. *Nano Lett.*, **2004**, *4*, 1175.

48 Jonkheijm, P.; Miura, A.; Zdanowska, M.; Hoeben, F. J. M.; De Feyter, S.; Schenning, A. P. H. J.; De Schryver, F. C. and Meijer, E. W. *Angew. Chem. Int. Ed.*, **2004**, *43*, 74.

49 Miura, A.; Jonkheijm, P.; De Feyter, S.; Schenning, A. P. H. J.; Meijer, E. W. and De Schryver, F. C. *Small*, **2005**, *1*, 131.

50 De Feyter, S. and De Schryver, F. C. *Chem. Soc. Rev.* **2003**, *32*, 139.

51 Zhang, X.; Chen, Q.; Deng, G. –J.; Fan, Q. –H. and Wan, L. –J. *J. Phys. Chem. C* **2009**, *113,* 16193.

52 De Feyter, S.; Gesquière, A.; De Schryver, F. C.;Meiners, C.; Sieffert, M. and Müllen, K. *Langmuir* **2000**, *16*, 9887.

53 Stevens, F.; Dyer, D. J. and Walba, D. M. *Angew. Chem. Int. Ed.* **1996**, *35*, 900–901.

54 De Feyter, S.; Gesquière, A.; Wurst, K.; Amabilino, D. B.; Veciana, J. and De Schryver, F. C. *Angew. Chem. Int. Ed.* **2001**, *40*, 3217.

55 Mamdouh, W.; Uji-i, H.; Gesquière, A.; De Feyter, S.; Amabilino, D. B.; Abdel-Mottaleb, M. M. S.; Veciana, J. and De Schryver, F. C. *Langmuir* **2004**, *20*, 9628.

56 Paci, I.; Szleifer, I. and Ratner, M. A. *J. Am. Chem. Soc.* **2007**, *129*, 3545.

57 Smith, D. P. E. *J. Vac. Sci. Tech. B* **1991**, *9*, 1119.

58 Wei, Y.; Kannappan, K.; Flynn, G. W. and Zimmt, M. B. *J. Am. Chem. Soc.* **2004**, *126*, 5318.

59 De Feyter, S.; Grim, P. C. M.; Rücker, M.; Vanoppen, P.; Meiners, C.; Sieffert, M.; Valiyaveettil, S.; Müllen, K. and De Schryver, F. C. *Angew. Chem. Int. Ed.* **1998**, *37*, 1223.

60 Qian, P.; Nanjo, H.; Yokoyama, T.; Suzuki, T. M.; Akasaka, K. and

Orhui, H. *Chem. Commun.* **2000**, 2021.
61 Lei, S.; Surin, M.; Tahara, K.; Adisoejoso, J.; Lazzaroni, R.; Tobe, Y. and De Feyter, S. *Nano Lett.* **2008**, *8*, 2541.
62 Li, C. –J.; Zeng, Q. –D.; Wang, C.; Wan, L. –J.; Xu, S. –L.; W. C. –R. and Bai, C. –L. *J. Phys. Chem. B* **2003**, *107*, 747.

Chapter 2: Tuning the Chirality at the Liquid-solid Interface by the Number of Stereogenic Centers

2.1 Introduction

Walba *et al*. were the first to report the ordering of chiral molecules and the expression of chirality on a surface observed by STM.[1,2] Since then, self-assembly of enantiopure molecules at the liquid-solid interface has been investigated by many researchers.[3,4,5,6] In most of these systems, the enantiomers form enantiomorphous monolayers, indicating the important effect of stereogenic centers on the molecular self-assembly. However, the effect that the number of stereogenic centers in molecules has on the amplification of chirality on a surface has never been reported. Many of these chiral molecules reported on contain only one stereogenic center. The lack of systematic studies on the effect of the number of chiral centers on the expression of chirality in molecular self-assembly motivated us investigate this aspect in detail.

The interesting optical and electronic properties of the nanostructures[7,8,9,10] that porphyrin molecules form make them popular building blocks.[11,12,13] Porphyrin derivatives **1**-**6** (Figure 2.1) that were investigated in this chapter were designed for several reasons. They contain amide groups as hydrogen-bonding functional unit and alkyl chains. Significant molecule-molecule and molecule-substrate interactions were anticipated, which support the self-assembly of these molecules, and subsequently also the STM imaging. The compounds differ from each other in the number and position of the stereogenic centers, creating a plateau to explore the role of multiple chiral centers in the molecular ordering at the liquid-solid interface.

2.2 Experimental

Scanning Tunneling Microscopy. All experiments were carried out at

room temperature. Scanning tunneling microscopy experiments were performed with a PicoSPM (Agilent) (using the constant-current mode). Pt/Ir STM tips were prepared by mechanical cutting from Pt/Ir wire (80%/20%, diameter 0.25 mm). Prior to imaging, the compounds under investigation were dissolved in 1-heptanol (Fluka). Saturated solutions were heated at 70 °C for 10 minutes, and a drop of this solution was applied on a freshly cleaved surface of highly oriented pyrolytic graphite (HOPG) (grade ZTB, Advanced Ceramics Inc., Cleveland, OH). Then, the STM tip was immersed into the solution. Prior to measuring, the sample was allowed to cool to room temperature. A bright (dark) contrast refers to a high (low) height.

Computational Methodology. Molecular mechanics and dynamics (MD) simulations were performed in the group of Prof. R. Lazzaroni (UMons) with the Tinker package[14] and the MM3 force field,[15] which has been reparameterized[16] to take into account the weak nonbonding interactions such as π-π stacking, CH-π interactions, and hydrogen bonds.

For the conformational analysis, MD simulations were run in the NVT canonical ensemble at 600 K using periodic boundary conditions (PBC). For the simulations on the HOPG surface, a periodic two-layer sheet of HOPG was built with dimensions 11.9 × 6.6 nm^2 in the plane of HOPG and 5.0 nm in the direction perpendicular to the HOPG surface. The HOPG structure was frozen during the simulation. A cutoff of 2.0 nm was applied for the van der Waals interactions. An MD simulation of 400 ps was first performed to equilibrate the system, which was then probed during the subsequent 400 ps (with frames recorded every 0.2 ps).

To study the self-assembly, the NVT canonical ensemble was used at 300 K. Eight porphyrin molecules were adsorbed on the HOPG bilayer in a box of 7.2 × 8.1 nm^2 in the plane of HOPG and 5.0 nm in the perpendicular direction to the plane of HOPG. A time of equilibration of 200 ps was used, and the lattice parameters were recorded during 200 ps (with steps of 0.2 ps).

In the case of the self-assembly without periodic boundary conditions, MD simulations were performed in the NVT canonical ensemble at 300 K and 16 molecules were laid down on the HOPG surface (with size 16.9×24.3nm^2). The system was first equilibrated by running a 100 ps MD

simulation, and the deviation of the porphyrin rows with respect to the HOPG reference axes <-1 1 0 0> was then investigated in a 100 ps long MD run (with steps of 0.1 ps).

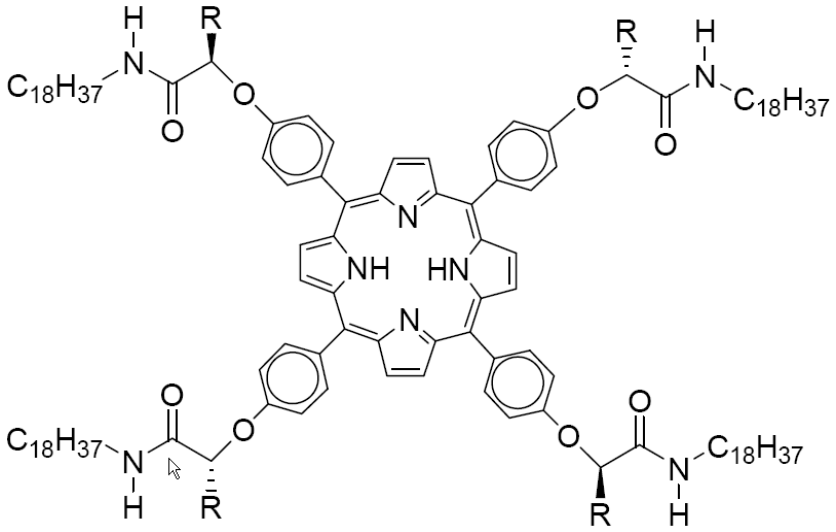

Abbreviations	Chiral substituents	Achiral substituents
(*R*,*R*,*R*,*R*)-**1**	5,10,15,20-R=CH_3	
(*R*,*R*,*R*)-**2**	5,10,15-R=CH_3	20-R=H
(*R*,*R*)-**3**	5,15-R=CH_3	10,20-R=H
(*R*,*R*)-**4**	5,10-R=CH_3	15,20-R=H
(S,S)-**4**	5,10-R=CH_3	15,20-R=H
(*R*)-**5**	5-R=CH_3	10,15,20-R=H
6		5,10,15,20-R=H

Figure 2.1 *Chemical structures of the compounds investigated in this chapter. Positions of stereogenic centers of each compound are listed in the table. The compounds were synthesized by Dr. P. Iavicoli in the group of Dr. D. Amabilino at ICMAB (Barcelona).*

2.3 Results and Discussion

Though porphyrin derivatives with different number of stereogenic centers are included in this chapter, only for **4** both enantiomers were investigated. The chiral nature of the monolayers formed by **4** is used as a reference for

the other compounds. Figure 2.2 shows a typical STM image of (*R,R*)-**4** and (*S,S*)-**4** physisorbed at the 1-heptanol - HOPG interface. Porphyrin cores appear as large bright spots packed in rows. The lines in darker regions running almost perpendicular to the porphyrin spots indicate alkyl chains. All alkyl chains are fully extended, adsorbed on the surface and interdigitated with those coming from adjacent porphyrin rows. The unit cell parameters are identical (within error) in both cases (as shown in Table 2.1). The chiral expression of both enantiomers in terms of the structure of the self-assembled monolayer can be recognized by the oblique shape of the unit cell. The monolayer structures of both enantiomers are identical, except for the fact that they are mirror images. Another approach to probe molecule-based two-dimensional chirality is by evaluating the orientation of a molecular row with respect to the HOPG (i.e. the angle (θ) between the normal of a main symmetry axis

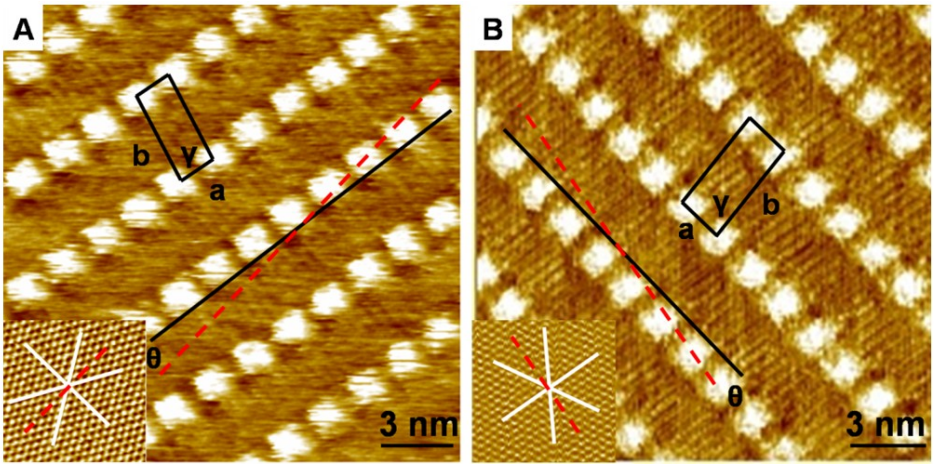

Figure 2.2 *STM images of both enantiomers of* ***4*** *physisorbed at the 1-heptanol - HOPG interface (I_{set} = 0.6 nA; V_{set} = -0.2 V). A) (R,R)-**4**. B) (S,S)-**4**. The insets show STM images of HOPG (not to scale) corresponding with sites underneath the monolayer (I_{set} = 0.6 nA; V_{set} = -0.001 V). The solid white lines in the insets indicate the direction of main symmetry axes of HOPG. The dashed red lines in both insets and main image are HOPG reference axes <-1 1 0 0>. Unit cells are indicated in black. The solid black lines run parallel to unit cell vector a. θ is the angle between HOPG reference axes <-1 1 0 0> and unit cell vector a. Each inset relates to the area underneath the monolayer.*

(*R,R*)-**4**, θ is +9±4° while for (*S,S*)-**4**, the angle θ is -8±2°. It shows that the orientation of molecular rows in monolayers of different enantiomers is reversed.

The monolayers of the other compounds are essentially isostructural (Figure 2.3). The only difference is the angle of the molecular propagation direction with respect to HOPG reference axes <-1 1 0 0>. Although the angles are always positive for *R*-enantiomers and negative for the

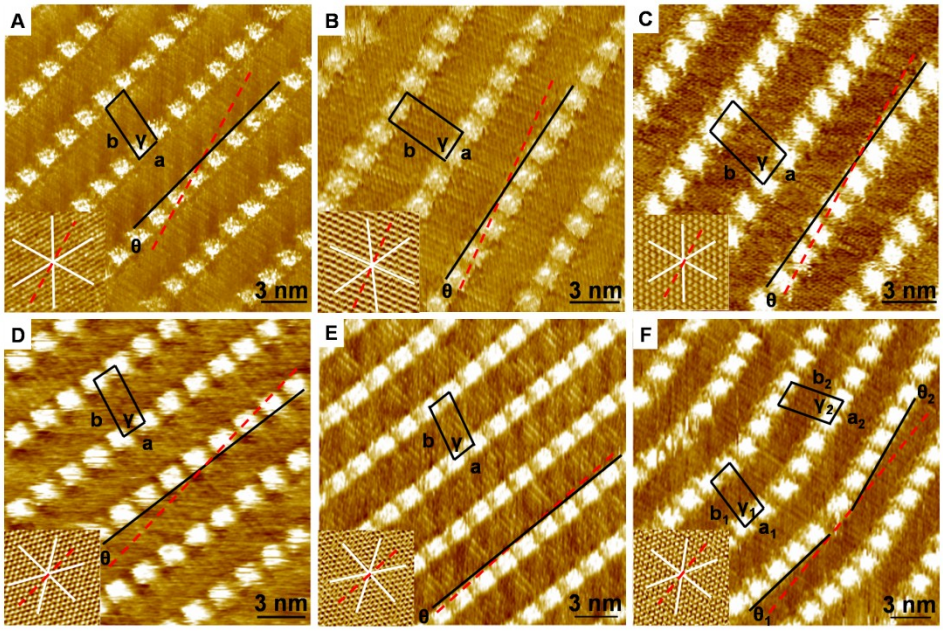

Figure 2.3 *STM images porphyrin derivatives* ***1-6*** *physisorbed at the 1-heptanol - HOPG interface (I_{set} = 0.6 nA; V_{set} = -0.2 V). The insets show STM images of HOPG (not to scale) corresponding with sites underneath the monolayer (I_{set} = 0.6 nA; V_{set} = -0.001 V). A) (R,R,R,R)-**1**. B) (R,R,R)-**2**. C) (R,R)-**3.** D) (R,R)-**4**. E) (R)-**5.** F) **6**. The insets show STM images of HOPG (not to scale) corresponding with sites underneath the monolayer. I_{set} = 0.6 nA; V_{set} = -0.001 V. The solid white lines in the insets indicate the direction of main symmetry axes of HOPG. The dashed red lines in all insets and main image are HOPG reference axes <-1 1 0 0>. Unit cells are indicated in black. The solid black lines are directions of unit cell parameter a. θ is the angle between HOPG reference axes <-1 1 0 0> and the direction of unit cell vector a. Each inset relates to the area underneath the monolayer.*

S-enantiomers, the absolute value decreases with the decreasing number of chiral centers in the molecules (Table 2.1). For instance, for (*R*)-**5**, the compound with only one stereogenic center, θ measures +7±4° while for (*R*,*R*,*R*,*R*)-**1**, the corresponding angle θ is +13±4°. The θ values for the compounds with two and three stereogenic centers are in between. Though the positions of both stereogenic centers in molecule **3** and **4** differ, STM results show that there are no obvious differences in their monolayer structure and registry with the HOPG substrate.

Table 2.1 *Unit cell parameters, angles of direction of unit cell vector a with respect to one of the HOPG reference axes <-1 1 0 0> (θ) and numbers of domains investigated of* ***1****-****6*** *at the 1-heptanol - HOPG interface. As achiral molecule* ***6*** *forms two types of domains with θ>0 and θ<0, values for these domains are calculated separately.*

	a (nm)	b (nm)	γ (°)	θ (°)	n
(*R*,*R*,*R*,*R*)-**1**	1.9±0.1	4.0±0.1	80±2	+13±4	29
(R,R,R)-**2**	2.0±0.1	4.2±0.3	80±5	+10±3	13
(R,R)-**3**	1.9±0.1	4.1±0.1	80±2	+7±2	21
(R,R)-**4**	1.9±0.1	4.0±0.1	81±4	+9±4	8
(R)-**5**	1.9±0.1	4.1±0.1	79±4	+7±4	19
6	2.0±0.2	4.1±0.2	79±4	+6±4	6
	1.9±0.1	4.3±0.3	75±3	-8±2	5
(S,S)-**4**	1.9±0.1	4.1±0.1	82±3	-8±2	9

An important finding is that for this class of molecules, molecular chirality is always expressed in the monolayer formation, regardless of the number of stereogenic centers. So even if only one of the arms carries a stereogenic center, exclusively enantiomorphous monolayer formation is observed.

In contrast to chiral molecules, the achiral molecule **6** forms both mirror-image type domains (θ>0 and θ<0). These domains share the same values for the unit cell parameters. Compared to other porphyrins with stereogenic centers, achiral molecules are more difficult to visualize because of the poor solubility in 1-heptanol at room temperature.

The STM data above show that porphyrin rows are always rotated

clockwise (CW) with respect to HOPG reference axes <-1 1 0 0> for the *R*-enantiomer and counterclockwise (CCW) for the *S*-enantiomer. Achiral molecules do not favor the formation of an achiral pattern, but they form mirror domains. This result clearly indicates that stereogenic centers strongly influence the molecule-substrate interactions.

The modeling and computation of the self-assembly of molecule **1** have been carried out by Lazzaroni *et al*.[17] For one single molecule, molecular dynamics (MD) simulations show the following (Figure 2.4):

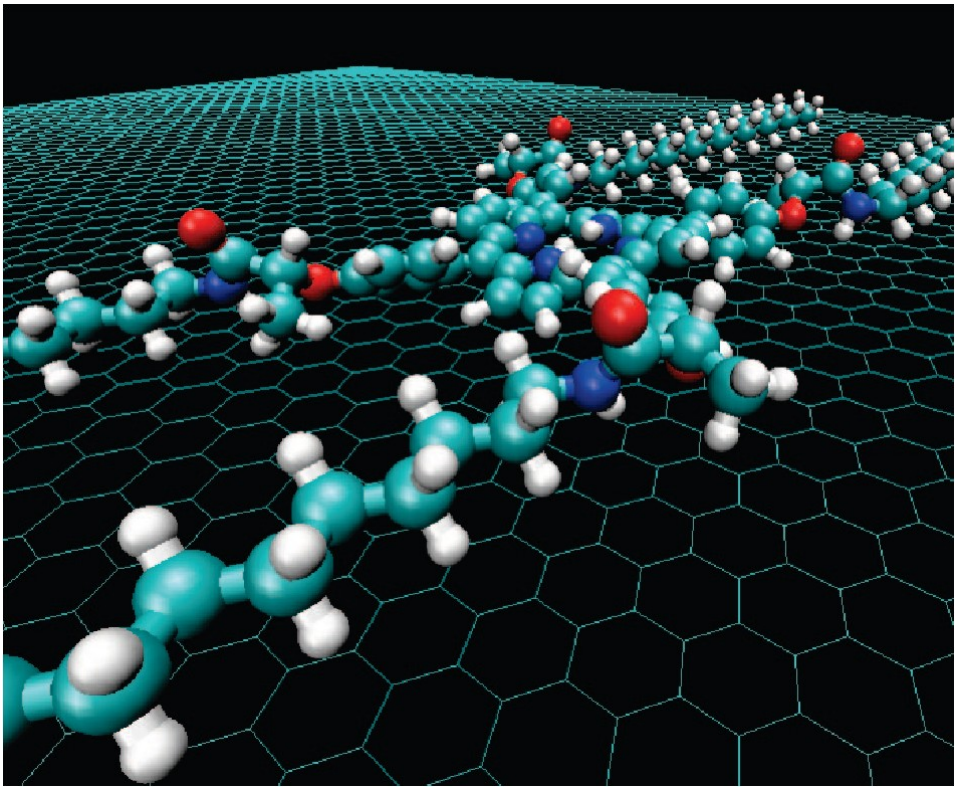

Figure 2.4 *Side view of the optimized structure of* ***1*** *adsorbed on HOPG. This image illustrates A) the orientation of the amide groups, with the C=O bonds pointing away from the surface (oxygen atoms in red), B) the orientation of the methyl group toward the surface.*[17]

1) The average height of the molecular core with respect to the HOPG surface is consistent with *π*-*π* interactions.
2) The hydrogen atom of the amide group points down to the surface

while the oxygen atom of the amide group points up to favor hydrogen bond formation with the solvent.

3) The methyl group which acts as stereogenic center also points toward the HOPG surface, so that CH-π interactions are established with the HOPG substrate. It's due to the presence of the stereogenic center close to the porphyrin core.
4) Alkyl side chains fully extend and align along one direction on the HOPG plane.

The structure of a single molecule **1** was then used as a starting point of a simulation which contained 16 molecules. Upon equilibration, the alkyl chains align perfectly along an axis parallel to one of the main HOPG axes. Unit cell parameters obtained after equilibration, a = 1.92 ± 0.12 nm, b = 4.20 ± 0.14 nm, γ = 87.4 ± 4.7°, are in good agreement with STM data. Such formation of the monolayer allows for perfect interdigitation between the alkyl chains of molecules in adjacent rows. The porphyrin rows are tilted with respect to HOPG reference axes <-1 1 0 0> by an angle of +12.2 ± 0.4°. The calculated value is quite close to the value obtained from STM data. In Figure 2.5A, the methyl groups of the stereogenic centers of (*R,R,R,R*)-**1** are pointing to the CCW direction with respect to the porphyrin core. As a matter of fact, once a molecule is lying on the surface, its neighbor is expected to shift in a direction perpendicular to HOPG reference axes <-1 1 0 0>, so that one of its methyl groups can accommodate in the empty space along the core of the neighboring molecule. This arrangement minimizes the free volume of the monolayer. This shifting leads to a deviation of the porphyrin row direction with respect to HOPG reference axes <-1 1 0 0>. A deviation in the opposite direction is expected for the other enantiomer (Figure 2.5B). The homochiral domain formed by enantiopure **1** indicates the transfer of chirality from the molecular level to the supramolecular level. The configuration of the stereogenic center sets the orientation of the methyl group, which in turn sets the deviation of the orientation of the porphyrin row with respect to HOPG reference axes <-1 1 0 0>.

Similar simulations were performed to study the deviation with respect to HOPG reference axes <-1 1 0 0> for rows of compounds **2** to **6**, by replacing sequentially all the methyl groups. The calculated values are reported in Table 2.2, together with the experimental data. The calculated

values for the deviation of rows of porphyrins with respect to the reference axis fit the experimental data quite well.

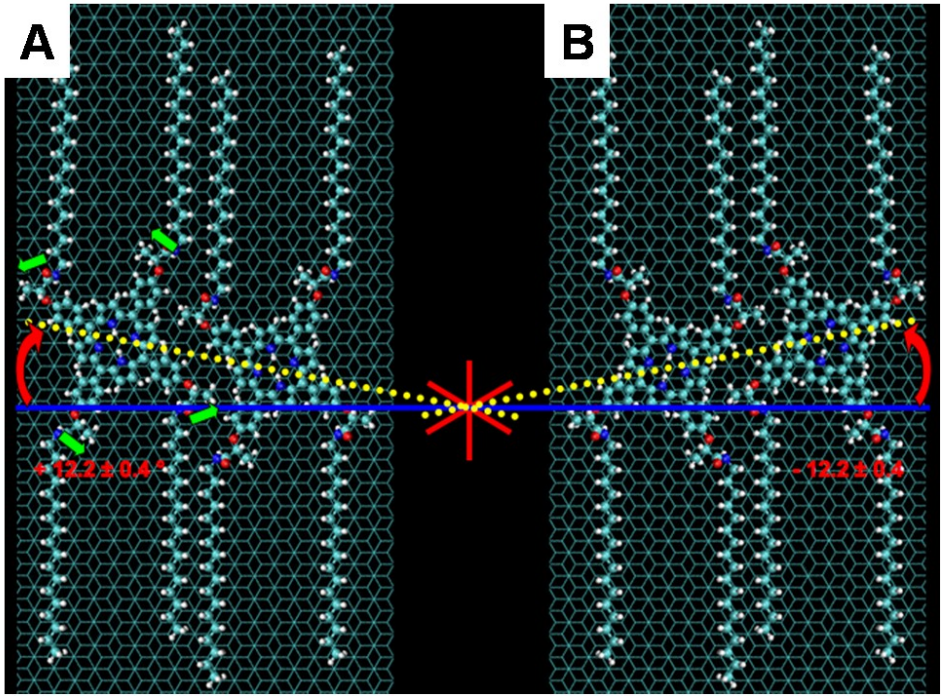

Figure 2.5 *Simulation of the self-assembly of* ***1*** *on HOPG. Top views of: A) (R,R,R,R)-****1*** *and B) (S,S,S,S)-****1*** *on the basal plane of HOPG. Red solid lines represent the main axes of HOPG. The HOPG reference axis is shown in blue solid line. Yellow dashed lines show the orientation of a porphyrin row with respect to one of the HOPG reference axes <1 1 0 0>. Green arrows are the orientations of the methyl groups of stereogenic centers with respect to the porphyrin core.*[17]

The calculated values for the deviation of rows of porphyrins with respect with the reference axis fit the experimental data quite well. Figure 2.6 shows the deviation angle with respect to the number of stereogenic centers. This clearly confirms that the number of chiral centers on these porphyrin compounds increases the deviation with respect to the HOPG reference axes, which is a measurement of the chirality at the nanoscale. The source of the increased angle appears to be the space required by the methyl group on the surface, which forces a displacement of one

porphyrin core with respect to the other.

Table 2.2 *Experimental and calculated deviation of the molecular row direction with respect to HOPG reference axes for monolayers of* ***1-6****. Only one mirror domain has been evaluated for compound* ***6****.*

	Measured Value (°)	Calculated Value (°)
(*R,R,R,R*)-**1**	13 ± 4	12.2 ± 0.4
(*R,R,R*)-**2**	10 ± 3	10.2 ± 0.2
(*R,R*)-**3**	7 ± 2	7.5 ± 0.2
(*R,R*)-**4**	9 ± 4	10.1 ± 0.3
(*R*)-**5**	7 ± 4	8.0 ± 0.3
6	6 ± 4	6.9 ± 0.4*

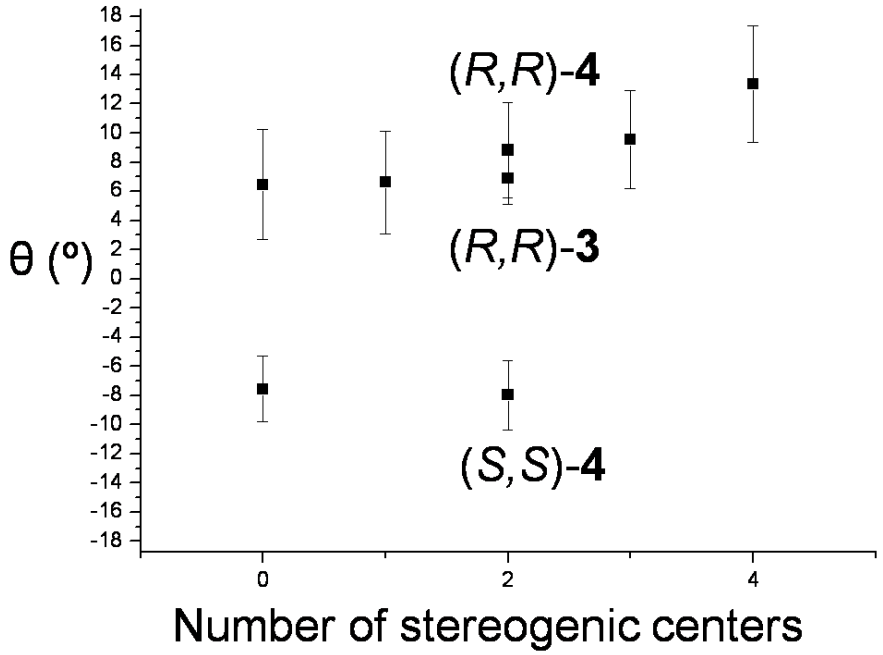

Figure 2.6 *Angle between the porphyrin rows along unit cell vector a and the HOPG reference axis, plotted as a function of the number of stereogenic centers in the porphyrins.*

2.4 Conclusions

Chiral and achiral porphyrin molecules were characterized by STM. The expression of molecular chirality can be identified by the angle between the molecular row direction and one of the HOPG reference axes <-1 1 0 0>. Molecules **1**-**6** containing different number of stereogenic centers form isostructural monolayers. The only difference is the degree of the deviation of the molecular row with respect to HOPG reference axes <-1 1 0 0>, indicating the importance of molecule-substrate interactions in directing the monolayer growth.

For this class of molecules, molecular chirality is always transferred to monolayer chirality, regardless of the number of stereogenic centers, which is quite remarkable given the size of the molecule. An important aspect is the fact that all alkyl chains (and stereogenic centers) are adsorbed on HOPG upon monolayer formation. Any out of plane orientation of the chiral arm could be detrimental for the transfer of molecular chirality into monolayer chirality.

MD simulations show that due to the presence of the stereogenic center close to the porphyrin core, methyl groups attached to the stereogenic centers on side chains are oriented toward the HOPG surface for stabilizing the CH-π interactions and rotate either CW or CCW with respect to porphyrin cores. To maximize the monolayer density, molecular cores are slightly shifted with respect to their neighbors, which lead to a deviation of the molecular row and the HOPG reference axes <-1 1 0 0>. The deviation is tuned by the number of stereogenic centers of the molecules. The amplification of the molecular chirality and the chiral expression with respect to the number of stereogenic centers were proven by both experimental and theoretical data.

2.5 References

1 Stevens, F.; Dyer, D. J. and Walba, D. M. *Angew. Chem. Int. Ed.*, **1996**, *35*, 900.

2 Walba, D. M.; Stevens, F.; Clark, N. A. and Parks, D. C. Acc. Chem. *Res.*, **1996**, *29*, 591.
3 De Feyter, S.; Gesquière, A.; Meiners, C.; Sieffert, M.; Müllen, K. and De Schryver, F. C. *Langmuir*, **1999**, *15*, 2817.
4 Yablon, D. G.; Guo, J. S.; Knapp, D.; Fang, H. B. and Flynn, G. W. *J. Phys. Chem. B*, **2001**, *105*, 4313.
5 Qian, P.; Nanjo, H.; Yokoyama, T. and Suzuki, T. M. *Chem. Lett.*, **1998**, *11*, 1133.
6 Gesquière, A.; Jonkheijm, P.; Schenning, A. P. H. J.; Mena-Osteritz, E.; Bäuerle, P.; De Feyter, S.; De Schryver, F. C. and Meijer, E. W. *J. Mater. Chem.*, **2003**, *13*, 2164.
7 Fuhrhop, J.-H.; Binding, U. and Siggel, U. *J. Am. Chem. Soc*. **1993**, *115*, 11036.
8 Schwab, A. D.; Smith, D. E.; Rich, C. S.; Young, E. R.; Smith, W. F. and De Paula, J. C. *J. Phys. Chem. B* **2003**, *107*, 11339.
9 Rotomskis, R.; Augulis, R.; Snitka, V.; Valiokas, R. and Liedberg, B. *J. Phys. Chem. B* **2004**, *108,* 1833.
10 Koepf, M.; Wytko, J. A.; Bucher, J. P. and Weiss J. *J. Am. Chem. Soc*. **2008**, *130*, 9994.
11 Marks, T. J. *Science* **1985**, *227*, 881.
12 Chen, Y. C.; Lee, M. W.; Li, L. L. and Lin, K. J. *J. Macr. Science B Physics* **2008**, *47*, 955.
13 Aziz, M. S. *Solid State Electronics* **2008**, *52*, 1145.
14 http://dasher.wustl.edu/tinker/.
15 Allinger, N. L.; Yuh, Y. H.; Lii, J. H. *J. Am. Chem. Soc.* **1989**, *111*, 8551.
16 Ma, B. Y.; Lii, J. H.; Allinger, N. L. J. *Comput. Chem.* **2000**, *21*, 813.
17 Linares, M.; Iavicoli, P.; Psychogyiopoulou, K.; Beljonne, D.; De Feyter, S.; Amabilino, D. B. and Lazzaroni, R. *Langmuir* **2008**, *24*, 9566.

Chapter 3: A Multivalent Hexapod: Chiral Expression and Conformational Dynamics of Six-Legged Molecules in Self-Assembled Monolayers at a Liquid-solid Interface

3.1 Introduction

In chapter 2, the self-assembly of enantiopure porphyrin molecules was investigated at the liquid-solid interface and the influence of the number of stereogenic centers on the expression of molecular chirality at the liquid-solid interface was discussed. However, enantiopure molecules do not necessarily form highly ordered homochiral monolayers.[1,2] In some cases, due to the chemical structure of the building blocks, especially for some "big" molecules, physisorption does (locally) lead to defects and disordered patterns. Monolayer defects may reveal useful information on certain aspects of the self-assembly process (i.e. conformational / rotational / translational dynamics) and the expression of chirality within the monolayers formed. With STM, molecular motions such as translational,[3,4,5,6] rotational,[7,8,9,10] and conformational dynamics[11,12,13,14] can be probed and traced, and this has been amply demonstrated under ultrahigh vacuum conditions.

In this chapter, the monolayer formation of a six-legged oligo(*p*-phenylene vinylene) (OPV)-substituted hexaarylbenzene **1** (Figure 3.1) that acts as molecular "hexapod" at the 1-phenyloctane - HOPG interface is investigated. This compound self-assembles in solution into perfect 1D fibers using a nucleation-growth mechanism.[15] The chirality of the 24 stereogenic centers is expressed at the supramolecular level, indicating the cooperative nature of the packing. Moreover, at the solid-liquid interface, a 2D lattice is formed, expressing molecular chirality at the supramolecular level. However, not all molecules were found to be perfectly aligned and a number of defects were observed. This study

reveals a multitude of dynamical events taking place in the monolayer (formation), at the liquid-solid interface.[16] The dynamics of **1** on the substrate is relatively slow on the STM time scale and can be followed in time. As a result, it's possible to probe the orientational, conformational, and translational behavior at the single-molecule level, at the solid-liquid interface, at room temperature. These slow dynamics at the liquid-solid interface are rather unique and the result of multivalent interactions involving six OPV legs.

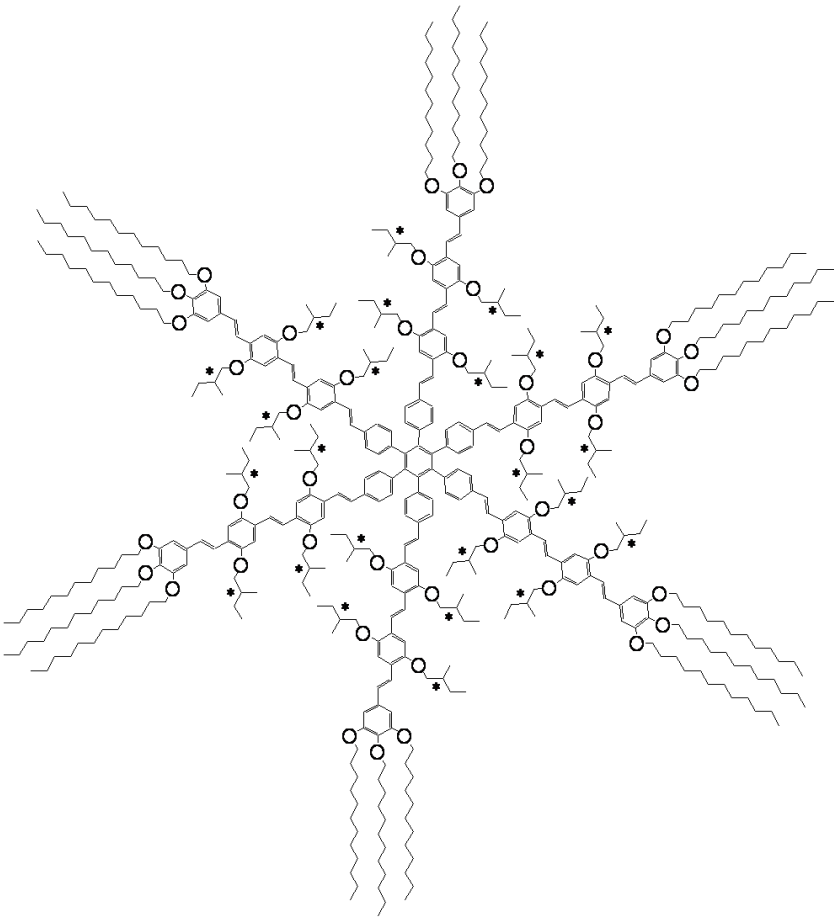

Figure 3.1 *Chemical structure of the six-legged oligo(p-phenylene vinylene)-substituted hexaarylbenzene* ***1****. The compounds were synthesized by Dr. Ž. Tomović in the group of Dr. A. P. H. J. Schenning at Eindhoven University of Technology (Eindhoven).*[15]

3.2 Experimental

Scanning Tunneling Microscopy. In this chapter, besides a PicoSPM (Agilent) (using the constant-current mode), a Topometrix Discoverer (using the constant-height mode) was also used for performing STM experiments. Both mechanical cut and electrochemical etched (in a 2 M KOH/6 M NaCN aqueous solution) tips were used in the measurements. The compounds under investigation were dissolved in 1-phenyloctane (Aldrich) at a concentration of approximately 10^{-4} M. The rest details refer to the experimental part in chapter 2.

Computational Methodology. Please refer to experimental part in chapter 2.

3.3 Results and Discussion

By self-assembly the spontaneous formation of a monolayer sets in. STM images recorded of **1** at the 1-phenyloctane - HOPG interface are shown in Figure 3.2, and the main structural characteristics of the molecules can easily be appreciated. The OPV units appear bright in the STM image, while the orientation of the alkyl chains is hardly visible. Those bright features typically reflect the anticipated star shape of the molecules. Space considerations and the few images where the alkyl chains can be identified point out that only two out of three alkyl chains are adsorbed on the surface. These are basically aligned along one of the main symmetry axes of HOPG. Also the unit cell vectors are almost aligned along the main symmetry axes of HOPG. Unit cell parameters are indicated in Table 3.1. The STM images are two-dimensionally chiral, and the molecules appear as stars, which belong to the crystallographic plane point group 6mm (the combination of a mirror with a hexad). Neglecting the intrinsic chirality of the molecules, these stars can only order into an achiral pattern if their “arms” are oriented parallel or perpendicular to the unit cell vectors. This is, however, not the case, and this has an effect on the relative distance between parallel oriented OPV-units of adjacent

molecules. Consider, for instance, the orientation of the long black and short white lines that connect the terminal phenyl groups of similarly oriented OPV units along unit cell vector b in Figure 3.2. Note that these marker lines are not in line. Their relative orientation can be described as short white and black long: **1** self-assembles into a chiral pattern in accordance with the plane group p6. Mirror plane images are never observed for a given enantiomer.

Table 3.1 *Structural parameters of the packing. Unit cell parameters (a, b, γ), angle of unit cell vector with respect to the main symmetry axis of HOPG (θ), and total number of domains (n) analyzed.*

	a (nm)	b (nm)	γ (°)	θ (°)	n
S-**1**	5.56 ± 0.07	5.56 ± 0.07	61 ± 2	+1 ± 2	5
R-**1**	5.67 ± 0.13	5.57 ± 0.13	62 ± 2	-4 ± 2	4

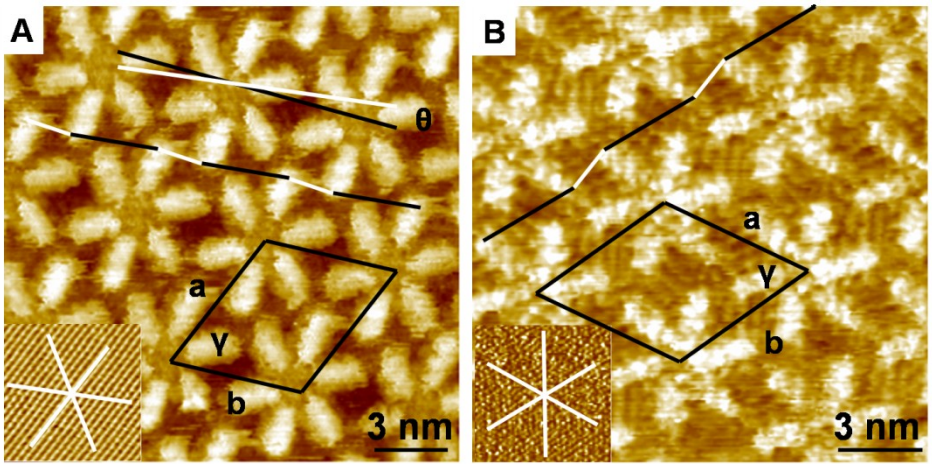

Figure 3.2 *STM images of **1** physisorbed at the 1-phenyloctane - HOPG interface. (A) S-**1** (I_{set} = 0.05 nA; V_{set} = -0.8 V); (B) R-**1** (I_{set} = 0.2 nA; V_{set} = -0.8 V). The insets show STM images of HOPG (not to scale) corresponding with sites underneath the monolayer (I_{set} = 0.2 nA; V_{set} = -0.001 V). The unit cell is indicated in black. The solid white lines coincide with the direction of the main symmetry axes of HOPG. The short white and long black lines connect the terminal phenyl groups of similarly oriented OPV units along unit cell vector b.*

Depositing a mixture of both eantiomers of **1** leads to a conglomerate: domains formed by *S*-**1** and *R*-**1** can be clearly distinguished (Figure 3.3). Due to the symmetry aspects of the self-assembly, co-adsorption of both enantiomers in the same domain would probably have led to an increase in the system's energy.

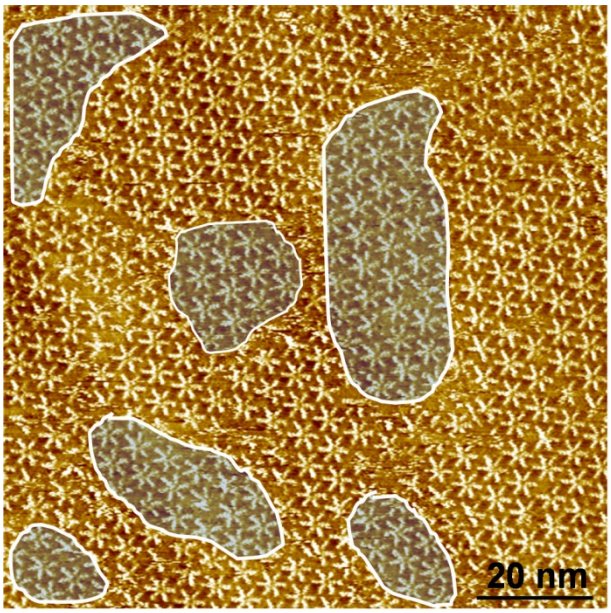

Figure 3.3 *STM image of a mixture of S-**1** and R-**1** physisorbed at the 1-phenyloctane - HOPG interface (I_{set} = 0.2 nA; V_{set} = -0.8 V). R-**1** domains are marked.*

Conformational Flexibility: Structurally defect-free 2D crystalline domains covering large areas are not observed though. Often "disordered" domains are observed in the midst of or between these crystalline domains. A group of molecules was identified as belonging to a disordered domain if the centers of the molecules are not on top of 2D crystalline lattice points within a given area or if the molecules have a different orientation than those in the crystalline matrix. For the statistical analysis, images with the size of about 100×100 nm were recorded and analysed, giving in total 20348 (*S*-**1**), 9642 (*R*-**1**) and 13169 (mixture of *S*-**1** and *R*-**1**) molecules. An example of the way the images were analysed is shown in Figure 3.4.

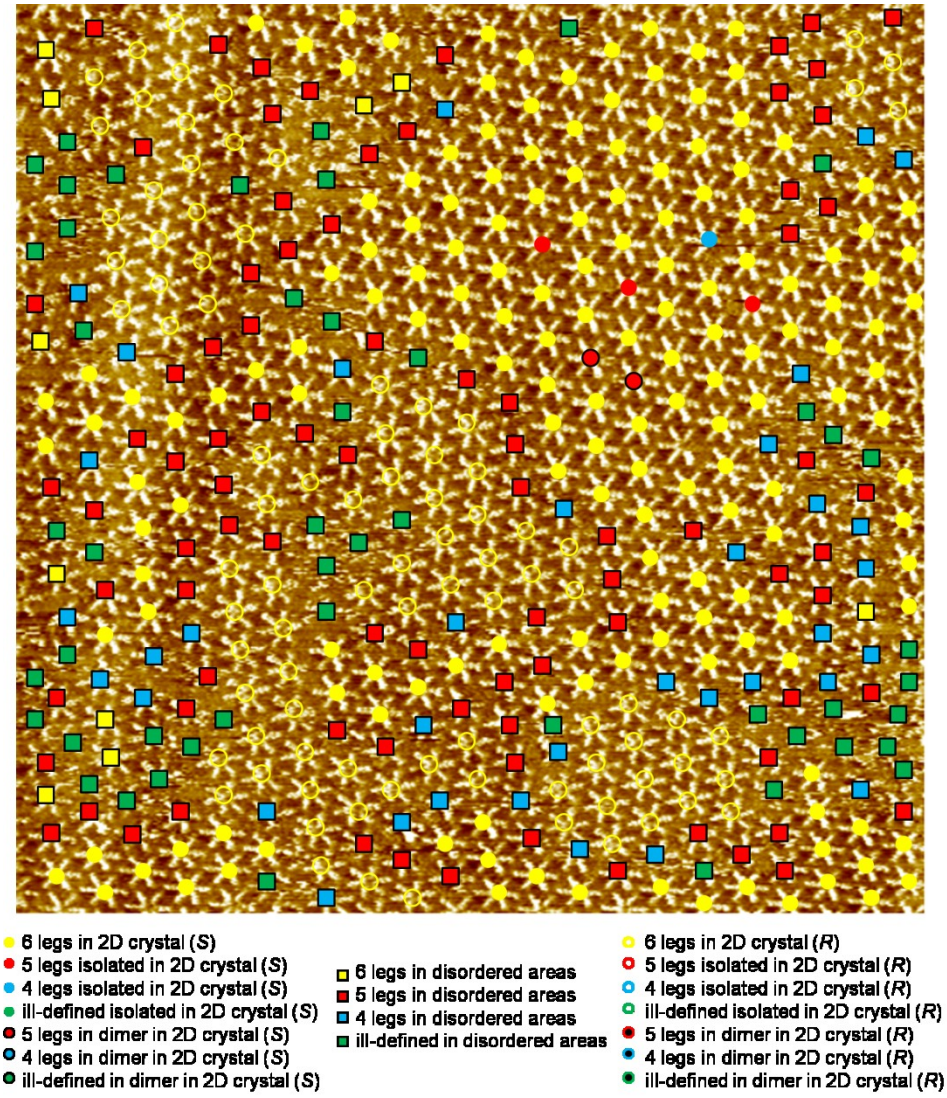

Figure 3.4 *Color-coded large-scale STM images (103.8×103.8 nm^2). The center of a molecule is indicated by a disk (ordered S-domain), a circle (ordered R-domain) or square (disordered area). Disks with black edge indicate dimer defects in ordered S-domains while disks without black edges indicate isolated defects in ordered S-domains. Circles with black center indicate dimer defects in ordered R-domains while circles without black center indicate isolated defects. The color refers to the number of visible OPV legs: yellow (6); red (5); blue (4); green (not defined).*

In enantiopure systems, about 2/3 of these molecules self-assemble into a regularly ordered matrix; 1/3 of the molecules are adsorbed in disordered domains.

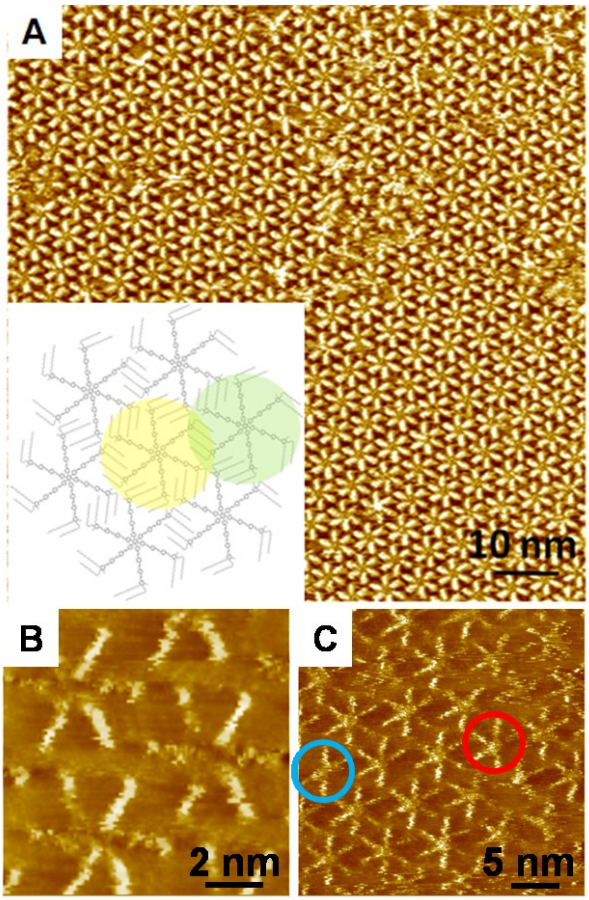

Figure 3.5 *STM images of **1** physisorbed at the 1-phenyloctane - HOPG interface. (A) Large domain (I_{set} = 0.05 nA, V_{set} = 0.8 V). Inset shows the model reflecting the ordering of the molecules in a 2D crystal. Two alkyl chains per OPV leg are adsorbed. The third one, which is omitted in the model, is most likely solvated. For clarity, the chiral 2-methylbutoxy groups are not shown. The intersection of the two colored disks coincides with the area of interaction between these two adjacent hexapods. (B) Magnified image showing the expected star shape of the molecules (I_{set} = 0.60 nA, V_{set} = 0.31 V). (C) In addition to the six-legged molecules, molecules are visible with apparently only five (red circle) or even four legs (blue circle) (I_{set} = 0.60 nA, V_{set} = 0.31 V).*[16]

Some of these molecules appear to have only five or four legs, as illustrated in Figure 3.5C. Strikingly, the situation in the so-called ordered and disordered domains is completely different. In ordered areas, most of the molecules appear as hexapods (*S*-**1**: 96.0%; *R*-**1**: 93.9%); 3.3% of the *S*-**1** (*R*-**1**: 4.8%) molecules appear with five legs and only 0.7% *S*-**1** (*R*-**1**: 0.9%) with four legs. In contrast, this ratio differs drastically in disordered domains. First note that a significant fraction (about 1/3) of the molecules in the so-called disordered domains is badly resolved, and it is not possible to identify their appearance (six or five or four legs) with certainty. However, of the remaining 3803 *S*-**1** (*R*-**1**: 1758) molecules, only 23% *S*-**1** (*R*-**1**: 20%) appear as hexapods, while the majority of the molecules (*S*-**1**: 57%; *R*-**1**: 61%) appear with five legs and 20% *S*-**1** (*R*-**1**: 18%) in disordered domains show four legs (detailed statistic results are shown in Table 3.2).

For the mixture of both enantiomers, the enantiomers self-assemble in separate domains. At boundaries between *S*- an *R*- domains, an increased number of defects is observed due to the packing incommensurability.

3.3% (635 out of 14033) of the *S*-**1** molecules adsorbed in an ordered "crystalline" hexagonal lattice are defects, i.e. they appear with five or four legs. Based on this experimental observation, in an ideal situation without edge defects (Figure 3.6), the possibility to observe a defect is

$$\eta = \frac{N_{defect}}{N_{total}}$$

where N_{defect} is the number of defects and N_{total} is the total number of sites. Each defect (shown as solid black circle) is surrounded by 6 equivalent sites. If one of these sites is also a defect, a dimer defect is formed (shown as dashed black circle). So the possibility to observe a dimer defect is

$$\eta_{dimer} = \frac{N_{defect}}{N_{total}} \times 6 \times \frac{N_{defect}}{N_{total}} = 6 \times \left(\frac{N_{defect}}{N_{total}}\right)^2$$

In this case, $N_{defect} = 635$, $N_{total} = 14033$

The possibility of a trimer defect can be ignored.

The calculation predicts that about 27% of these defects would appear in dimers. In contrast, experimentally, a significantly higher population of molecules in dimers is observed (S-**1** & *R*-**1**: 40%), indicating that a defect

promotes the presence of another one in its periphery.

Table 3.2 *Statistic results of the appearance of S-**1**, R-**1** and the mixture of both enantiomers.*

		S-**1**	*R*-**1**	*S*-**1** & *R*-**1**
2D crystals	6 legs	13398 (95.5%)	6739 (93.9%)	6982 (97.5%)
	5 legs isolated	289 (2.1%)	206 (2.9%)	94 (1.3%)
	4 legs isolated	51 (0.4%)	38 (0.5%)	20 (0.3%)
	ill-defined isolated	39 (0.3%)	19 (0.3%)	6 (0.1%)
	5 legs in dimer	179 (1.3%)	137 (1.9%)	45 (0.6%)
	4 legs in dimer	46 (0.3%)	28 (0.4%)	7 (0.1%)
	ill-defined in dimer	31 (0.2%)	11 (0.2%)	6 (0.1%)
Disordered areas	6 legs	890 (14.1%)	360 (14.6%)	385 (6.4%)
	5 legs	2176 (34.5%)	1081 (43.9%)	2559 (42.6%)
	4 legs	737 (11.7%)	317 (12.9%)	915 (15.2%)
	ill-defined	2512 (39.8%)	706 (28.7%)	2150 (35.8%)
Total images		60	22	30
Total molecules		20348	9642	13169
Order : disorder ratio		2.2 : 1	2.9 : 1	1.2 :1
5 legs : 4 legs ratio in ordered domain		4.8 : 1	5.2 : 1	5.1 : 1
Isolated : dimer ratio in ordered domain		1.5 : 1	1.5 : 1	2.1 : 1

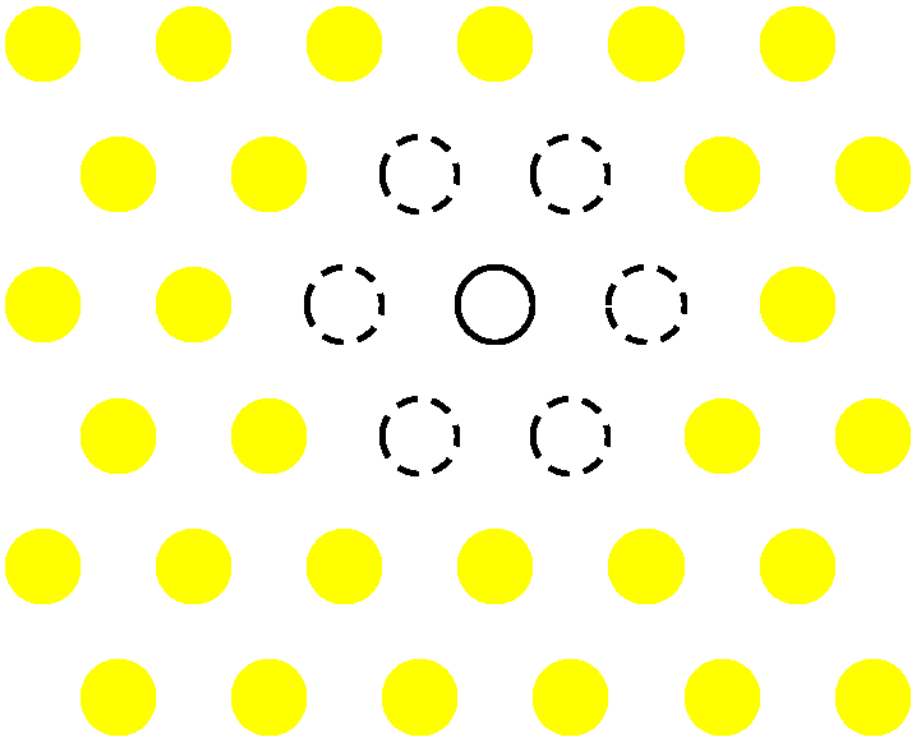

Figure 3.6 *Model of ideal molecular packing in 2D crystals.*[16]

In addition to the fact that synthesis and purification were carried out according to the highest possible standards making use of recycling GPC, the appearance of the molecules changed during the STM acquisition, that is, as far as the number of visible legs and their orientation is concerned. This was interpreted as definite proof that the "defective" molecules are not impurities.

Conformational Dynamics: Certain molecules show indeed some interesting changes in appearance. Quite often, the number of "legs" changes: legs disappear and reappear. Figure 3.7A shows a series of images zooming in on the different appearances of one *S*-**1** molecule as a function of time (molecule A).

In frame A3, the molecule only shows five legs; the leg at 4 o'clock is missing, while in frame A4, all legs are visible. The image in frame A13 is blurred and marks the transition from six visible legs (frame A12) to five visible legs (frame A14). In frame A15, all six legs appear again. Another example of a similar transition is shown in Figure 3.7B. This *S*-**1** molecule

starts off with four visible legs (frame B3) and evolves into a situation where five legs are visible (from frame B5 on).

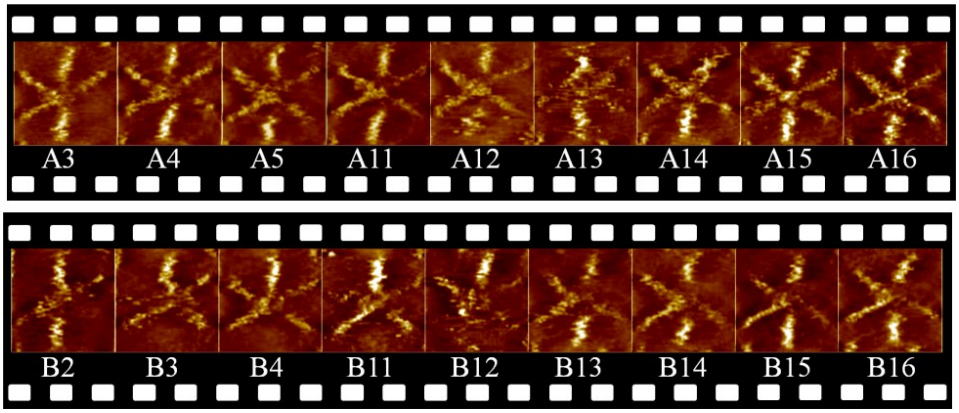

Figure 3.7 *Sequence of STM images zooming in on one S-**1** molecule. Top: molecule A. Bottom: molecule B. The frame numbers are indicated below each image. The time difference between two consecutive frames (e.g., An→A(n + 1)) is about 14 s.*[16]

Not only does the number of visible legs change but their orientation changes in time. Basically, two types of orientational changes can be observed. A first type involves a transition where the desorption-adsorption of legs results in an apparent rotation of the molecules. For instance, in Figure 3.8A, at the position of the red arrow, a leg appears, while at the position of the green arrow, a leg disappears. Overall, the molecule appears to be rotated. This rotation hypothesis is unlikely as it involves the desorption and adsorption of all legs. Note that the position of the other legs has not changed.

In addition, these molecules are not rigid as far as the position of the legs is concerned. The molecule in Figure 3.8B undergoes a transition from five adsorbed legs to six adsorbed legs. Note, however, that the "readsorption" of the sixth leg follows the reorientation of the leg indicated in green: originally at 1 o'clock, it appears subsequently at the 12 o'clock position. Also more subtle orientational changes can be observed (Figure 3.8C, *S*-**1**). The legs indicated by the red arrows slightly change their orientation from frame to frame, though the overall orientation of the molecule remains unchanged. The effect is that the angle between the legs is not always 60° but can change considerably.

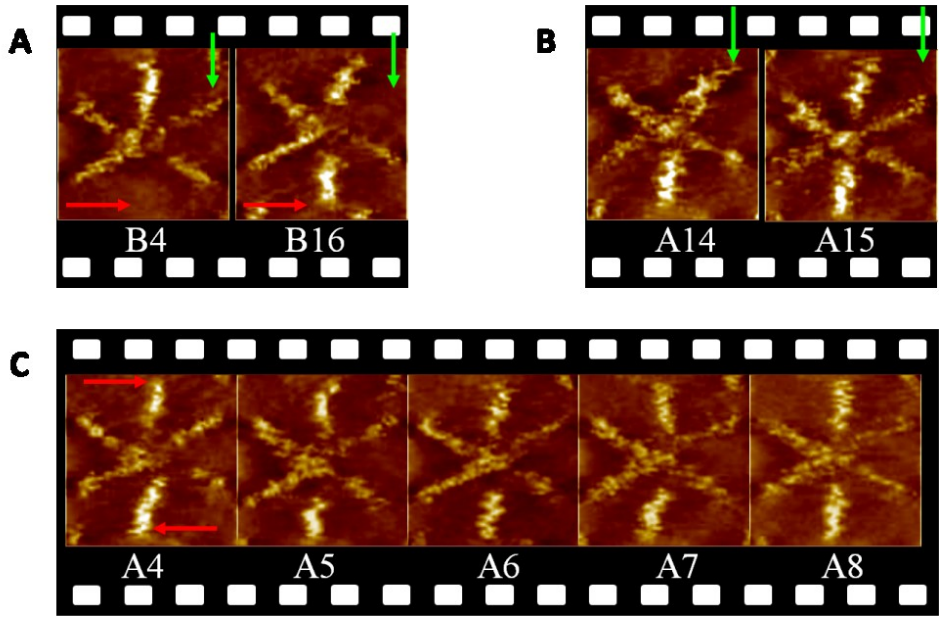

Figure 3.8 *Sequence of STM images zooming in on one S-**1** molecule highlighting different dynamics. (A) The molecule appears to rotate. At the position of the red arrow, a leg appears, while at the position of the green arrow, a leg disappears. (B) Readsorption of a leg, affecting the orientation of the leg originally at 1 o'clock. (C) The legs indicated by the red arrows slightly change their orientation from frame to frame, though the overall orientation of the molecule remains unchanged. The frame numbers are indicated below each image.*[16]

These data strongly suggest that the origin of the "defects" is the desorption/readsorption or reorientation of legs. More evidence will follow for the fact that the disappearance and reappearance of the bright legs are not merely due to differences in the tunneling efficiency as the result of orientational changes that do not involve desorption of the legs.
With the disappearance and reappearance events of the legs being identified as the desorption and readsorption of these legs, respectively, one can now estimate the differences in energy between a hexapod and molecules with five or four adsorbed legs in 2D crystalline lattices based on a Boltzmann distribution:
The fractional number of particles N_i / N occupying a set of states i with energy E_i is

$$\frac{N_i}{N} = e^{-\frac{E_i}{k_B T}}$$

where k_B is the Boltzmann constant ($k_B = 8.617 \times 10^{-5}$ eV/K, T is temperature, N is the total number of particles:

$$N = \sum_i N_i$$

The energy difference between two different states is:

$$\Delta E = k_B T \ln \frac{N_A}{N_B}$$

Therefore, N_{six} is the number of sites occupied by molecules with 6 visible legs. N_{five} is the number of sites occupied by molecules with 5 visible legs. N_{four} is the number of sites occupied by molecules with 4 visible legs.

The energy difference between a molecule with 6 legs adsorbed and 5 legs adsorbed in *S*-**1** domains is:

$$\Delta E_{five-six} = k_B T \ln \frac{N_{six}}{N_{five}} = 0.097 \text{ eV}$$

The energy difference between a molecule with 6 legs adsorbed and 4 legs adsorbed in S-1 domains is:

$$\Delta E_{four} = k_B T \ln \frac{N_{six}}{N_{four}} = 0.14 \text{ eV}$$

These values are much lower than one could expect based on the adsorption energy of an alkyl chain on HOPG, which is about 0.07 eV/ CH_2. Therefore, solvation of the OPV unit and alkyl chains must be crucial to support the desorption process of individual legs.

In addition, the larger than statistically predicted number of dimer defects in the 2D crystalline lattice indicates that molecules mutually interact and that desorption of a leg in a hexapod promotes the desorption of a leg in a hexapod next to it. Some clue to the origin of this behavior comes from a detailed analysis of the nature of these dimers. The relation between two adjacent *S*-**1** molecules is shown in Figure 3.9. Alkyl chains at the end of each leg are always oriented clockwise. In each molecule there is one leg desorbed. There are 36 possible combinations but pairs of equal numbers (e.g. 1-6' equals 6-1') are identical which leaves us with 21 unique combinations (1-1', 1-2', 1-3', 1-4', 1-5', 1-6', 2-2', 2-3', 2-4', 2-5', 2-6', 3-3', 3-4', 3-5', 3-6', 4-4', 4-5', 4-6', 5-5', 5-6', 6-6'). On statistical grounds, the probability for the 1-1' combination (and any of the x-x' combinations) is

(100/36) = 2.78%, while 5.56% for the other combinations. However, this more favored combination where both parallel OPV units of which the alkyl chains in principle could interact via van der Waals interactions was observed more frequently (17% of dimer defects). The desorption of a leg has therefore a direct impact on the stability of the OPV leg in the adjacent hexapod it is interacting with and favors its desorption.

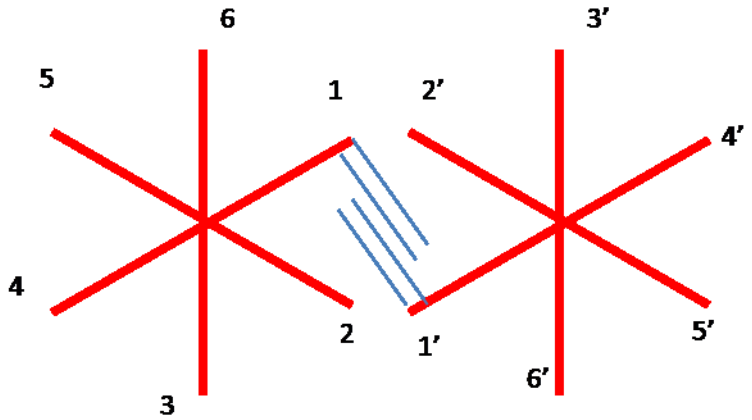

Figure 3.9 *Model of two adjacent S-**1** molecules.*[16]

Atomistic simulations based on force-field techniques have been used to model the dynamics of a single *S*-**1** molecule on a HOPG surface. All the simulations were carried out with the molecular modeling package TINKER 4.2 using the MM3 (2000) force field. This force field has been recently parameterized to give an accurate description of weak intermolecular interactions, which are likely to play an important role in physisorption and self-assembly phenomena. The HOPG surface is made of two frozen layers of HOPG. Experimentally, the lateral mobility of the legs is observed together with the "disappearance" of individual legs, which based on the experimental data is attributed to desorption.

The molecule is characterized by an extended π-delocalization and changes in the molecular geometry, such as tilting of the phenylene rings or distortion of a leg, can reduce the extent of conjugation. The first step consists in estimating the molecular geometry when one leg is in the solvent phase, in order to study the readsorption process. For that purpose, a *S*-**1** molecule having already one leg pointing in the solvent

phase was modeled and let the molecule relax (Figure 3.10). In this model, the environment is treated explicitly by introducing solvent molecules in the system. A high temperature molecular dynamic (MD) at 650K, in the NVT ensemble, has been then performed to investigate the behavior of the desorbed leg, by recording the evolution of the height of atoms within that leg with respect to the surface during the last 100ps of the MD run.

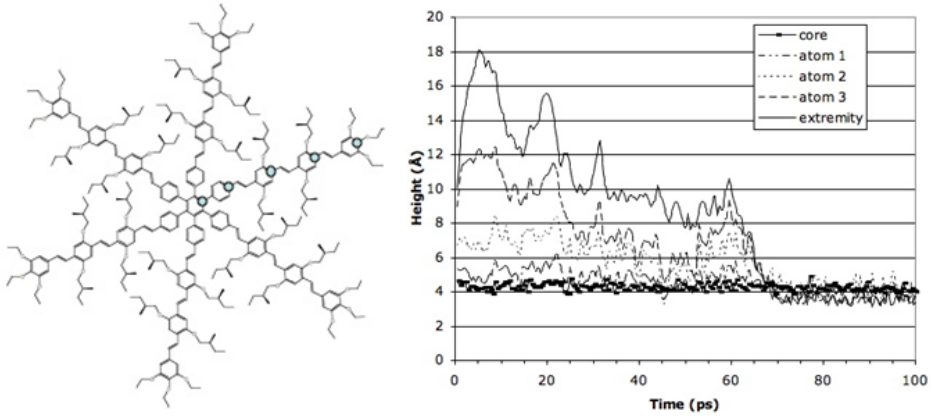

Figure 3.10 *Left: S-**1** molecule with alkyl chains replaced by ethyl groups. The circles indicate the carbon atoms used to sample the sorption process of the arm pointing into the solvent phase. These atoms are called, from the core outwards: core, atom 1, atom 2, atom 3, extremity. Right: Evolution of the height of the atoms of the desorbed arm during the simulation. The height for an atom is defined as its vertical distance with respect to the upper HOPG layer.*[16]

As expected, the phenyl rings attached to the central benzene ring are rotated to form a kind of chiral propeller[17] and make the adsorption of the central benzene to the HOPG difficult. The atoms of and at the next phenyl groups are not significantly out of the plane of the molecule at the surface, while the largest variations occur for the atoms close to the extremity of the leg. Interestingly, at the end of the simulation, the leg is fully adsorbed on the surface, which means that one leg can desorb and be re-adsorbed despite the lateral relaxation of the other legs (i.e., the fact that parts of the neighboring legs may slide and fill the space left empty by the desorbed leg). At the end of the simulation, the atoms at the end of the leg are closer to the HOPG surface than the 'core' carbon atoms. The

terminal phenyl ring can adsorb flat, with strong π-π interactions with HOPG, while the tilting of the phenylene units closest to the core (due to steric hindrance) induces the core ring to be slightly 'lifted up' with respect to the equilibrium adsorption distance for an unperturbed benzene ring. Another aspect of the tilted orientation of the phenylene rings closest to the core is that the orientation of the double bond near the center tends to be opposite from the other double bonds.

Figure 3.11A-D shows some snapshots of the system along the MD simulation. In control simulations, the desorption involving the last three phenylene units of the leg was observed, while the one directly attached to the core is not able to desorb (as this would imply a highly energetic geometrical distortion close to the core).

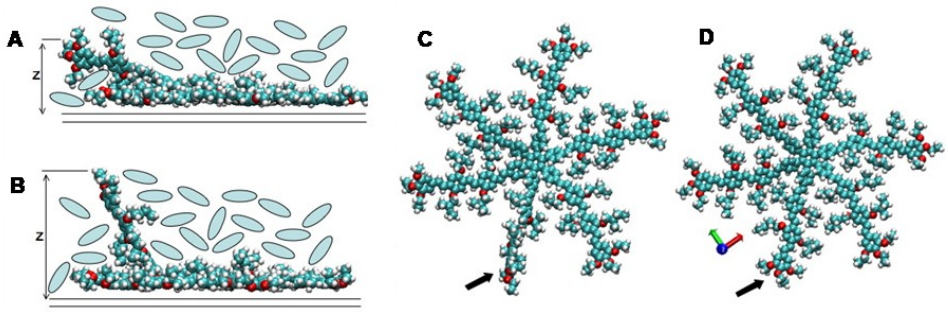

Figure 3.11 *Snapshots from the MD simulations: in A) and B) the solvent and the surface are schematically represented by the ovals and the two lines beneath the S-**1** molecule, respectively. In the top views (C) and (D), the solvent and the surface are not shown, for the sake of clarity. (A) shows the starting geometry, where one leg is in the solvent phase. In (B) the leg is moving even further away from the surface into the solvent. In (C) it is going back towards the surface (black arrow) adopting a tilted conformation, to be finally adsorbed flat on the surface (D).*[16]

Lateral mobility of the legs: A convenient way to model the lateral mobility of the legs remaining adsorbed on HOPG when one leg is desorbed consists in considering a molecule on the surface having in silico one leg chopped off, with only the first phenyl ring left, since this is the part of the leg that cannot desorb, as mentioned above. This approach is more convenient from a molecular dynamics point of view and resembles the situation where the desorbed leg chain would be "frozen" in the solvent.

All the following simulations are conducted at room temperature in the NVT ensemble, involving the *S*-**1** molecule in Figure 3.12 adsorbed on HOPG. To reduce the computational effort, the solvent is now represented as a continuous medium and its influence is included in the model via its dielectric constant. Statistical analysis of the molecular geometry has been performed on the last 150 ps of the MD trajectory.

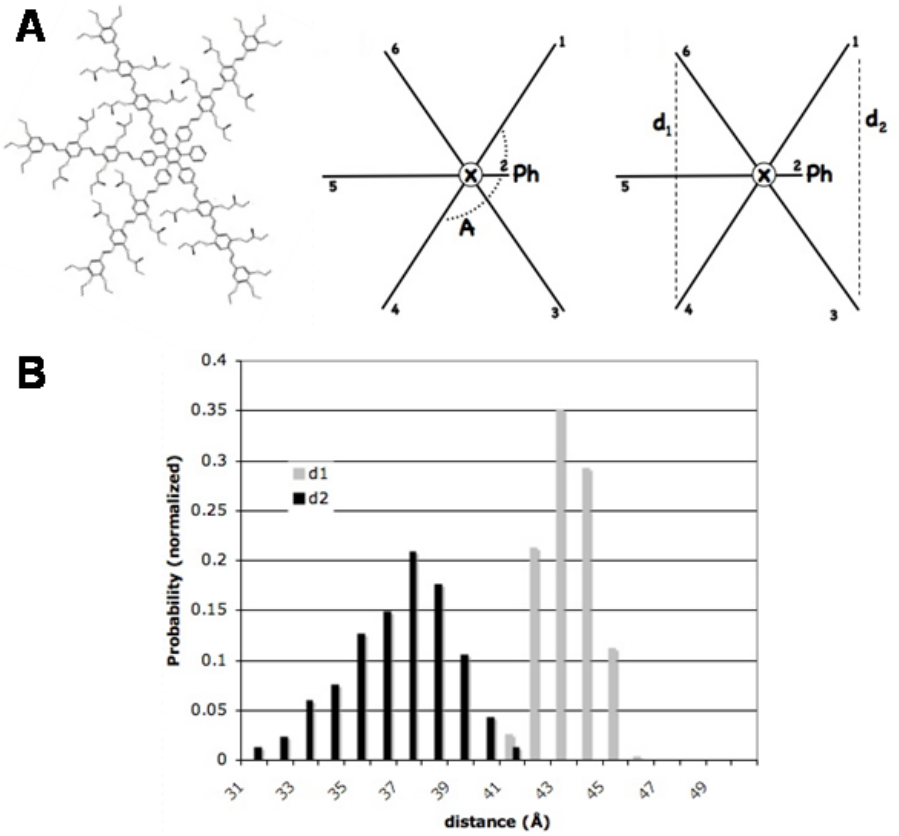

Figure 3.12 *A) Five-leg model S-**1** molecule used to study the lateral mobility of the adsorbed legs and schematic representations. The angle A between legs 1 and 4 is used to follow the legs' relaxation. Another way to express the lateral mobility of the legs consists in following the distances d1 and d2 along the MD simulation. B) Distribution of the values for the distances d1 and d2.*[16]

The lateral mobility of the adsorbed legs was followed in two different ways: (i) in terms of the angle between opposite legs with respect to the center of the molecule; and (ii) in terms of the distance d1 and d2 between the ends of legs 1-3 and 4-6, respectively. In Figure 3.12A, three angles A, B and C corresponding to those between the legs 1-4, 2-5 and 3-6 can be defined, respectively. The average values and the standard derivations of these angles are 164.6 ± 9.4 for A (legs 1-4), 171.2 ± 3.3 for B (legs 2-5) and 166.3 ± 6.2 for C (legs 3-6). The angles A and C are significantly smaller than 180°, indicating a displacement of legs 1 and 3 towards the empty space resulting from the absence of leg 2. The large values of the standard deviation for those two angles suggest a “breathing” motion of the legs when leg 2 is in the solvent phase. The breathing motion also suggests that the space left by a desorbed leg is not occupied in a stable way, allowing adsorption/desorption dynamics of the legs, consistent with the experimental observations.

In order to determine whether this relaxation involves the entire molecule or mainly the “defective” part, the values of distances d1 and d2 were examined. Figure 3.12B shows the distribution of those distances along the MD simulation. d2 (36.99 ± 2.08 Å) is considerably shorter than d1 (43.73 ± 0.94 Å) and shows larger fluctuations around its average value.

This confirms that legs 1 and 3 tend to fill the empty space (thereby bringing their extremities closer to each other) and that those legs remain quite mobile while occupying the empty space. Comparison with the data obtained for a molecule having all six legs adsorbed (42.90 ± 1.00 Å) also indicates that the behavior of legs 4 and 6 is not affected by the desorbed leg. In other words, only the two neighboring legs are affected by the desorption of a leg. In the model of molecular Dynamics of a molecule having already one arm pointing in the solvent phase, the environment is treated explicitly by introducing solvent molecules in the system. A high temperature molecular dynamic (MD) at 650K, in the NVT ensemble, has been then performed to observe the behaviour of the desorbed arm, by recording during the last 100ps the evolution of the height with respect to the surface of five carbon atoms along that arm.

Translational Dynamics: In the conformational dynamics presented, simulated, and discussed above, the position of the center of mass of the molecules was not found to change. However, in addition, translational

motion was also observed, as highlighted in these three frames (Figure 3.13). In this sequence of images, there is translational motion on the surface in areas that are characterized by nonideal ordering of the molecules, in other words in areas with free space. For the molecules (*S*-**1**) that are indicated by the colored rings, the center of mass position changes. Those molecules, which undergo translational changes, simultaneously also undergo orientational changes of their legs. Due to the limited number of observations, no conclusions can be drawn if certain translational directions, for example, along one of the symmetry axes of HOPG, are preferred.

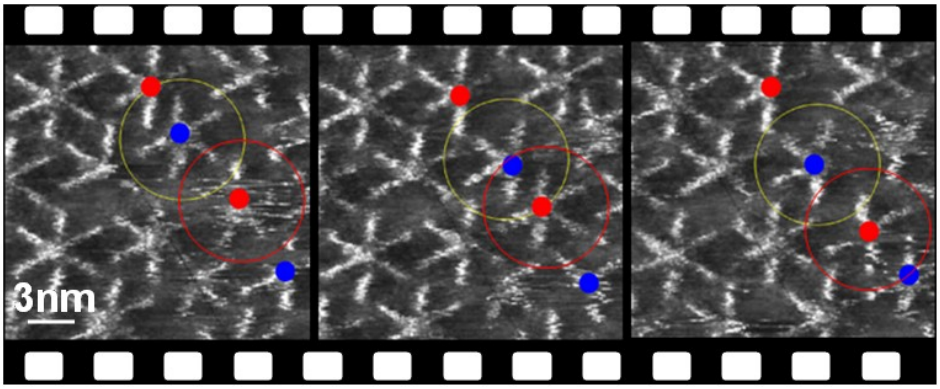

Figure 3.13 *Sequence of STM images zooming in on conformational and translational events of S-**1** at the 1-phenyloctane - HOPG interface. The time gap between the frames is 26 and 68 s. Colored disks and circles indicate the center and periphery of a number of selected molecules, respectively.*[16]

Can one be sure that orientational/translational motions take place in the plane of the substrate? Though it is appealing to consider that these molecules are moving on the surface, there is also the possibility of molecular desorption-adsorption dynamics (*i.e.*, vertical dynamics) as the experiments are carried out at the solid-liquid interface. Desorption-adsorption phenomena have been demonstrated for alkylated isophthalic acid derivatives and other alkylated molecules. However, for the hexapod system, the desorption-adsorption dynamics are considered to take place at a much longer time scale than observed for smaller alkylated systems. One molecule has 18 dodecyloxy chains. Even if only

a fraction of the alkyl chains are adsorbed, the overall interaction energy at 0.07 eV/CH_2 is sufficiently high to slow down the desorption dynamics considerably. Therefore, it is safe to conclude that the observed dynamics are surface confined and do not reflect desorption-adsorption dynamics.
The translational dynamics confirms also that the disappearance and reappearance of the bright legs is due to a desorption-readsorption process and not to a change in electron tunneling efficiency through the OPV legs as a result of some other orientational changes. Consider, for instance, the two molecules marked in the upper half of the left frame of Figure 3.8. In both molecules, only five legs are visible. The invisible legs must be desorbed from the surface: the core to core distance between these "colliding" molecules (3.91 nm) and the distance between parallel legs (1.82 nm) are much smaller than for the regular arrangement, and there is just no space for the "sixth" leg of each molecule to be adsorbed (Figure 3.13 A&B). In line with the previous arguments, the apparent rotation of five-legged molecules (Figure 3.8A) should be described as the desorption of one leg and the simultaneous adsorption of another leg, rather than the rotation of the molecules within the plane of the substrate or a molecular desorption-adsorption process.
Figure 3.14 shows a comparative histogram of the nearest neighbor distance (measured between the central phenyl groups) in ordered and disordered *S*-**1** areas. Clearly, disorder goes along with an on average reduced nearest neighbor distance. The clear bias toward smaller values for disordered domains explains in part the drastic difference in population in ordered and disordered domains. At small intermolecular distances, the molecules cannot have all OPV legs adsorbed because of steric hindrance, as illustrated above, naturally leading to a shift in population from molecules with all OPV units adsorbed to molecules with only five or four OPV units adsorbed.
Random or Collective Processes? In the previous paragraphs, different dynamics (desorption-adsorption of legs), orientational/conformational flexibility, and translation at the level of individual molecules have been described. This description did not take into account the relation between the motion of individual molecules and the (lack of) dynamics of its surroundings. Figure 3.15 summarizes the different aspects of the motion by a color code revealing the following for *S*-**1**: (i) desorption-readsorption

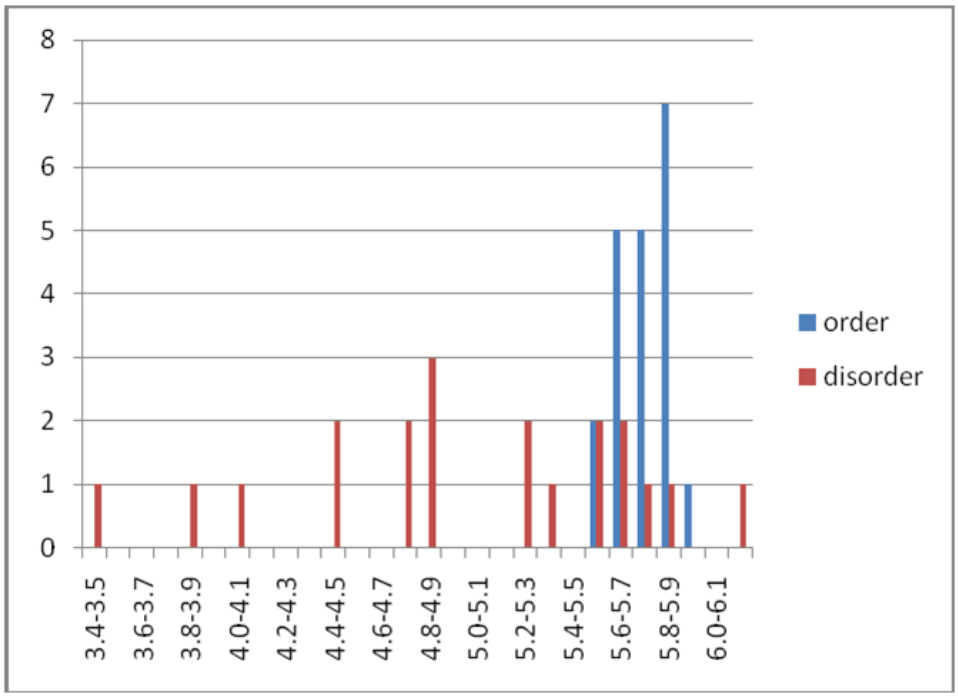

Figure 3.14 *Histogram of the nearest neighbor distance in ordered and disordered S-**1** domains.*[16]

phenomena of individual legs occur both in a noncorrelated (green) and correlated (yellow) fashion; (ii) a reorientation of the legs (*e.g.*, a five-star that "rotates") goes always together with the desorption or reorientation of legs of adjacent molecules; (iii) not surprisingly, quite some conformational dynamics occurs in the area of the translationally mobile molecules. The conclusion to draw is that the conformational or translational motion of a given molecule will favor simultaneous dynamics of adjacent molecules. This is in line with the steady-state picture which revealed the high tendency to form dimer defects.

Why there is huge difference in population in ordered and disordered domains? Basically, the data show that both reduced intermolecular interactions and increased intermolecular interactions promote the conformational dynamics.

When being part of a 2D crystalline lattice, the molecules are trapped and stabilized by intramolecular and intermolecular alkyl chain-alkyl chain van der Waals interactions. Only a small percentage of molecules have one or

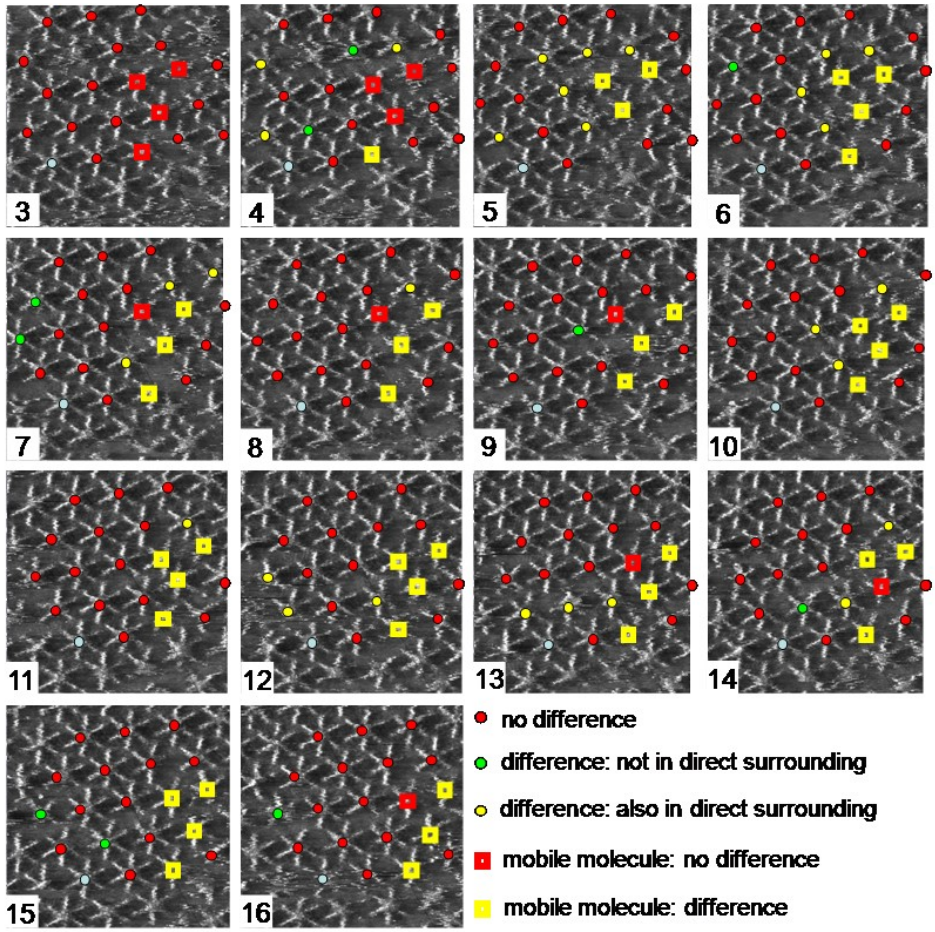

Figure 3.15 *Color-coded sequence of STM images of monolayers of S-**1**. The center of a molecule is indicated by a disk (translational immobile) or square (translational mobile). Red indicates that there is no difference with the previous frame. Green indicates there is a difference in the number of legs adsorbed or orientation with the previous frame. However, no apparent change is observed in the surrounding molecules which could be correlated with that motion. Yellow indicates there is a difference in the number of legs adsorbed or orientation with respect to the previous frame. Changes are observed in the surrounding molecules too. The blue disk is a reference point. The frame number is indicated in the lower left corner.*[16]

two legs desorbed (*S*-**1**: 4%, *R*-**1**: 6%). The presence of a defect was shown to promote the coexistence of another defect adjacent to it. When being part of a disordered domain, the majority of the molecules (*S*-**1**: 77%, *R*-**1**: 80%) appear as defects. This is in part due to the molecular mobility led by the on average reduced distance and increased intermolecular interactions between molecules (steric hindrance). In addition, reduced alkyl chain-alkyl chain interdigitation interactions most likely contribute to the high fraction of defect sites.

Multivalency: Another way to look at the peculiar dynamic behavior of the hexapod is the following. If the total interaction energy with the substrate would be too strong (van der Waals interactions between the six OPV units, the alkyl chains, and the substrate), the mobility of such a molecule would be very slow and it would take a long time before ordered self-assembly sets in. For having such a strong interaction, all six legs should be able to be adsorbed in a perfect way, or in other words, self-assembly would be impaired, or the self-assembly kinetics too slow, if the multivalency[18] effect is too strong. When the fit between molecule and surface is just off, this “wrongly” designed multivalency favors the self-assembly process to set in relatively fast. In that case, a limited number (four or five) of legs will be adsorbed perfectly, while the remaining ones are searching for their ideal binding place. On average, the binding of all six legs is diminished compared to a perfectly fitted hexapod molecule.

3.4 Conclusions

These molecular hexapods form distinct chiral monolayers at the liquid-solid interface, and mixtures of both enantiomers lead to conglomerate formation. The chirality at the level of the monolayer is not or only very weakly expressed in terms of the monolayer orientation with respect to the substrate.

In addition to ordered domains, disordered areas are frequently observed. Careful analysis shows that a significant fraction of the molecules undergo conformational dynamics.

The dynamics reflects to some extent the motion of hexapods, occurs

"spontaneously", and is not the result of heat or light treatment. Intramolecular conformational dynamics were shown to be promoted by nearest neighbor interactions. In addition, translational motion of individual molecules was observed, which could be correlated with conformational dynamics that occurred simultaneously.

This high molecular weight molecule allows probing dynamic phenomena at a solid-liquid interface in a unique way. However, conformational and translational dynamics are by no means unique to this molecule. Upon self-assembly into 2D crystalline matrices, the typically low molecular weight molecules probably undergo (slight) conformational dynamics, but these dynamical phenomena are expected to occur so fast that averaged images are obtained: the different conformational states are not resolved.[19] Thanks to the specific structure of the molecular hexapod and its size, giving rise to a relatively large interaction with HOPG, these submolecular dynamic phenomena could be followed. Molecular dynamics simulations confirmed the possibility of adsorption/desorption processes for individual legs.

Out-of-plane conformational dynamics also relate to the vertical dynamics-adsorption and readsorption-of small molecular weight molecules at a solid-liquid interface, mediated by desolvation and solvation. In physisorbed systems at a solid-liquid interface, these desorption-adsorption dynamics typically remain unnoticed-the site of a desorbed molecule is immediately filled by another one-except if marker molecules are used.[20,21] Solvation must play an important role, but it is difficult to probe.

It would, therefore, be interesting to see how these dynamics are influenced by changing the solvent, temperature, the composition of the monolayers or the chemical nature of one or two of the legs of the molecular hexapod. This will further develop our understanding of the dynamics of molecules in self-assembled monolayers, bring insight into solvation at solid-liquid interfaces, and lead to additional understanding in the multivalency concept.

3.5 References

1 De Feyter, S.; Gesquière, A.; Meiners, C.; Sieffert, M.; Müllen, K. and. De Schryver, F. C *Langmuir* **1999**, *15*, 2817.
2 Yablon, D. G.; Guo, J. S.; Knapp, D.; Fang, H. B. and Flynn, G. W. *J. Phys. Chem. B* **2001**, *105*, 4313.
3 Berner, S.; Brunner, M.; Ramoino, L.; Suzuki, H.; Guntherodt, H.-J. and Jung, T. A. *Chem. Phys. Lett.* **2001**, *348*, 175.
4 Schunack, M.; Linderoth, T. R.; Rosei, F.; Laegsgaard, E.; Stensgaard, I. and Besenbacher, F. *Phys. Rev. Lett.* **2002**, *88*, 156102.
5 Otero, R.; Hummelink, F.; Sato, F.; Legoas, S. B.; Thostrup, P.; Laegsgaard, E.; Stensgaard, I.; Galvao, D. D. and Besenbacher, F. *Nat. Mater.* **2004**, *3*, 779.
6 Schull, G.; Douillard, L.; Fiorini-Debuisschert, C.; Charra, F.; Mathevet, F.; Kreher, D. and Attias, A.-J. *Nano Lett.* **2006**, *6*, 1360.
7 Hou, S. M.; Sagara, T.; Xu, D. C.; Kelly, T. R. and Ganz, E. *Nanotechnology* **2003**, *14*, 566.
8 Wintjes, N.; Bonifazi, D.; Cheng, F. Y.; Kiebele, A.; Stohr, M. and Jung, T. A. *Angew. Chem. Int. Ed.* **2007**, *46*, 4089.
9 Wahl, M.; Stohr, M.; Spillmann, H.; Jung, T. A. and Gade, L. H. *Chem. Commun.* **2007**, *13*, 1349.
10 Manzano, C.; Soe, W.-H.; Wong, H. S.; Ample, F.; Gourdon, A.; Chandrasekhar, N. and Joachim, C. *Nat. Mater.* **2009**, *8*, 576.
11 Jung, T. A.; Schlittler, R. R. and Gimzewski, J. K. *Nature* **1997**, *386*, 696.
12 Scherer, L. J.; Merz, L.; Constable, E. C.; Housecroft, C. E.; Neuburger, M. and Hermann, B. A. *J. Am. Chem. Soc.* **2005**, *127*, 4033.
13 Weigelt, S.; Busse, C.; Petersen, L.; Rauls, E.; Hammer, B.; Gothelf, K. V.; Besenbacher, F. and Linderoth, T. R. *Nat. Mater.* **2006**, *5*, 112.
14 Lingenfelder, M.; Tomba, G.; Costantini, G.; Ciacchi, L. C.; De Vita, A. and Kern, K. *Angew. Chem. Int. Ed.* **2007**, *46*, 4492.
15 Tomović, Ž.; van Dongen, J.; George, S.; Xu, H.; Pisula, W.; Leclère, P.; Smulders, M. M. J.; De Feyter, S.; Meijer, E. W. and Schenning, A. P. H. J. *J. Am. Chem. Soc.* **2007**, *129*, 16190.

16 Xu, H.; Minoia, A.; Tomović, Ž.; Lazzaroni, R. Meijer, E. W.; Schenning, A. P. H. J. and De Feyter S. *ACS NANO* **2009**, *3*, 1016.
17 Gross, L.; Moresco, F.; Ruffieux, P.; Gourdon, A.; Joachim, C. and Rieder, K.-H. *Phys. Rev. B* **2005**, 71, 165428.
18 Broeren, M. A. C.; van Dongen, J. L. J.; Pittelkow, M.; Christensen, J. B.; van Genderen, M. H. P. and Meijer, E. W. *Angew. Chem. Int. Ed.* **2004**, *43*, 3557.
19 Stabel, A.; Heinz, R.; Rabe, J. P.; Wegner, G.; De Schryver, F. C.; Corens, D.; Dehaen, W. and Sueling, C. *J. Phys. Chem.* **1995**, *99*, 8690.
20 Gesquiere, A.; Abdel-Mottaleb, M. M.; De Feyter, S.; De Schryver, F. C.; Sieffert, M.; Mullen, K.; Calderone, A.; Lazzaroni, R. and Bredas, J. L. *Chem. –Eur. J.* **2000**, *6*, 3739.
21 Stevens, F. and Beebe, T. P. *Langmuir* **1999**, *15*, 6884.

Chapter 4: Tuning the Ordering, Orientation and Expression of Chirality of Monolayers of Oligo(*p*-phenylenevinylene) Derivatives

4.1 Introduction

In the previous chapter, the self-assembly of a six-legged OPV hexapod has been investigated.[1,2] This π-conjugated molecule shows very interesting chiral expression and dynamic behavior at the supramolecular level.

Functional properties of monolayers are defined by the supramolecular structures. Thus controlling the self-assembly process by tuning molecule-molecule and molecule-substrate interactions is important.

In this chapter, instead of using covalently linked oligo(*p*-phenylene vinylene) moieties, OPV derivatives which are designed to interact via non-covalent interactions (Figure 4.1) are used as building blocks of the monolayer. Their tunable chemical structure makes it possible to investigate the relation between the structural properties of the building blocks and the monolayer formed. The good solubility of this type of molecules in solvents that commonly are used for STM measurements (Figure 4.2) offers the possibility to explore the role solvent molecules play in self-assembly at the liquid solid interface.

4.2 Experimental

Scanning Tunneling Microscopy. The STM equipments and tip preparation are the same as mentioned in chapter 3. The compounds under investigation were dissolved in 1-phenyloctane (Aldrich), 1,2,4-trichlorobenzene (Aldrich), 1-octanol (Aldrich) and 1-octanoic acid (Sigma) at a concentration of approximately 10^{-4} M.

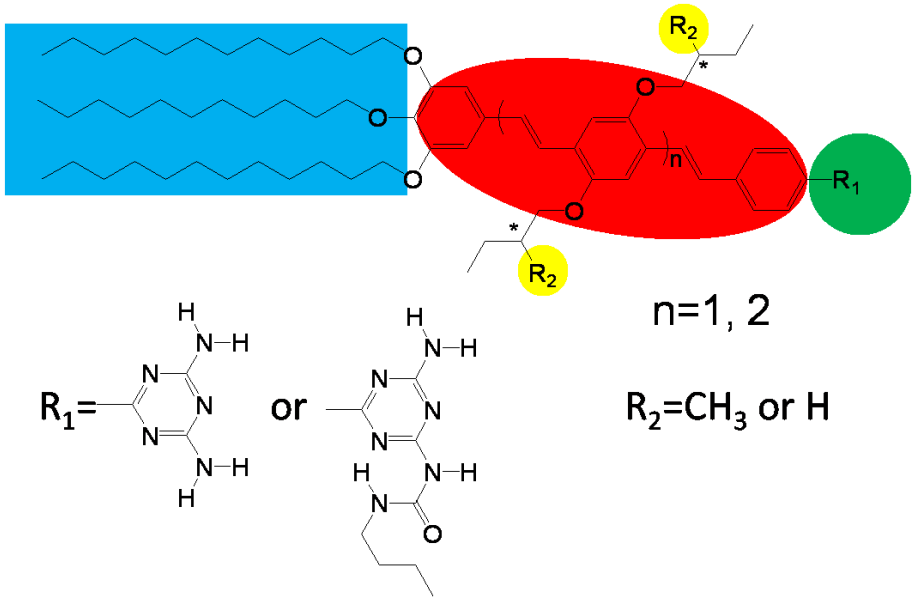

Figure 4.1 *Chemical structure of oligo(p-phenylene vinylene) derivatives. The tunable parts are indicated in color. Red: the conjugated backbone (its length can be modified). Green: terminal functional group (its nature can be changed). Yellow: stereogenic centers if R_2=CH_3. Blue: terminal alkyl chains (their length can be modified). The compounds were synthesized by Dr. P. Jonkheijm in the group of Dr. A. P. H. J. Schenning and Prof. E. W. Meijer at Eindhoven University of Technology (Eindhoven).*[3]

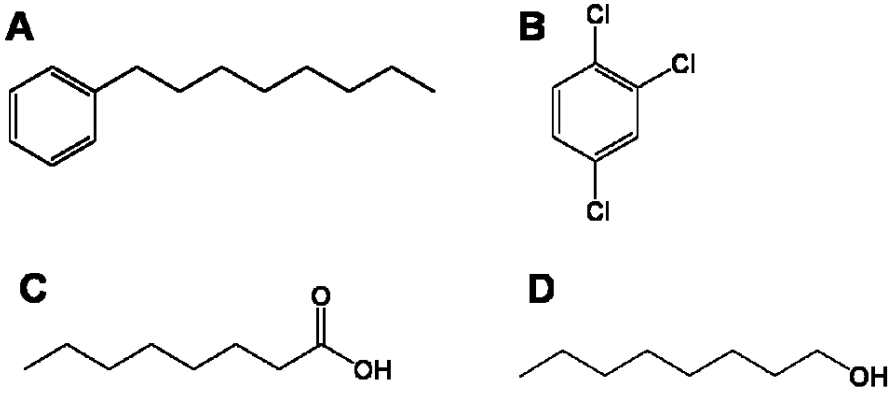

Figure 4.2 *Chemical structures of solvents used in this chapter: A) 1-phenyloctane, B) 1,2,4-trichlorobenzene, C) 1-octanoic acid, D) 1-octanol.*

4.3 Results and Discussion

Influence of terminal functional groups

Besides molecule-substrate interactions which will be treated later on, molecule-molecule interactions decide if well ordered supramolecular structures can form. In this chapter, OPV molecules with diamino triazine (-T) and ureido-s-triazine (-UT) functional groups are used as building blocks. Both molecules provide the possibility of forming intermolecular hydrogen bonds. Figure 4.3 shows typical STM images of (*S*)-OPV4T and (*S*)-OPV4UT at the liquid-solid interface. The OPV backbones appear bright in the STM image, while the alkyl chains appear in the dark regions. (*S*)-OPV4T shows '5' supramolecular rosettes and these rosettes propagate almost along one of the three main symmetry axes of HOPG.[3] OPV4UT molecules form dimer structures and propagate also along one of the main symmetry axes of HOPG. Dimers always rotate CCW with respect to the HOPG reference axis.[4] Unit cell parameters are shown in Table 4.1.

Influence of the length of backbones

Changing the length of the backbones of the OPV molecules not only changes the unit cell vectors, but also the molecular packing and orientation.[5] Figure 4.4 shows the monolayer formed by (*S*)-OPV3T and (*S*)-OPV3UT.

In case of *(S)*-OPV3T, the molecules form again supramolecular rosettes via hydrogen bonds (Figure 4.4A). However, the orientation for OPV3T rosettes is '2' (CW), while the orientation for OPV4T rosettes is '5' (CCW). In addition, the angle between the directions of rows of rosettes with respect to the main symmetry axes of HOPG (θ=+18±2°) also indicates the homochirality of the monolayers formed.

On the one hand, modeling (Figure 4.5) suggests that the empty space, i.e. the substrate area which is not covered by molecules, is minimal in case of OPV4T rosettes showing a '5' orientation. On the other hand, the experimentally not-observed '5' rotation for OPV3T is expected to be

unstable due to the steric interactions of the OPV and dodecyloxy chains.[3,5]

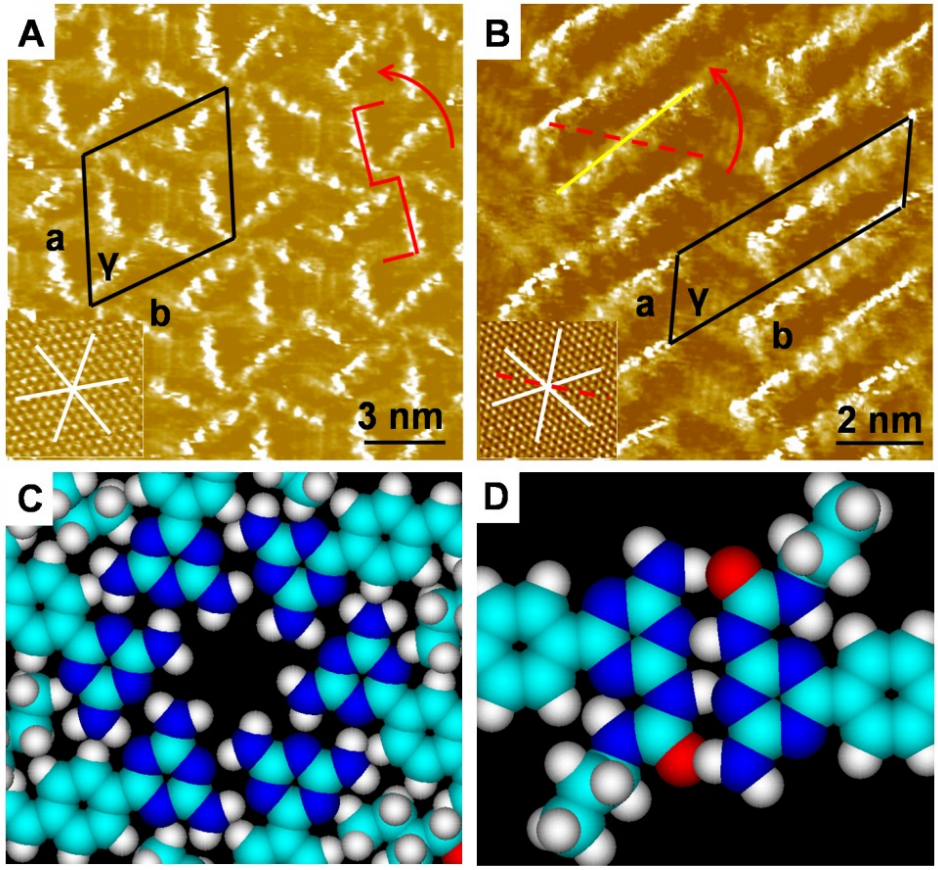

Figure 4.3 *STM images of OPV monolayers. A) (S)-OPV4T at 1-phenyloctane - HOPG interface, B) (S)-OPV4UT at 1,2,4-trichlorobenzene - HOPG interface. Unit cells are indicated in black. The '5' (CCW) orientation of rosettes is shown in red. White lines in inset show the HOPG main symmetry axes. Red dashed line in B) indicates a HOPG reference axis. The direction of dimers is indicated with a yellow solid line. A red arrow in A) shows the CCW orientation of dimers with respect to the HOPG reference axis. C) Model of hydrogen bonded moiety of (S)-OPV4T hexamer. D) Model of hydrogen bonded moiety of (S)-OPV4UT dimer. Sky blue=C, white=H, dark blue=N, red=O.*[3,4]

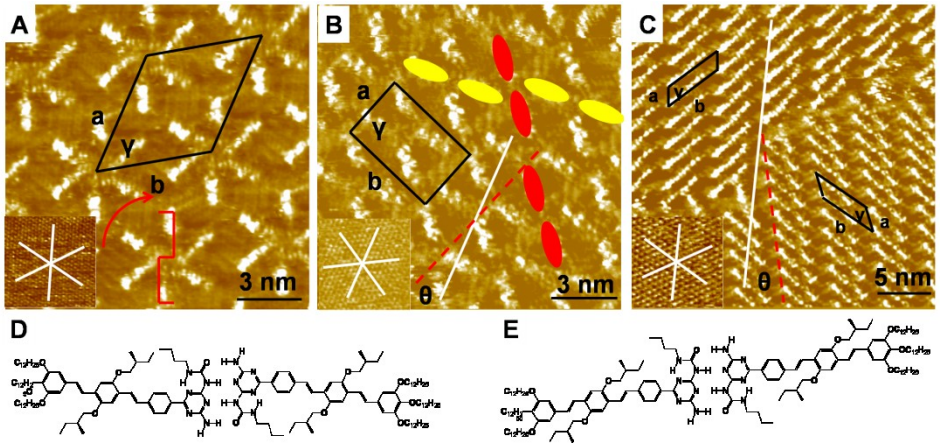

Figure 4.4 *STM images of OPV monolayers. A) Majority packing of (S)-OPV3T at 1-phenyloctane - HOPG interface, B) Minority packing of (S)-OPV3T at 1-phenyloctane - HOPG interface, C) (S)-OPV3UT at 1,2,4-trichlorobenzene - HOPG interface. D) Tentative model of majority packing of (S)-OPV3UT. Dimer shows a pronounced shift between two molecules, E) Tentative model of minority packing of (S)-OPV3UT. Dimer shows a linear packing. Unit cells are indicated in black. The '2' (CW) orientation of rosettes is shown in red in A). White lines in the images and insets show the HOPG main symmetry axes. Red dashed lines indicate the directions of unit cell vector a.*[3,4]

Besides a rosette structure, a dimer packing is also observed in a few domains for OPV3T (Figure 4.4B). Dimers, which are probably hydrogen bonded, propagate along two directions, leading to a paired dimer motif. The angle between unit cell vector a and the main symmetry axis of HOPG θ=+21±1° clearly indicates the homochiral packing of the monolayer. Note that not all alkyl chains follow the main symmetry axis of HOPG.

For *(S)*-OPV3UT, dimer structures are also observed in large areas. The domain on the top of Figure 4.4C shows a very similar molecular packing as in monolayers of *(S)*-OPV4UT. Molecular rows propagate along the main symmetry axis of the HOPG. Dimers rotate CCW with respect to short lamella axis. However, this typical packing of *(S)*-OPV4UT is not a majority orientation for *(S)*-OPV3UT. The packing shown on the bottom of Figure 4.4C dominates the *(S)*-OPV3UT monolayer. In this packing, the

lamella propagation direction rotates CCW with respect to the main symmetry axis of HOPG. Dimers rotate CW with respect to the HOPG reference axis. Note that the CW and CCW domains cannot be converted into each other by a mirror-symmetry operation: CW and CCW domains are the result of different packing motifs, i.e. they are polymorphs. More specifically, the backbones of the respective dimers are either shifted or co-linear.

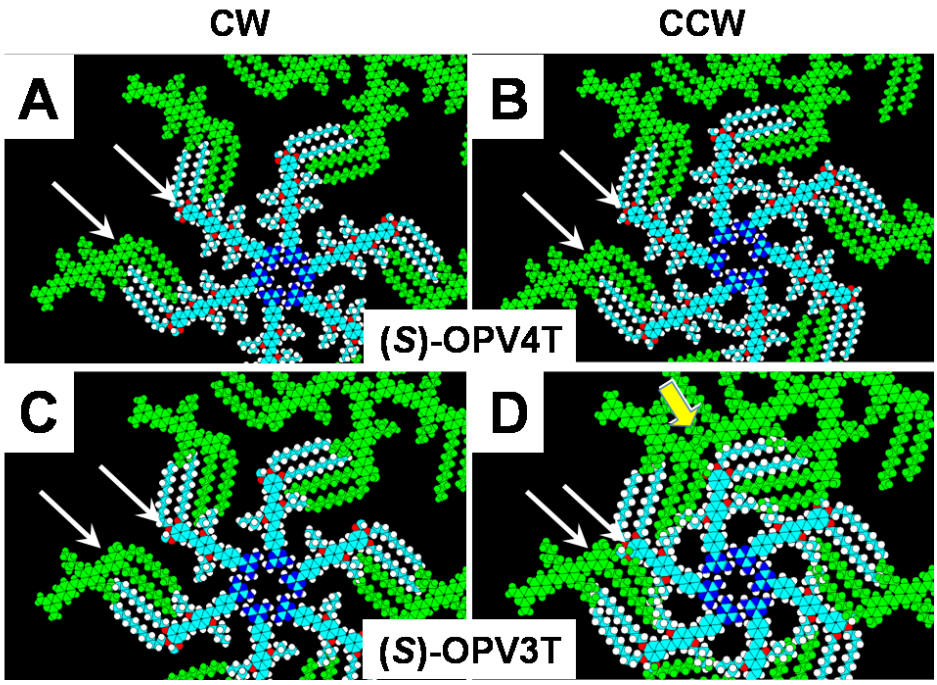

Figure 4.5 *Possible CW (A, C) and CCW (B, D) rosettes of OPV3T and OPV4T, respectively. Experimentally, the CCW rosettes were observed for OPV4T and the CW rosettes for OPV3T. Arrows indicate the nearest phenyl rings from adjacent rosettes.*[5]

Influence of the length of alkyl chains

Interactions between molecule and substrate are often keys to the outcome of the self-assembly process at the liquid-solid interface. The length of alkyl chains is a parameter which can be used for tuning the supramolecular structures. In this chapter, OPV derivatives always have three alkyl chains at one end of the backbone. The self-assembly of two

(*S*)-OPV4T (R_1=diamino triazine, R_2=CH_3, n=2) derivatives with alkyl chain length of C_6 ((*S*)-OPV4T-C_6) and C_{12} ((*S*)-OPV4T), respectively, is investigated to explore the influence of the alkyl chain length. The motivation is the difference in the supramolecular chirality of the OPV3T and OPV4T rosettes. One would expect that the rosettes formed show the same orientation, independent of the number of stereogenic centers or the length of the OPV units. This is clearly not the case. Models of '2' and '5' (S)-OPV4T rosettes show that the distance between the terminal phenyl rings of adjacent OPV rods in the '2' rosette structure is larger than for the '5' rosette structure. Thus, '5' rosettes structures lead to less free surface area and are expected to be more stable. In case of (S)-OPV3T, the formation of a '5' rosettes structure would also lead to a minimum in free surface area. However, the terminal phenyl rings and the alkyl chains of adjacent molecules overlap in '5' rosette structures and cause unfavorable steric interactions. By tuning the alkyl chain length, the steric interactions between the backbones and the alkyl chains of adjacent molecules are expected to change and lead to different orientation.

Figure 4.6 shows STM images of the monolayers formed by the (*S*)-OPV4T derivatives with different alkyl chain length at the

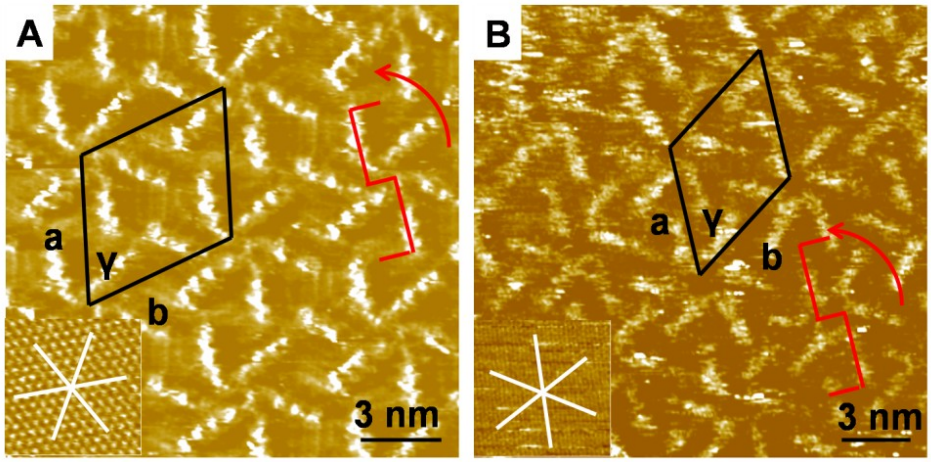

Figure 4.6 *STM images of (S)-OPV4T physisorbed at the 1-phyneloctane - HOPG interface. A) Alkyl chain length = 12, B) alkyl chain length = 6. Unit cells are indicated in white. Red arrows show the CCW orientation of rosettes. White lines in inset images show the HOPG main symmetry axis.*[3]

1-phenyloctane - HOPG interface. In both cases, alkyl chains provide enough molecule-substrate interactions and molecules form well ordered rosettes. The expression of chirality can be easily distinguished by the CCW rotation rosettes adopt. As shown in Table 4.1, angles of lamellae with respect to the HOPG main symmetry axis ((*S*)-OPV4T-C_{12}: -2±1°; (*S*)-OPV4T-C_6: -10±1°) also indicate that homochiral domains are formed in both cases. As expected, due to the alkyl chain length difference, vector a and b in C_6 are smaller than C_{12}. However, the difference is not big enough to influence the orientation of conjugated backbones of OPV molecules. This path has not been explored any further.

Influence of stereogenic centers

Stereogenic centers on side chains of OPV molecules are keys to amplify and transfer molecular chirality to supramolecular structures. Figure 4.7A shows the STM image of a monolayer formed by (*R*)-OPV4T. As expected, rosettes with an almost identical unit cell as found for (*S*)-OPV4T are observed and the monolayer can be considered to be the mirror image of the one formed by (*S*)-OPV4T. Rosettes adopt a '2' rotation. Unit cell vector a rotates CW with respect to the main symmetry axis of HOPG (θ=+6±1°).

For the achiral A-OPV4T, both '5' and '2' and randomly packed molecules can be observed after deposition. The monolayer needs quite long time to reach equilibrium. After 5 hours, a paired dimer packing which is similar to

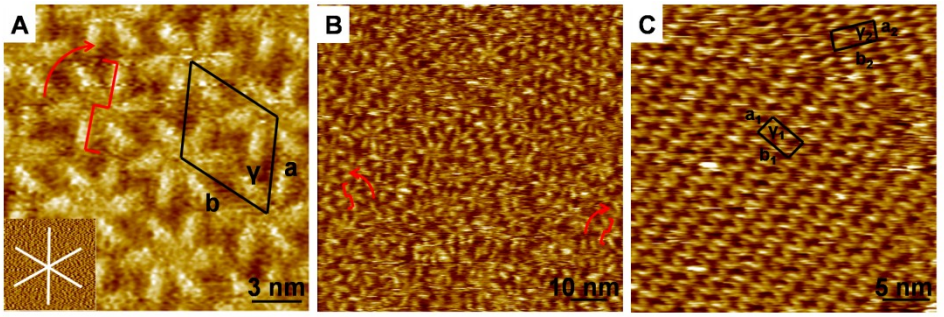

Figure 4.7 *STM images of OPV4T physisorbed at the 1-phenyloctane - HOPG interface. A) (R)-OPV4T, B) A-OPV4T, recorded 3 hours after deposition, C) A-OPV4T, 5 hours after deposition. Unit cells are indicated in black. Orientations of rosettes are in red.*

the one shown in Figure 4.4B dominates the monolayer. Two types of domains can be found. They share the same unit cell parameters, but have different chiral expression. Unit cell vector a rotates either CW (θ=+25±1°) or CCW (θ=-27±1°) with respect to the main symmetry axis of HOPG. Mirror domains are present and a conglomerate is formed.
For A-OPV3T, no rosettes are observed. Soon after deposition, dimer patterns can be observed, followed by the formation of paired dimer patterns. In both cases, the monolayers form a conglomerate (Figure 4.8).

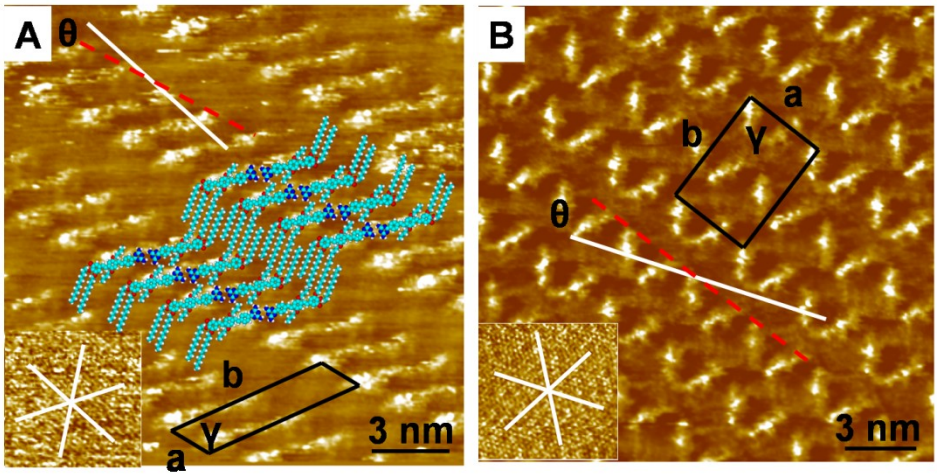

Figure 4.8 *STM images of A-OPV3T physisorbed at the 1-phenyloctane - HOPG interface. A) dimers, B)* paired dimer *patterns. Unit cells are indicated in black. Red dashed lines show directions of unit cell vector a. The exact position and orientation of the alkyl chains is not known.*

As expected, A-OPV3UT molecules form conglomerate dimer structures, with an identical unit cell as (*S*)-OPV3UT. However, instead of forming dimers, A-OPV4UT molecules self-assemble into well-ordered tetramer structures. Due to the absence of stereogenic centers in achiral molecules, A-OPV4UT can flip over on the surface and provide more possibilities of hydrogen-bond formation (Figure 4.9).
OPVT molecules can form several different types of packing. Besides disordered domains, well ordered rosettes, paired dimer patterns and dimer structures are all observed. The differences in packing density for the three cases are small (Table 4.2). OPV4T doesn't form regular dimer structures. Only at the 1-octanoic acid - graphite interface (see below), a

new non-stable low-density dimer pattern is observed.

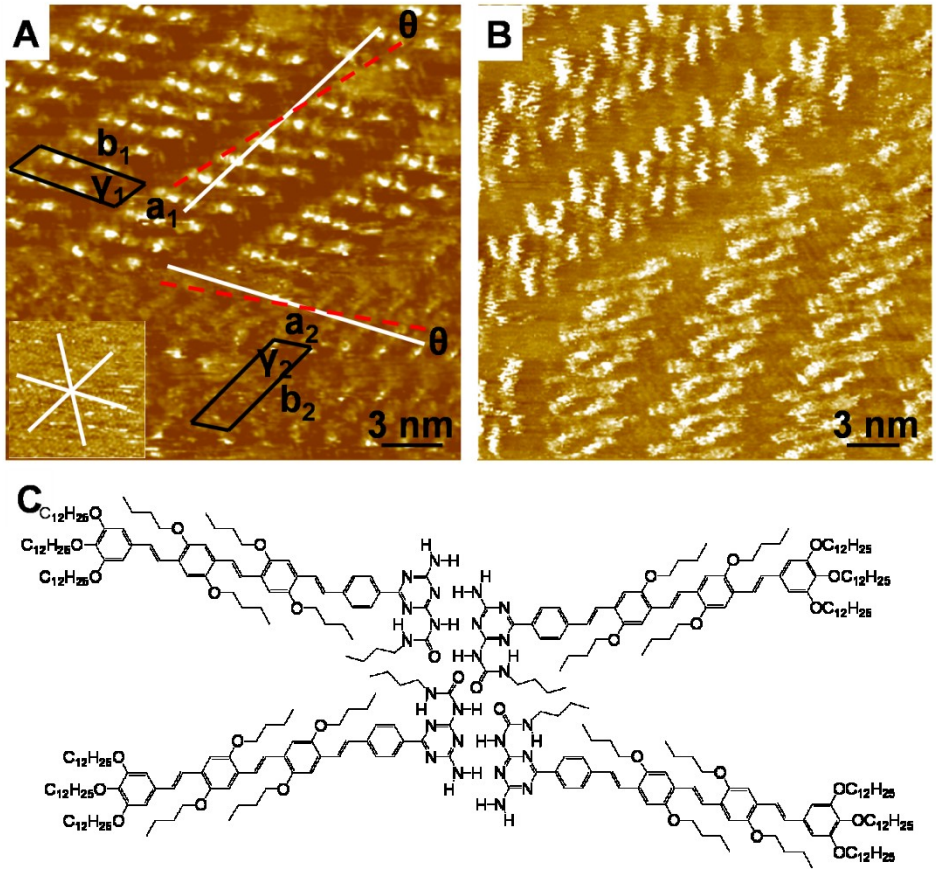

Figure 4.9 *A) and B) are STM images of A-OPVUT physisorbed at the 1,2,4-trichlorobenzene - HOPG interface. A) A-OPV3UT, B) A-OPV4UT. Unit cells are indicated in white. Red dashed lines show directions of unit cell vector a. C) Tentative model of A-OPV4UT tetramers.*

It is clear that for this class of molecules the presence or absence of stereogenic centers affects the molecular organization. For achiral molecules, it's apparently more difficult to have six molecules adopting the same orientation and to self-assemble into well ordered rosette patterns. Several factors could contribute. The achiral molecules are less soluble in 1-phenyloctane than their chiral analogues. In addition, the achiral molecules experience more possibilities to adsorb on the surface as they can do so with both enantiotopic faces. Both factors are expected

to slow down the self-assembly process, at least the trajectory to the thermodynamically favored pattern.

Table 4.1 *Unit cell parameters, and angle of vector a with respect to the HOPG main symmetry axis (θ). Alkyl chain length is 12 carbon atoms if not specifically indicated.*

	a (nm)	b (nm)	γ (°)	θ (°)	Packing
(*S*)-OPV4T	6.1±0.1	6.1±0.1	60±1	-2±1	Rosette
(*R*)-OPV4T	6.1±0.2	6.1±0.1	61±1	+6±1	Rosette
A-OPV4T	3.1±0.1	6.2±0.1	87±1	+25±1	Paired dimer
	2.8±0.1	6.6±0.1	87±1	-27±1	Paired dimer
(*S*)-OPV4TC_6	5.9±0.1	5.8±0.1	61±1	-10±1	Rosette
(*S*)-OPV3T	5.5±0.1	5.6±0.1	61±5	+18±2	Rosette
	3.1±0.1	4.8±0.1	90±1	+21±1	Paired dimer
A-OPV3T	3.4±0.1	5.3±0.1	89±1	+19±1	Paired dimer
	3.4±0.1	5.3±0.1	89±1	-19±1	Paired dimer
	1.8±0.1	5.1±0.1	62±1	+13±1	Dimer
	1.8±0.1	5.1±0.1	65±1	-12±1	Dimer
(*S*)-OPV4UT	2.0±0.1	6.7±0.1	54±3	0	Dimer
(*S*)-OPV3UT	1.7±0.1	5.6±0.1	53±1	0	Dimer
	2.0±0.1	5.9±0.1	49±1	-14±1	Dimer
A-OPV3UT	1.8±0.1	6.0±0.1	48±1	+14±1	Dimer
	1.8±0.1	6.1±0.1	48±1	-14±1	Dimer

Table 4.2 *Molecular densities (nm^2/molecule) of different types of OPV3T and OPV4T monolayers at the 1-phenyloctane - HOPG interface. '-' means that no experimental data are available.*

	Chiral OPV3T	Achiral OPV3T	Chiral OPV4T	Achiral OPV4T
Dimers	-	3.717-4.513	-	-
Paired dimer	3.524-3.920	4.287-4.725	-	4.377-5.037
Rosettes	4.101-4.860	-	5.110-5.841	-

Influence of solvent

Solvent also plays a very important role in the formation of supramolecular structures.[6,7,8,9,10,11] OPVT molecules have good solubility in many solvents which are commonly used for STM measurements including 1-phenyloctane, 1,2,4-trichlorobenzene, 1-octanoic acid and 1-octanol. Generally, four types of supramolecular structures are observed (Figure 4.10). The patterns that OPVT molecules form in different solvents are listed Table 4.3.

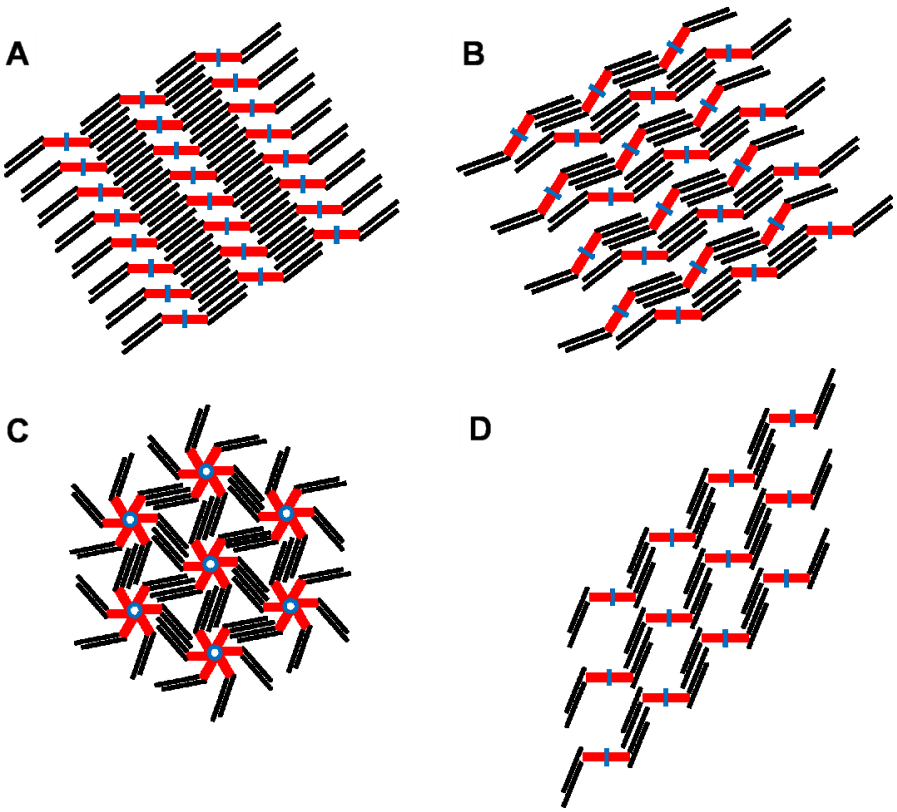

Figure 4.10 *Tentative model of the supramolecular structures that OPVT molecules form. A) dimers, B) paired dimers, C) rosettes, D) low density dimers. Red rods show OPV backbones. Black lines indicate alkyl chains. Blue rods or circles are the functional groups which form hydrogen bonds. In all cases, two out of three alkyl chains can be observed. Although the fate of the third alkyl chain is not clear, invisible chains are considered to be directed into the solution.*

1-phenyloctane

The interaction of solvent molecules like 1-phenyloctane with OPV is believed to be rather small. Except for weak π-π interactions, no other significant interaction modes are anticipated. In this solvent, both chiral and achiral OPV molecules need quite long time to reach the equilibrium state (normally several hours). Figure 4.11 shows dynamic phenomena in monolayers of OPV4T. Though the final stable supramolecular structures are different, 2D Fourier spectra indicate that monolayers become more ordered in time. A similar dynamic behavior is also observed in OPV3T systems. Different from OPV4T, both chiral and achiral OPV3T molecules form two types of ordered structures. In both cases, two types of patterns were observed after several hours. Minority packings only appeared shortly (less than 30 minutes) and evolved into majority packings (Figure 4.4A and Figure 4.8B).

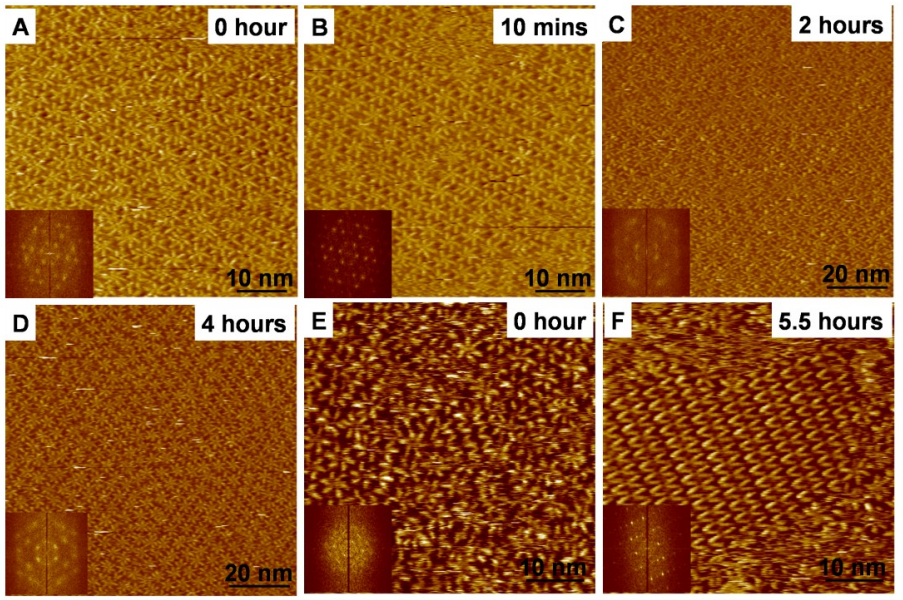

Figure 4.11 *STM images of OPV4T physisorbed at the 1-phenyloctane - HOPG interface. A) & B) (S)-OPV4T (I_{set} = 0.02 nA; V_{set} = -0.65 V), C) & D) mixture of (S)- and (R)-OPV4T (1:1) (I_{set} = 0.02 nA; V_{set} = -0.80 V), E) & F) A-OPV4T (I_{set} = 0.01 nA; V_{set} = -0.65 V). Insets show 2D FFT. The delay between sample formation (drop casting) and image recording is indicated on the top right corner.*

1,2,4-trichlorobenzene

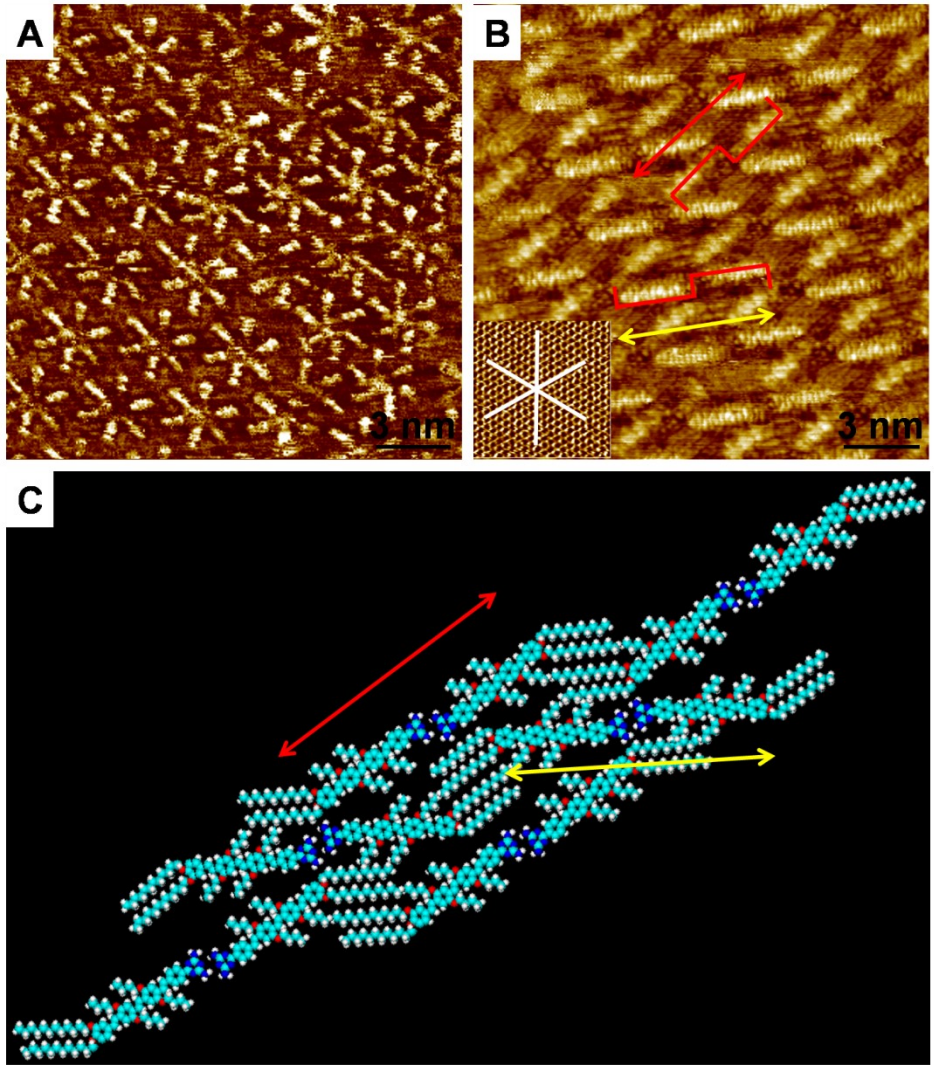

Figure 4.12 *A) and B) are STM images of OPV4T physisorbed at the 1,2,4-trichlorobenzene - HOPG interface. A) (S)-OPV4T, B) A-OPV4T (I_{set} = 0.25 nA; V_{set} = -0.65 V). White lines in inset image show HOPG main symmetry axes. C) Tentative Model of* paired dimer *pattern formed by A-OPV4T. Two propagation directions of dimers are indicated in red and yellow arrows, respectively.*

Similar as in 1-phenyloctane, (*S*)-OPV4T molecules form '5' rosettes and

A-OPV4T molecules form conglomerate paired dimer structures in 1,2,4-trichlorobenzene (TCB), respectively (Figure 4.12). Generally, the equilibration time is shorter than in 1-phenyloctane. High resolution STM images allow one to determine in detail the packing of the paired dimer structures. Namely, two types of dimers are formed (‘2’ and ‘5’ type) which propagate along two different directions, respectively.

1-octanol

When 1-octanol is chosen as solvent, it is expected to compete with the OPV units in terms of hydrogen bonding and assist the monolayer to reach equilibrium. Sometimes, 1-octanol is observed to adsorb on HOPG, by the formation of a self-assembled layer or by co-adsorption in a self-assembled layer composed the compound of interest. However, for OPV systems, there is no evidence that solvent molecules are involved in the monolayer formation. However, the molecular packing and the dynamics of monolayer formation are different from 1-phenyloctane and 1,2,4-trichlorobenzene. At the 1-octanol - HOPG interface, monolayers of well-ordered rosettes are observed within 30 minutes after deposition (Figure 4.13). For chiral OPVT, depending on the length of OPV backbone,

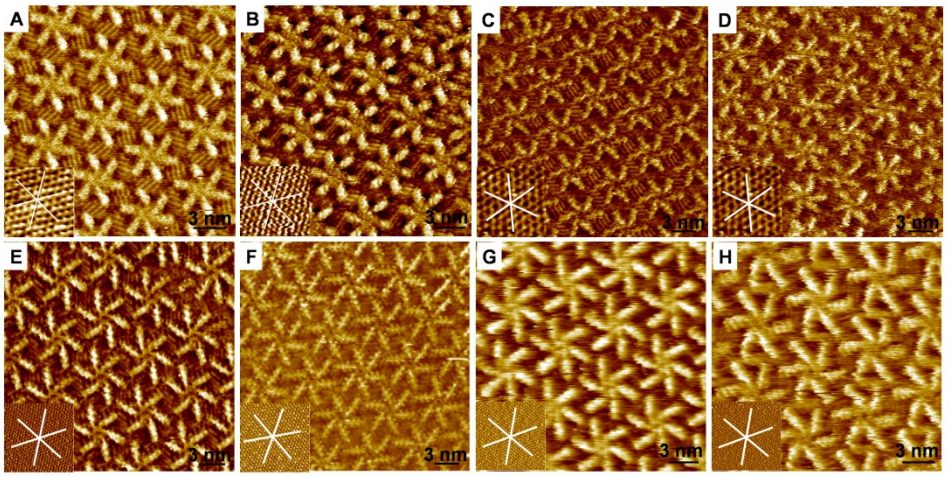

Figure 4.13 *STM images of OPVT monolayers at the 1-octanol - HOPG interface. A) (S)-OPV3T, B) (R)-OPV3T, C) & D) A-OPV3T, E) (S)-OPV4T, F) (R)-OPV4T, G) & H) A-OPV4T. White solid lines in insets are HOPG main symmetry axes.*

the orientation of the rosettes is either ‘2’ or ‘5’. In case of achiral molecules, conglomerate packing is observed.

1-octanoic acid

However, the reasoning developed above is challenged by experiments at the 1-octanoic acid - HOPG interface. There are many interactions possible between the OPV diamino triazine unit and the carboxylic acid group of 1-octanoic acid. Compared to other solvents, OPVT molecules have a very high solubility in 1-octanoic acid, which may reflect the relatively strong interactions between OPVT and solvent molecules.

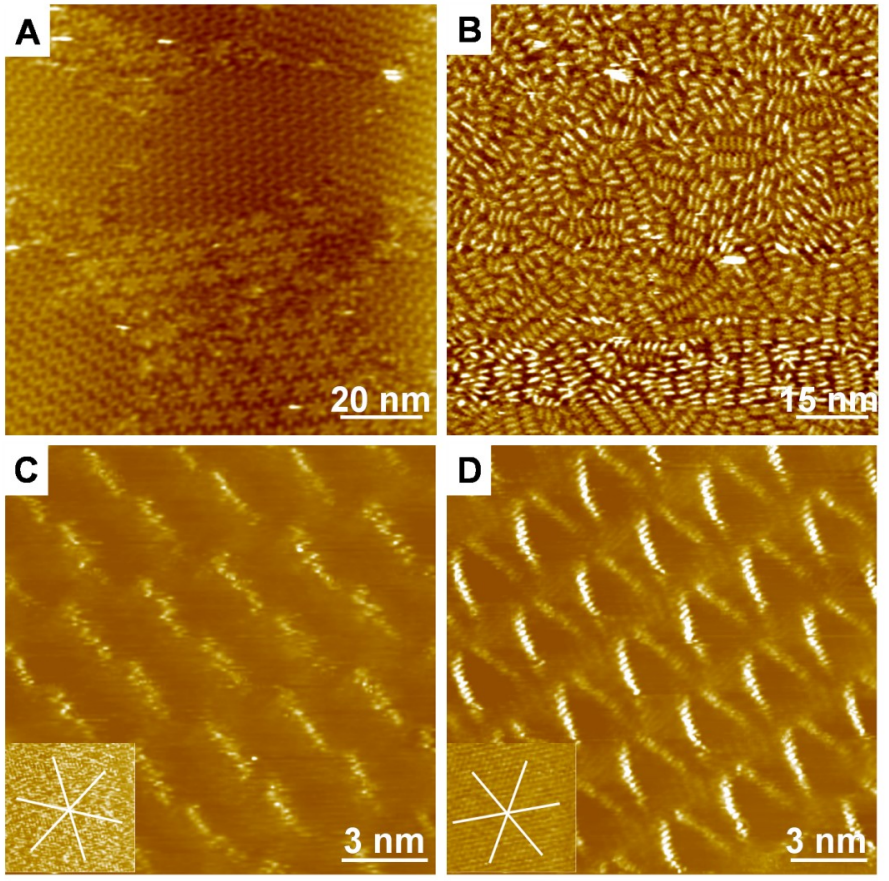

Figure 4.14 *STM images of OPVT monolayers at the 1-octanoic acid - HOPG interface. A) (S)-OPV3T, B) (S)-OPV4T, C) & D) achiral-OPV4T. White solid lines in insets are HOPG main symmetry axes.*

Figure 4.14 shows typical STM images of monolayers of chiral and achiral OPVT derivatives. Though OPV molecules are observed soon after the deposition, no ordered 2D structures are formed. Most of the domains are composed of disordered dimer-like structures. Only after several hours, ordered structures were visualized. Rosettes only appear for (*S*)-OPV3T. In addition, it forms paired dimer patterns. Solvent molecules are considered either to co-adsorb with OPV or to interact on top of monolayers and hamper the formation of rosettes. Achiral-OPV4T forms initially low density dimer-like patterns, followed by the formation of paired dimer patterns. Unit cell parameters of the two types of patterns A-OPV4T formed are shown in Table 4.3.

Table 4.3 *Unit cell parameters, angles of direction of unit cell vector a with respect to the main symmetry axes of HOPG. Due to the limited data, only one type of domain was observed in both cases.*

	a (nm)	b (nm)	(°)	θ (°)
Low density dimers	2.8±0.1	5.6±0.1	81±2	+27±1
paired dimer	3.1±0.1	6.8±0.1	90±1	-26±2

The patterns which are observed for the chiral and achiral OPV derivatives in the different solvents are summarized in Table 4.4.
Basically, four different patterns are observed: rosette, dimer and paired dimer pattern, both for the achiral and chiral molecules. Solvent clearly plays a role in the self-assembly process because not all patterns are observed in all solvents. The exact nature of the role solvent plays is still not clear though. Solvent molecules were never observed co-adsorbing with OPV derivatives. However, the preformation of hydrogen bonded complexes in aprotic solvents (e.g. 1-phenyloctane, TCB) could slow down the self-assembly process or favor the formation of a disordered phase. In solvents with –OH or –COOH groups, hydrogen bonds may form between solvent molecules and OPV molecules on top of the monolayers. In this case solvent molecules actively participate in the self-assembly process which could also affect the dynamic behavior.

Table 4.4 *Supramolecular structures formed by OPV molecules in different solvents. '-' means that related experiments haven't been carried out yet.*

	1-phenyl-octane	TCB	1-octanol	1-octanoic acid
(S)-OPV3T	rosettes, paired dimer	-	rosettes	rosettes, paired dimer
(R)-OPV3T	-	-	rosettes	-
A-OPV3T	dimers, paired dimer	-	rosettes	-
(S)-OPV4T	rosettes	rosettes	rosettes	paired dimer
(R)-OPV4T	rosettes	-	rosettes	-
A-OPV4T	rosettes, paired dimer	rosettes, paired dimer	rosettes	Low density dimers, paired dimer

4.4 Conclusions

In summary, the self-assembly of some oligo(*p*-phenylene vinylene) derivatives at the liquid-solid interface has been investigated. By varying the structural characteristics of the OPV molecules (type of functional terminal groups, the length of backbones, the length of alkyl chains and the existence of stereogenic centers), molecule-molecule and molecule-substrate interactions are tuned. The result is the formation of various monolayers which differ in the ordering, orientation and expression of chirality.

The effect of solvent has been investigated by recording the self-assembly of OPVT molecules in four different achiral solvents. Though no evidence shows that solvent molecules co-adsorb with OPV derivatives, in all cases, there is a clear effect of the solvent on the pattern formation and the dynamics involved. In some solvents several patterns

are formed which co-exist (polymorphism), or which appear to be intermediates while the system evolves toward thermodynamic equilibrium. 1-Octanol appears to be special in that respect as only one type of pattern is observed for all compounds. It is fair to say though that solvent effects are to a large extent unpredictable so far.
Important though is that the expression of chirality does not depend on the nature of the solvent, i.e. a pattern which appears in more than one solvent has always the same chirality for a given enantiomer.

4.5 References

1 Xu, H.; Minoia, A.; Tomović, Ž.; Lazzaroni, R.; Meijer, E. W.; Schenning, A. P. H. J. and De Feyter, S. *ACS NANO* **2009**, *3*, 1016.
2 Tomović, Ž.; van Dongen, J.; George, S. J.; Xu, H.; Pisula, W.; Leclere, P.; De Feyter, S.; Meijer, E. W. and Schenning, A. P. H. J. *J. Am. Chem. Soc.* **2007**, *129*, 16190.
3 Jonkheijm, P.; Miura, A.; Zdanowska, M.; Hoeben, F. J. M.; De Feyter, S.; Schenning, A. P. H. J.; De Schryver, F. C. and Meijer E. W. *Angew. Chem.* **2004**, *116*, 76.
4 Gesquière, A.; Jonkheijm, P.; Hoeben, F. J. M.; Schenning, A. P. H. J.; De Feyter, S.; De Schryver, F. C. and Meijer E. W. *Nano Lett.* **2004**, *4*, 1175.
5 Miura, A.; Jonkheijm, P.; De Feyter, S.; Schenning, A. P. H. J.; Meijer, E. W. and De Schryver F. C. *Small* **2005**, *1*, 131.
6 Vanoppen, P.; Grim, P. C. M.; Rücker, M.; De Feyter, S; Moessner. G; Valiyaveettil, S.; Müllen, K. and De Schryver, F. C. *J. Phys. Chem.* **1996**;*100* 196363.
7 Yang, Y. and Chen, W. *Curr. Opin. Colloid Interface Sci.* **2009**, *14*, 135.
8 Takami, T.; Mazur, U. and Hipps K. W. *J. Phys. Chem. C* **2009**, *113*, 17479.
9 Mamdouh, W.; Uji-i, H.; Dulcey, A. E.; Percec, V.; De Feyter, S. and De Schryver, F. C. *Langmuir* **2004**, *20,* 7678.
10 Lackinger, M.; Griessl, S.; Heckl, W. M.; Hietschold, M. and Flynn, G. W. *Langmuir* **2005**, *21*, 4984.
11 Li, C. J.; Zeng, Q. D.; Wang, C.; Wan, L. J.; Xu, S. L.; Wang, C. R. and

Bai, C. L. *J Phys Chem B* **2003**;*107*:747.

Chapter 5: Emerging Solvent-Induced Homochirality by the Confinement of Achiral Molecules against a Solid Surface

5.1 Introduction

In previous chapters, the emergence, transmission and amplification of chirality in ordered self-assembled monolayers have been discussed. Due to the geometrical restrictions introduced by 2D confinement,[1,2,3,4] chiral information can be easily transferred by chiral molecules in most of the cases. Achiral molecules are also able to form locally chiral 2D structures. Certain achiral molecules can be described as prochiral – one desymmetrising step away from chirality – if they become asymmetric when they are constrained to a surface. However, for some achiral systems, both chirality and ordering are lost due to the lack of stereogenic centers. Homochirality in achiral enantiomorphous monolayers can be realized by merging chiral modifiers in the monolayer[5] or by exposing monolayers to magnetic fields.[6] Alternatively, the potential role of solvents in amplification of chirality and emergence of homochirality at surfaces remains unexplored to date.

How solvent-induced macroscopic chirality emerges within self-assemblies of achiral molecules on achiral surfaces is shown in this chapter. It is an exclusive surface-confined process, and as such it differs from “chiral-solvent-” or “chiral-guest-induced” chirality of supramolecular systems in solution.

As shown in chapter 4, the chiral molecule, (*S*)-oligo(*p*-phenylenevinylene) diamino triazine ((*S*)-OPV4T, Figure 5.1)), assembles exclusively in a counter-clockwise (CCW) hydrogen-bonded rosette motif at the liquid–solid interface, with 1-phenyloctane or 1-octanol as the achiral solvent.[7,8] Molecular homochirality is expressed at the supramolecular level as a result of the 2D packing of the chiral rosette.

In this chapter, the corresponding achiral analogue is used to

demonstrate that supramolecular homochirality emerges at the interface between a chiral liquid and the surface of HOPG.[9]

The choice of a particular chiral solvent was guided by the anticipated need to maximize possible interactions between the chiral solvent and A-OPV4T, i.e. π-stacking and hydrogen bonding interactions, in order to facilitate the transmission of chiral information to A-OPV4T assemblies. On the other hand, technical limitations related to imaging at the liquid-solid interface, such as electrochemical inertness of the solvent at the bias voltages applied (to avoid Faraday currents), low vapor pressure (to avoid evaporation), and low substrate affinity (to avoid solvent monolayer formation), furthermore limited the range of chiral solvents to be selected. Considering these restrictions, solvents such as 1-phenyl-1-octanol (Figure 5.1B), 2-octanol (Figure 5.1C) and citronellol (Figure 5.1D) turned out to be particularly promising candidates. 1-Phenyl-1-octanol represents the logical hybrid form between 1-phenyloctane and 1-octanol, solvents typically used for scanning tunneling microscopy (STM) imaging at the liquid–solid interface. Furthermore, it was expected that 1-phenyl-1-octanol would be a good solvent, as it has the possibility to interact with the diamino triazine moiety in A-OPV4T through hydrogen bonding. In addition, 1-phenyl-1-octylacetate (Figure 5.1E) was considered to be an interesting reference solvent because of the anticipated difference in

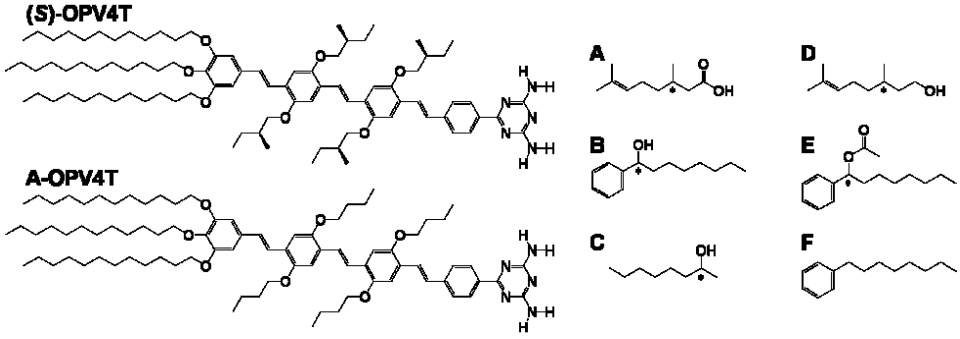

Figure 5.1 *Molecular structures of the chiral ((S)-OPV4T) and achiral (A-OPV4T) 1,3-diamino triazine oligo(p-phenylenevinylene) oligomers. Solvents used in this study: A) citronellic acid, B) 1-phenyl-1-octanol, C) 2-octanol, D) citronellol, E)1-phenyl-1-octylacetate and F) 1-phenyloctane.*

hydrogen-bonding interactions: whereas the acetate group is a hydrogen-bond acceptor, the hydroxy group can function both as hydrogen-bond acceptor and donor.

5.2 Experimental

Scanning Tunneling Microscopy. Prior to imaging, A-OPV4T or (*S*)-OPV4T were dissolved by sonication (few minutes) and heating at 40 °C (15 minutes). The solutions obtained had a concentration ranging between 10^{-4} to 10^{-5} M. 2-Octanol (Fluka), citronellol (SAFC) and citronellic acid (Aldrich) are commercially available. Other details can be found in the experimental part in chapter 2.

Organic Synthesis. The OPV derivatives were provided by Dr. A. P. H. J. Schenning and Prof. E. W. Meijer (TUEindhoven). 1-phenyl-1-octanol and 1-phenyl-1-octylacetate were synthesized by the group of Prof. B. Feringa (Universiteit Groningen). Since these two chiral solvents were specially designed and prepared for the investigation in this chapter, the synthesis procedure will be introduced below.

Racemic 1-phenyl-1-octanol was prepared by Grignard addition of heptyl magnesium bromide to benzaldehyde using standard techniques (Figure 5.2). Purification was achieved by column chromatography over SiO_2 (gradient heptane - heptane/EtOAc 9:1). To obtain samples for use in STM measurements, the compound was further purified by Kugelrohr distillation.

Acetylation was achieved by subjecting 1-phenyl-1-octanol to acetic anhydride in pyridine at 0 ºC overnight (Figure 5.3).

Enantiomerically pure 1-phenyl-1-octanol was prepared by applying the procedure of Mori and Bernotas on a large scale (Figure 5.4).

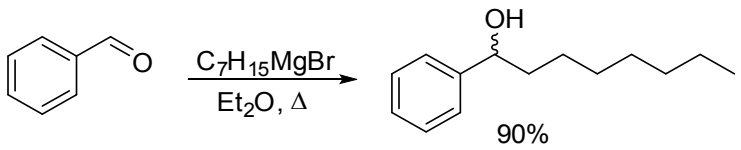

Figure 5.2 *Synthesis of racemic 1-phenyl-1-octanol.*

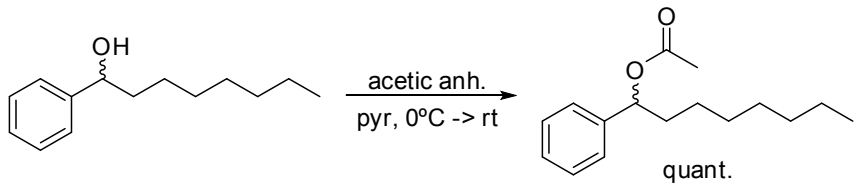

Figure 5.3 *Acetylation of 1-phenyl-octanol.*

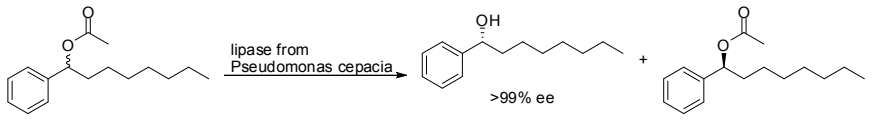

Figure 5.4 *Enzymatic kinetic resolution of 1-phenyl-octyl acetate.*

UV/Vis and CD spectroscopy. Circular-dichroism (CD) spectra were recorded using a JASCO J-600 spectropolarimeter, where the sensitivity, time constant and scan-rate were chosen appropriately; UV/vis spectra were obtained using a Perkin Elmer Lambda 40P. A Peltier temperature programmer model 1 (PTP-1) was used to measure temperature variable UV/vis spectra between 0° and 80°. Measurements at low temperature were not possible at lower temperatures because the used solvents freeze at -5°C.

5.3 Results and Discussion

When depositing solutions of A-OPV4T in achiral solvents (e.g., 1-phenyloctane, 1-octanol) on HOPG, the monolayer is characterized by large disordered areas, which in addition to dimers contain tetramers and cyclic rosettes.

In chapter 4, it was shown that solvents have a pronounced influence on the monolayer patterns, degree of ordering and orientation of the monolayers formed by A-OPV4T. To investigate any amplification of chirality induced by chiral solvents, the supramolecular structures formed by A-OPV4T must be stable and well-ordered so that their chiral nature can be evaluated. Figure 5.5 shows STM results of a monolayer of

A-OPV4T formed at the (*S*)-citronellic acid - HOPG interface. As observed in 1-phenyloctane, A-OPV4T molecules need a long time to form a stable monolayer. In the first several hours after deposition of a droplet of (*S*)-citronellic acid containing A-OPV4T, mainly rows of dimers are observed which propagate along different directions. Due to the high degree of disorder, it is not feasible to evaluate the chirality of these monolayers. Only after 7 hours, "2" (CW) supramolecular rosettes are observed which form locally homochiral domains. However, due to the slow dynamics of the monolayer formation, it is difficult to obtain large homochiral areas, which makes a reliable analysis difficult. The effect of chiral solvent on the structural changes of the monolayer is hard to conclude because when the solvent evaporates, the concentration of the solution on the surface may change.

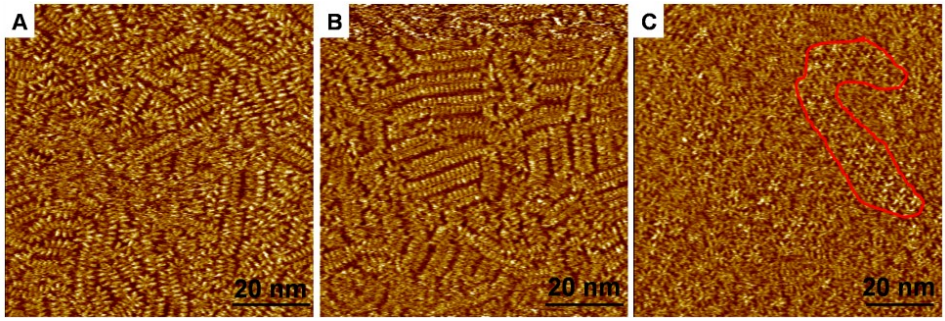

Figure 5.5 *STM images of A-OPV4T physisorbed at the (S)-citronellic acid - HOPG interface (I_{set} = 0.015 nA; V_{set} = -0.6 V). A) recorded 1 hour after deposition, B) recorded 5 hours after deposition, C) recorded 7 hours after deposition. The area indicated in red contains an assembly of locally ordered homochiral A-OPV4T rosettes.*

As shown in the previous chapter, achiral alkylated alcohols such as 1-octanol promote the fast self-assembly of A-OPV4T into well-ordered 2D crystals at equilibrium. In contrast, depositing A-OPV4T at the *racemic*-1-phenyl-1-octanol - HOPG interface leads to amorphous areas at the initial stage of the self-assembly process. The monolayer is indeed characterized by large disordered areas, which in addition to dimers, tetramers and other (cyclic) oligomers also contains small ordered domains of rosettes (Figure 5.6A). In time and depending on experimental conditions, larger areas of ordered rosettes with "2" (CW) and "5" (CCW)

orientations were obtained (Figure 5.6B).

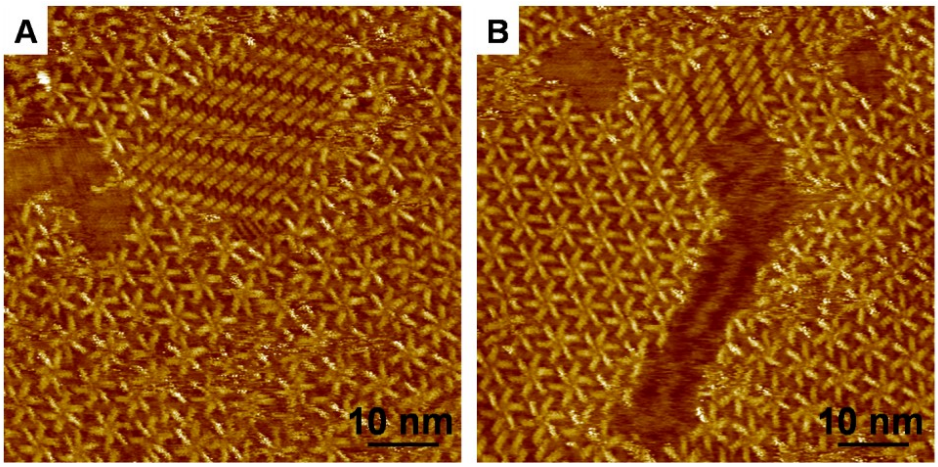

Figure 5.6 *STM images of A-OPV4T physisorbed at the racemic-1-phenyl-1-octanol - HOPG interface (I_{set} = 0.6 nA; V_{set} = -0.2 V). A) recorded 0.5 hour after deposition, B) recorded 2.5 hours after deposition.*

Although results varied from session to session, by using enantiopure 1-phenyl-1-octanol as solvent, the surface coverage of well-ordered rosettes increases faster during a measuring session (Figure 5.7A). Similar to enantiopure OPV4T molecules in achiral solvent - HOPG interface, rosettes formed by A-OPV4T can be classified in the same way: “2” type (CW) or “5” type (CCW) orientations. From large scale images (Figure 5.7A), it appears that, within the observed monolayer, there is a clear bias towards “2” (CW) orientation in (*S*)-1-phenyl-1-octanol and “5” (CCW) orientation in (*R*)-1-phenyl-1-octanol. This finding indicates that because of the chiral confinement of A-OPV4T against the surface, “2” (CW) and “5” (CCW) rosette motifs formed at the interface between HOPG and a chiral solvent are energetically non-equivalent and there is a strong preference for a given rosette's chirality.

In addition to the expression of chirality at the level of the rosettes, the next level in their hierarchical self-assembly, that is, the relative orientation of the rosettes within the monolayer, is chiral and solvent-dependent too (Note the sequence of the longer black and shorter white marker lines in Figure 5.7B and Figure 5.7C, which connect the

terminal phenyl groups of similarly oriented OPV units along unit cell vector b. Their sequence and relative orientation highlight the chiral

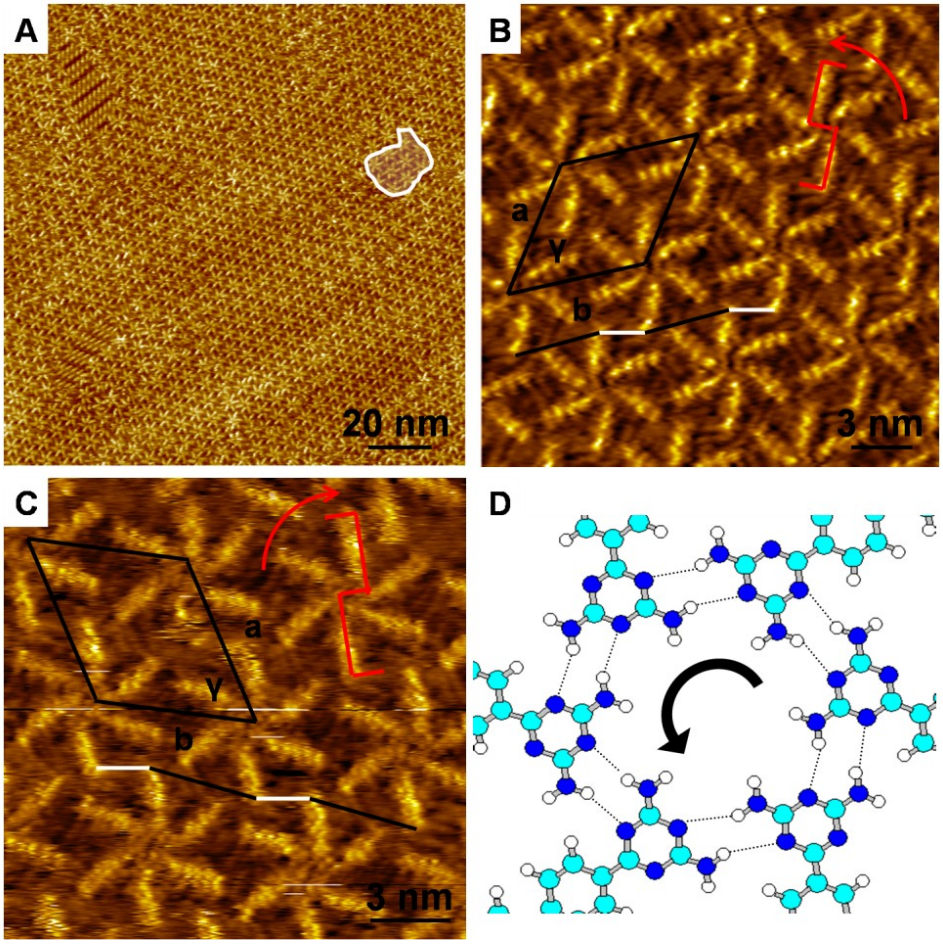

Figure 5.7 *A) and B) STM images of an A-OPV4T monolayer at the (R)-1-phenyl-1-octanol - HOPG interface. A) In addition to several domains of "5" (CCW) rosettes, one "2" (CW) domain is observed as marked (I_{set} = 0.03 nA; V_{set} = -0.57 V). B) Zoomed image of the "5" (CCW) rosette (I_{set} = 0.01 nA; V_{set} = -0.65 V). C) STM image of an A-OPV4T monolayer at the (S)-1-phenyl-1-octanol - HOPG interface (I_{set} = 0.01 nA; V_{set} = -0.65 V) D) Anticipated hydrogen-bonding motif of the "5" (CCW) orientation, involving six A-OPV4T molecules. Blue arrows indicate the nitrogen atoms which remain free to interact by hydrogen bonding with the solvent molecules; dark blue N, light blue C, white H. Unit cells are indicated in black. Orientations and rotations are shown in red.*[9]

nature of the monolayer). In both enantiomeric pure solvents, many ordered domains of variable size were observed. Within a given domain, the rosettes are ordered in rows and form a homochiral crystalline lattice characterized by the following unit cell parameters which are within experimental error identical to those of (*S*)-OPV4T at the 1-phenyloctane - HOPG interface and A-OPV4T at the 1-octanol - HOPG interface: a = 6.11± 0.06 nm, b = 6.13 ± 0.04 nm, γ = 60 ± 1° in (*S*)-1-phenyl-1-octanol (Figure 5.7C) and a = 6.09 ± 0.06 nm, b = 6.04 ± 0.05 nm, γ = 62 ± 2° in (*R*)-1-phenyl-1-octanol (Figure 5.7B). A-OPV4T self-assembles into a chiral pattern in accordance with the plane group *p*6, which is one of the five chiral plane groups.[10,11]

To confirm solvent-induced asymmetric induction at the liquid-solid interface, a statistical analysis was performed indexing the individual rosettes as “2” (CW) or “5” (CCW). This analysis was carried out by using several batches of solvent and substrates, and by probing more than a thousand rosettes for each experiment. The results show that monolayer formation in enantiomeric pure 1-phenyl-1-octanol solvents clearly leads to solvent-induced asymmetric induction (Table 5.1). A 100% asymmetry induction is never observed though, likely because of the slow kinetics of the ordering process. The measured enantiomeric ratios (“5” versus “2”) range from 17:83 (“5”:“2”) in (*S*)-1-phenyl-1-octanol to 91:9 (“5”:“2”) in (*R*)-1-phenyl-1-octanol. These values are comparable within the experimental error. Whereas high enantiomeric ratios are obtained in enantiopure solvents, the proportion of “2” and “5” rosettes of A-OPV4T at the interface between the racemic solvent mixture and HOPG is approximately equal.

These results demonstrate the crucial influence of the solvent in inducing macroscopic chirality of achiral molecules at the liquid-solid interface. To get more insight in the role of the solvent and its specific interaction with A-OPV4T, the influence of the solvent was screened and in particular of the H-bonding interactions between A-OPV4T and the solvent. Similar experiments were performed in (*R*)-1-phenyloctylacetate and (*S*)-1-phenyl-octylacetate, which differ from (*R*)-1-phenyl-1-octanol and (*S*)-1-phenyl-1-octanol in their H-bonding properties: the former bear an –OH group and the latter an –OAc group. Similar to the experiments in 1-phenyloctane, the monolayers are disordered with only locally small

rosette domains. The statistical analysis of sets of STM images reveals a

Table 5.1 *Asymmetric induction in A-OPV4T monolayers at various liquid–solid interfaces. All STM images were obtained at least one hour after deposition on the surface, to allow the monolayers to organize in view of the dynamics taking place. Typically, the waiting time was longer for rac-1-phenyl-1-octanol than for the corresponding enantiomeric pure solvent. A significant number of areas per solvent was probed: (R)-1-phenyl-1-octanol (16 areas), (S)-1-phenyl-1-octanol (17), rac-1-phenyl-1-octanol (52), (R)-1-phenyl-1-octyl acetate (13), (S)-1-phenyl-1-octyl acetate (15),* (*S*)-2-octanol (30) and (*S*)-β-citronellol (20)*. The standard deviation of the weighted mean of the enantiomeric ratio (so corrected for the number of chiral rosettes per area) is given in parentheses. Note that the standard deviation for a constant number of probed rosettes should become smaller by scanning larger areas, which is limited though by the need for high spatial resolution.*[9]

Solvent	1) No. of rosettes analyzed 2) % of distinct rotating rosettes ("5" + "2")	1) Enantiomeric ratio "5":"2" 2) (Stand.Dev.)
(*R*)-1-phenyl-1-octanol	2209 86	91 : 9 (9)
(*S*)-1-phenyl-1-octanol	1948 71	17 : 83 (14)
rac-1-phenyl-1-octanol	4190 78	54 : 46 (14)
(*R*)-1-phenyl-octyl acetate	1019 44	55 : 45 (15)
(*S*)-1-phenyl-octyl acetate	1194 42	48 : 52 (12)
(*S*)-2-octanol	3663 89	69 : 31 (5)
(*S*)-β-citronellol	3242 88	63 : 37 (6)

very small bias in favor of either “5” or “2” rosettes in (*R*)-1-phenyl-1-octylacetate and in (*S*)-1-phenyl-octylacetate, respectively. This bias, however, is negligible and within the experimental error. These results demonstrate that hydrogen bonding interactions between the solvent molecules and A-OPV4T are keys in inducing surface chirality, most probably by allowing H-bonding of the molecules from the self-assembled monolayer, with the solvent. The alcohol moiety from the solvent may opens the possibility to form a hydrogen bond with one of the nitrogen atoms from the A-OPV4T diamino triazine unit, which remains unbound despite the formation of the rosettes (Figure 5.7D).

The key role of the –OH group in alcoholic solvents can be further proven by using other chiral solvents. The orientations of the rosettes formed by A-OPV4T at the (*S*)-2-octanol - HOPG or (*S*)-β-citronellol - HOPG also show a clear bias. The enantiomeric ratio of “5” : ”2” rosettes is 69 :31 in (*S*)-2-octanol and 63 : 37 in (*S*)-β-citronellol. In time, the ordering and the enantiomeric ratio of a specific area increased (Figure 5.8). Note that both the enantiomeric ratio in (*S*)-2-octanol and (*S*)-β-citronellol is reversed in

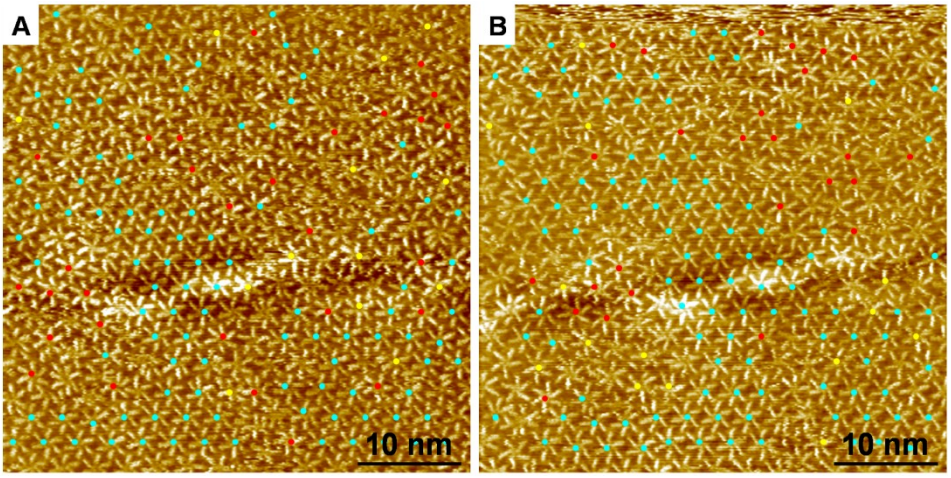

Figure 5.8 *A) First and B) last frame of a sequence of STM images of an A-OPV4T monolayer at the (S)-2-octanol - HOPG interface recorded at the same area. The time gap between the frames is about 3 minutes. The center of the rosettes is color-coded: “5” (blue), “2” (red), n-o (not-ordered) orientation (yellow). The irregular HOPG boundary in the middle of the images indicates that both images are captured at the same location. The enantiomeric ratio is 77 : 23 and 81: 19 in A) and B), respectively.*

comparison to (*S*)-1-phenyl-1-octanol. As far as (*S*)-2-octanol and (*S*)-1-phenyl-1-octanol are observed, this is to be expected, as the chirality of the stereogenic centers is different (by replacing a 'methyl' group by a 'phenyl' group, the absolute configuration changes following the Cahn-Ingold-Prelog rules; so, (S)-2-octanol is the equivalent of (*R*)-1-phenyl-1-octanol). For citronellol, a comparison is not possible. The limited number of chiral protic solvents tested does not allow yet to draw general conclusions concerning the effect of the absolute configuration of the solvent on the amplification of chirality.

To obtain further evidence for the specific role played by interfacial confinement in the formation of chiral rosettes, the behavior of A-OPV4T in solution was examined by UV/Vis absorption and circular dichroism (CD) measurements (Figure 5.9). The aim of these experiments was to demonstrate that potential *pre*-formation of the rosettes in solution does not occur. For typical concentrations used for STM (c = 3 x 10^{-5} mol/L) and at room temperature, no significant CD signal was ever observed in either 1-phenyloctane, (*R*)- or (*S*)-1-phenyloctanol, -1-phenyl-1-octylacetate and the UV/Vis absorption spectra were characteristic for molecularly dissolved oligomers showing that there is neither chiral nor achiral aggregation of A-OPV4T in these solvents. Therefore, the rosettes exclusively form at the liquid-solid interface. This conclusion is supported by complementary evidence from STM measurements. Indeed, at an early stage of deposition on the surface (typically after a few minutes), the observed monolayer has a morphology

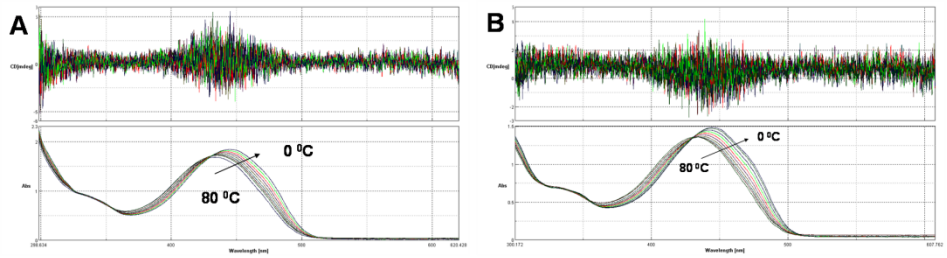

Figure 5.9 *CD spectra (top panel) and Uv/Vis spectra (bottom panel) of A-OPV4T in A) (R)-1-phenyloctanol (2.7 x 10^{-4} M), B) (R)-1-phenyl-1-octylacetate (2.0 x 10^{-4} M), for a range of temperatures comprised between 0° and 80°. The spectra have been registered in a 1 mm thick cuvette.*[9]

resembling strongly that of the disordered monolayers typically observed from achiral solvents.

A solvent monolayer acting as a chiral template underneath the rosettes is unlikely because at room temperature, in the absence of the A-OPV4T molecules, deposition of (*R*)-1-phenyl-1-octanol or (*S*)-1-phenyl-1-octanol on HOPG never resulted in the observation of any ordered layer. In addition, the unit cell parameters of ordered rosette domains in the different solvents are identical, regardless if chiral induction is observed or not. Combined with the fact that the unit cell parameters are also identical to those of (*S*)-OPV4T, it is safe to conclude that solvent molecules are not co-adsorbed within the plane of the monolayer, that is, there are no solvent molecules between the rosettes.

STM at the liquid–solid interface not only allows the extent of chiral induction on the surface to be evaluated, but also enables how homochirality emerges to be observed (Figure 5.10). Therefore, series of STM images were recorded at the (*R*)-1-phenyl-1-octanol - HOPG interface over a period of 50 min. For each frame, the number of “5”, “2” rosettes, and ill-defined cyclic hexamers with no identifiable orientation (not-ordered (n-o)) have been measured and their evolution in time is indicated in Figure 5.10C, revealing a clear correlation between the appearance of order and the emergence of chirality. Over time, the number of “5” rosettes increases at the expense of those with no identifiable orientation (n-o) and, to a lesser extent, of the “2” rosettes. In this time-dependent sequence, the enantiomeric ratio increases from about 50 : 50 “5” : “2” to 80 : 20 “5” : “2” after 50 min. For the same sample, but at a different area, a similar sequence of images was recorded, but starting three hours later. In this case the initial enantiomeric ratio is already at a high level and doesn’t change significantly in time. This evolution from non-ordered rosettes to “5” or “2” rosettes, or the evolution from “2” rosettes into “5” rosettes (or vice versa), depending on the chirality of the solvent, was observed in all our experiments. As an example, Figure 5.11 shows the evolution of a “2” rosette into a “5” rosette. The conversion of n-o rosettes to “2” or “5” rosettes happens both at domain boundaries and in the bulk of the disordered domains. This conversion is not necessarily faster at domain boundaries but there the nature of the conversion (forming “2” or “5” rosettes) is clearly dictated by

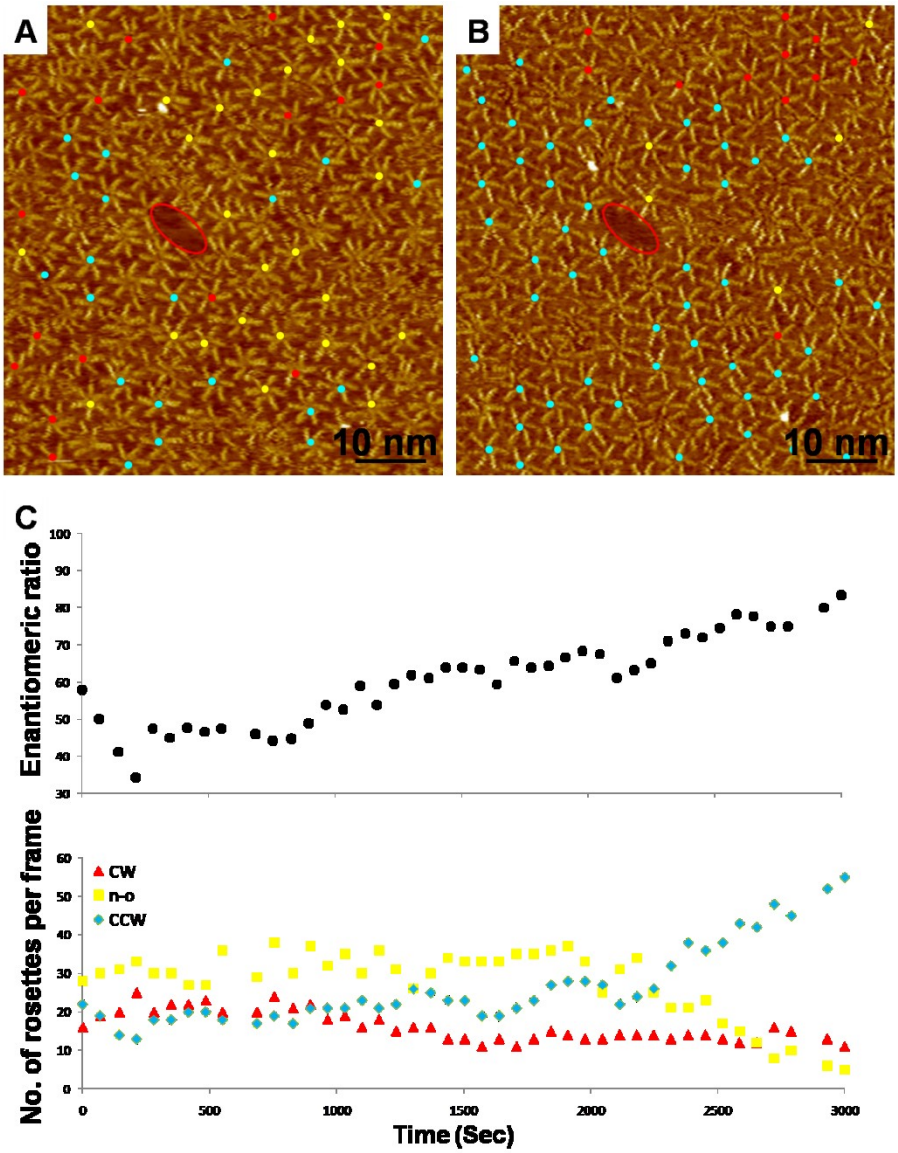

Figure 5.10 *A) First and B) last frame of a sequence of STM images of an A-OPV4T monolayer at the (R)-1-phenyl-1-octanol - HOPG interface recorded at the same area. The time gap between the frames is 50 minutes. The center of the rosettes is color-coded: "5" (blue), "2" (red), n-o (not-ordered) orientation (yellow). The red bordered dark defect area acts as a marker region. C) Evolution of the enantiomeric ratio ("5"/("5"+"2")) and the number of rosettes of a given orientation ("5", "2", or n-o orientation) as a function of time.*[9]

the chirality of the ordered domain. Clearly, as a result of the confinement, in well packed domains the conversion of “2” into “5” rosettes (or vice versa) happens primarily at the domain boundaries. Similarly, the transition of other structures, such as dimers to rosette-type objects has also been identified.

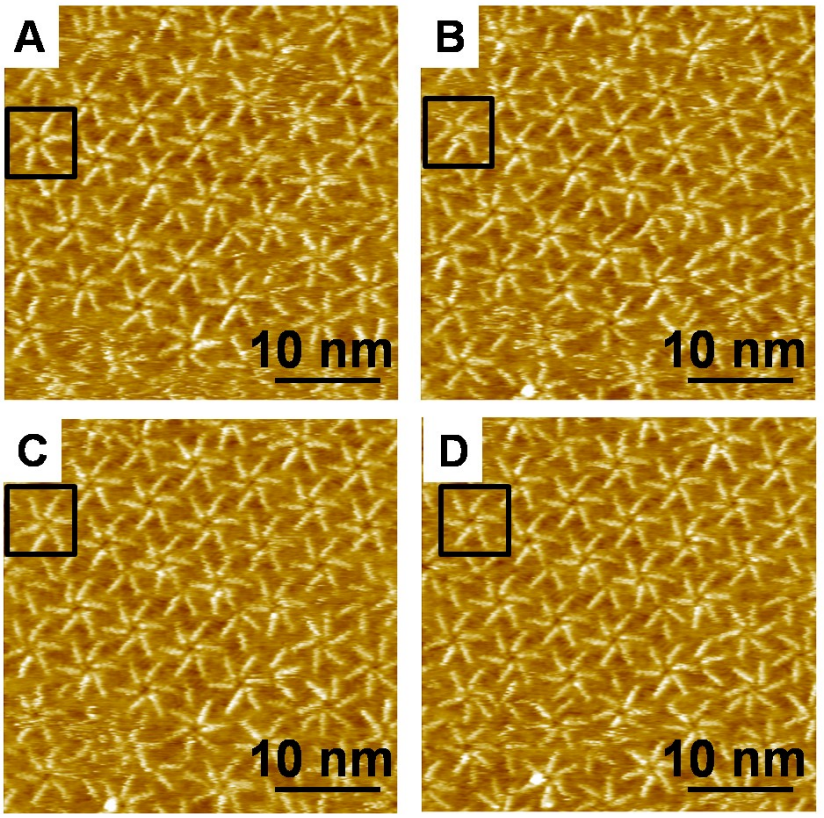

Figure 5.11 *A sequence of STM images of an A-OPV4T monolayer at the (R)-1-phenyl-1-octanol - HOPG interface recorded at the same area. The area of interest is indicated by the black square. The time gap between two adjacent images is 47 seconds. Over time, the irregular cyclic hexamer indicated in the square evolves into a “5” rosette.*

Multiple pathways to the emergence of homochirality coexist. Disorder-order transitions occur not only at the level of the individual rosettes but also at the monolayer level. It is hard to foresee how an isolated rosette will have the preferred chirality because 2D crystallization also plays a role in the chiral selection: in the 2D lattice, the preference of

a conglomerate 2D lattice over the racemic lattice will lead to the addition of small energy differences at the supramolecular level.
The actual mechanism of chiral selection that favors the formation of rosettes with a particular handedness during 2D crystallization is not known. It probably involves interactions between the solvent and the rosettes, chiral desolvation processes, steric restrictions within the monolayer-in which order is favored-or, most probably, an interplay of all these effects. The time dependence reflected in our experiments does not support a hypothesis of emergence of homochirality purely resulting from improved order and underlines the importance of additional kinetic effects. One possible scenario is that upon surface-mediated self-assembly, individual rosettes are formed. The unbound nitrogen atoms in these rosettes (Figure 5.7D) are likely to transiently interact through hydrogen bonding with the solvent molecules. In an achiral solvent, physisorption by desolvation leads to the disappearance of these complexes and the formation of physisorbed rosettes, without any favored handedness. However, the use of a chiral solvent favors the formation of transient complexes with a particular handedness. Upon desolvation, rosettes with a particular handedness are formed on the surface. The self-assembly of rosettes with the same handedness further improves the order within the monolayer. Other weak interactions such as π-π interaction may also be involved in the formation of transient complexes.

5.4 Conclusions

In summary, 2D crystallization at the interface between an achiral surface and a chiral solvent can produce enantiomerically enriched, and even homochiral organic surfaces. In other words, chirality on one scale (a stereocenter in a chiral solvent molecule) has been manifested on the larger scales of a surface-confined hierarchical supramolecular assembly. The demonstration of control of chirality on surfaces in synthetic achiral molecular systems by chiral solvents is a simple method and is of considerable interest for asymmetric synthesis, heterogeneous asymmetric catalysis, chiral separation, or the fabrication of advanced functional materials.

5.5 References

1 Ortega Lorenzo, M.; Baddeley, C. J.; Muryn, C. and Raval, R. *Nature* **2000**, *404*, 376.

2 Kühnle, A.; Linderoth, T. R.; Hammer, B. and Besenbacher, F. *Nature* **2002**, *415*, 891.

3"Supramolecular surface chirality": Ernst, K. H. *Top. Curr. Chem.* **2006**, *269*, 209.

4 De Feyter, S. and De Schryver F. C. in Scanning Probe Microscopies beyond Imaging: Manipulation of Molecules and Nanostructures, Wiley-VCH, Weinheim, **2006**.

5 Parschau, M.; Romer, S.and Ernst, K.-H. *J. Am. Chem. Soc.* **2004**, *126*, 15398.

6 Berg, A. M.and Patrick, D. L. *Angew. Chem. Int. Ed.* **2005**, *44*, 1821.

7 Jonkheijm, P.; Miura, A.; Zdanowska, M.; Hoeben, F. J. M.; De Feyter, S.; Schenning, A. P. H. J.; De Schryver, F. and Meijer, E. W. *Angew. Chem. Int. Ed.* **2004**, *43*, 74.

8 Miura, A.; Jonkheijm, P.; De Feyter, S.; Schenning, A. P. H. J.; Meijer, E.W. and De Schryver, F. C. *Small* **2005**, *1*, 131.

9 Katsonis, N.; Xu, H.; Haak, R. M.; Kudernac, T.; Tomović, Ž.; George, S.; Van der Auweraer, M.; Schenning, A. P. H. J.; Meijer, E. W.; Feringa, B. L. and De Feyter, S. *Angew. Chem. Int. Ed.* **2008**, *47*, 4997.

10 Barlow, S. M. and Raval, R. *Surf. Sci. Rep.* **2003**, *50*, 201.

11 Plass, K. E.; Grzesiak, A. L. and Matzger, A. J. *Acc. Chem. Res.* **2007**, *40*, 287.

Chapter 6: Molecular Recognition of Monolayers at a Liquid-solid Interface

6.1 Introduction

In the previous chapter, solvent induced two-dimensional chirality has been discussed. Solvent molecules such as 1-phenyl-1-octanol act as chiral modifiers in the self-assembly of an achiral building block on an achiral substrate and produce enantiomerically enriched, and even homochiral organic surfaces. Though the actual mechanism of chiral selection is still unclear, solvent molecules do play a very important role in the amplification of chirality. In few studies, monolayers have been formed upon mixing achiral and chiral molecules. For instance, chiral molecules can co-adsorb with structurally similar achiral molecules and act as mere chiral markers in co-adsorbed domains, i.e. they don't affect the overall monolayer structure.[1,2] Alternatively, the expression of chirality at the liquid-solid interface can be amplified or expressed by the co-adsorption of achiral molecules.[3,4] From a fundamental point of view, there is clearly need for a more comprehensive study of multicomponent systems.

Besides these fundamental aspects, the separation of enantiomers is an area of great interest and activity because of its importance in for instance the pharmaceutical industry. In a number of separation techniques, the interaction of molecules with a surface is crucial (e.g. the use of chiral columns in liquid chromatography). In several studies, surfaces have been modified to direct the enantioselective self-assembly (crystallization) of different enantiomers.[5,6,7] Such enantioselective adsorption processes are not yet demonstrated on achiral surfaces.

In this chapter, molecular recognition at the liquid-solid interface was introduced by using two chiral components: resorcinol and diaminocyclohexane (Figure 6.1). The acid and amine functional groups make it possible for these two building blocks to co-adsorb on the surface, which makes this system a perfect plateau to investigate the roles each chiral component plays in the chiral expression of the co-adsorbed

monolayers.

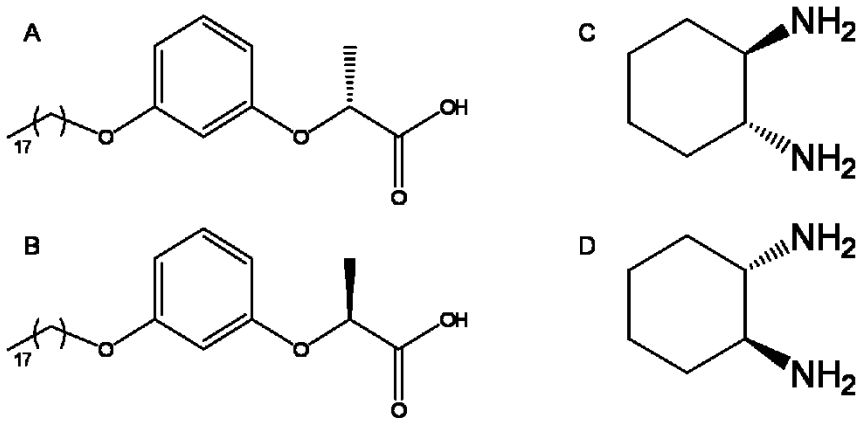

Figure 6.1 *Molecular structures of the chiral resorcinol and diaminocyclohexane. (A) (R)-resorcinol (R-**1**), (B) (S)-resorcinol (S-**1**), (C) (1R,2R)-(-)-diaminocyclohexane ((R,R)-**2**), (D) (1S,2S)-(+)-diaminocyclohexane ((S,S)-**2**).*

6.2 Experimental

Scanning Tunneling Microscopy. (*R*)- and (*S*)-**1** were dissolved in 1-phenyloctane at a concentration of 7.6×10^{-3} M. Without specific indication, the sum of the resorcinol concentrations was kept constant in all experiments. (*R*,*R*)-**2** and (*S*,*S*)-**2** solutions were premixed with resorcinol solutions. Premixed samples were always heated to approximately 70 °C before imaging. Other experimental details are similar to those reported in chapter 2.

6.3 Results and Discussion

First, each component was investigated independently. Resorcinol molecules contain acid groups as hydrogen-bonding units and alkyl chains which favor self-assembly at the liquid-solid interface. Figure 6.2 shows STM images of monolayers of enantiopure *R*-**1** and *S*-**1** molecules adsorbed on HOPG. The aromatic head groups can often but not always

be distinguished as bright spots. Sometimes, the STM contrast at the level of the resorcinol groups is complex and does not allow resolving individual resorcinol groups, which may indicate a certain flexibility in their orientation. Those cases where individual resorcinol groups can be identified show that nearest neighbor molecules of different rows form dimer structures which most likely are stabilized by hydrogen bonding. These dimers propagate along one direction and lamellae type patterns can be observed in large areas. Alkyl chains are fully extended, adsorbed on the surface and interdigitated with those of adjacent rows. The width of a row (D) is about 3.7 nm (Table 6.1). By eye it is not possible to identify the chiral nature of the supramolecular patterns and as individual resorcinol groups are not always distinguishable, describing the monolayer packing in terms of a unit cell is not very meaningful, nor useful.

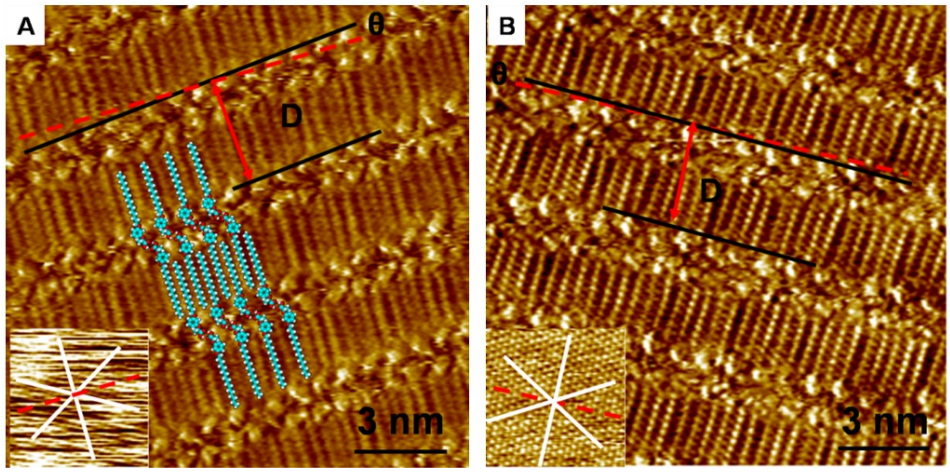

Figure 6.2 *STM images of **1** physisorbed at the 1-phenyloctane-HOPG interface. A) R-**1** (I_{set} = 0.02 nA; V_{set} = 1.0 V), B) S-**1** (I_{set} = 0.02 nA; V_{set} = 1.04 V). The insets show STM images of HOPG (not to scale) corresponding with sites underneath the monolayer (I_{set} = 1.09 nA; V_{set} = 0.02 V). White solid lines indicate main symmetry axes of HOPG. Red dashed lines indicate the selected HOPG reference axis running perpendicular to one of the main symmetry axes. Black solid lines indicate the direction of molecular rows. Double-headed red arrows show the width (D) of the bi-component rows. In a tentative molecular model, resorcinol molecules are superimposed on the STM image to highlight their respective location.*

Luckily, the propagation direction of the dimer rows with respect to a HOPG reference axes <-1 1 0 0> reveals the monolayer chirality. In case of *S*-**1**, the dimer rows are rotated exclusively clockwise over a small angle (+5±3°: Table 6.1) with respect to the HOPG reference axes <-1 1 0 0>. In case of *R*-**1**, a small anticlockwise rotation (-4±2°: Table 6.1) is observed.

Deposition of a mixture of *R*-**1** and *S*-**1** leads to a conglomerate. Two different types of domains are observed which are identical in structure to those of the pure enantiomers. Moreover, the relative abundance of the enantiomorphous patterns (in terms of the surface coverage) reflects the solution composition of the enantiomers.

Prior to investigating the mixture of **1** and **2**, an attempt was made to probe the monolayer structure of **2**. Molecule **2** is not able to self-assemble though at the 1-phenyloctane - HOPG interface under the conditions used for STM imaging. This not that surprising as the molecule is not flat (relatively weak molecule-substrate interactions) and the lack of strong hydrogen bonding

As will be shown below, under some conditions co-adsorbed patterns of **1** and **2** can be observed upon premixing. Importantly, molecule **2** recognizes the handedness of molecule **1** as in diastereomeric complex formation.

Figure 6.3 shows monolayers formed by *R*-**1**+(*R*,*R*)-**2** and *S*-**1**+(*S*,*S*)-**2** at a ratio of 2:1. In both cases, a similar pattern is fomed which differs though from the monolayer structures formed by **1** itself. Molecules order into rows. The width of such a row (D) is about 5.3 nm which is much larger than for enantiopure **1** (3.7 nm). In addition to alkyl chains, STM images reveal sometimes 'blobs' which often appear brighter than the alkyl chains and contain streaks (Figure 6.3b). Alternatively, in some images (e.g. Figure 6.3a) the molecular rows are separated by dark troughs. As suggested by the STM contrast, especially at the level of the alkyl chains, rows consist of tail-to-tail dimers of **1**. Alkyl chains are not interdigitated. This explains only in part though the increased width of the rows. Although molecules **2** cannot be identified in the STM images, the best fit of the molecular models with the STM images requires the formation of a **1**-**2**-**1** complex, the diaminocyclohexane being sandwiched between two resorcinol groups (Figure 6.3). Based on the orientation and

packing of the alkyl chains, the distance between resorcinol groups of adjacent molecules along the row propagation directions measures only ca. 0.7 nm, which is significantly less than for the enantiopure system (ca. 1.0 nm). This result indicates that the aromatic part of **1** can't lie flat on the surface, but must be tilted, which is in line with the streaky features observed.

In contrast to the enantiopure systems, two-dimensional chirality of the monolayers can clearly be determined by the orientation of the alkyl chains with respect to the molecular propagation direction. For *R*-**1**+(*R*,*R*)-**2**, alkyl chains are rotated clockwise (CW) with respect to the normal on the row propagation direction and counter-clockwise (CCW) in the *S*-**1**+(*S*,*S*)-**2** case. In addition, monolayer chirality is also established by the relative orientation of the row propagation directions with respect to the graphite lattice. The angle between the propagation direction of the

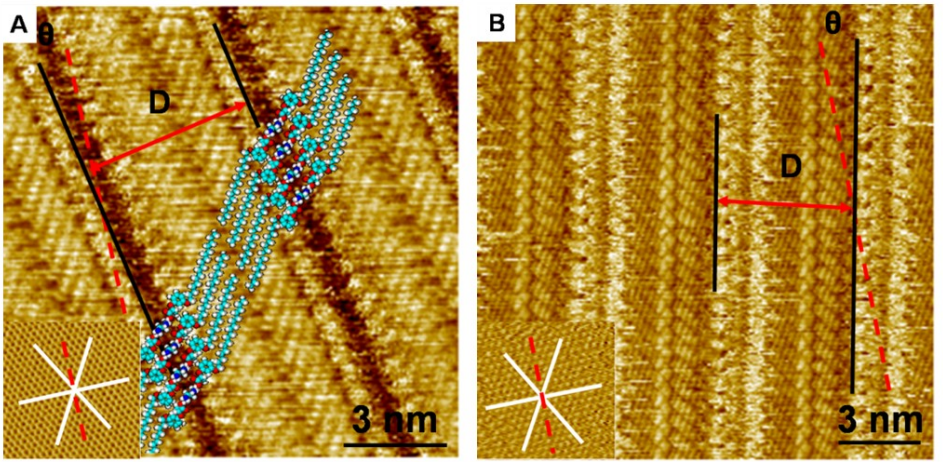

Figure 6.3 *STM images of monolayers formed upon premixing **1** and **2** at the 1-phenyloctane - HOPG interface. A) R-**1**+(R,R)-**2** (2:1) (I_{set} = 0.25 nA; V_{set} = 1.00 V), B) S-**1**+(S,S)-**2** (2:1) (I_{set} = 0.20 nA; V_{set} = 1.00 V). White solid lines indicate graphite main symmetry axes. Red dashed lines indicate the selected graphite reference axis running perpendicular to one of the main symmetry axes. Black solid lines indicate the direction of molecular rows. Double-headed red arrows show the width (D) of the bi-component rows. In a tentative molecular model, resorcinol and diamine molecules are superimposed on the STM image to highlight their respective location.*

rows and the HOPG reference axes <-1 1 0 0> measures -10±2° in monolayers of *R*-**1**+(*R*,*R*)-**2** and +12±3° for *S*-**1**+(*S*,*S*)-**2**.

Different from the combinations mentioned above, mixtures of *R*-**1**+(*S*,*S*)-**2** and *S*-**1**+(*R*,*R*)-**2** with the same ratio 2:1 don't lead to co-adsorption. Only resorcinol molecules are observed in STM images. The molecular packing and chiral expression are identical to those of the enantiopure resorcinol systems.

This opens the possibility to use the resorcinol derivatives as resolving agents for the resolution of a racemic mixture of diaminocyclohexanes, at the liquid-solid interface, without the need of 3D crystallization.

To confirm the ability of **1** to selectively co-adsorb one of the enantiomers of **2**, *R*-**1** or *S*-**1** are premixed with (*R*,*R*)-**2** and (*S*,*S*)-**2** at a ratio of 4:1:1. As hoped, exclusively one enantiomer of **2** is selectively co-adsorbed on the surface. Figure 6.4 shows the STM images of these two

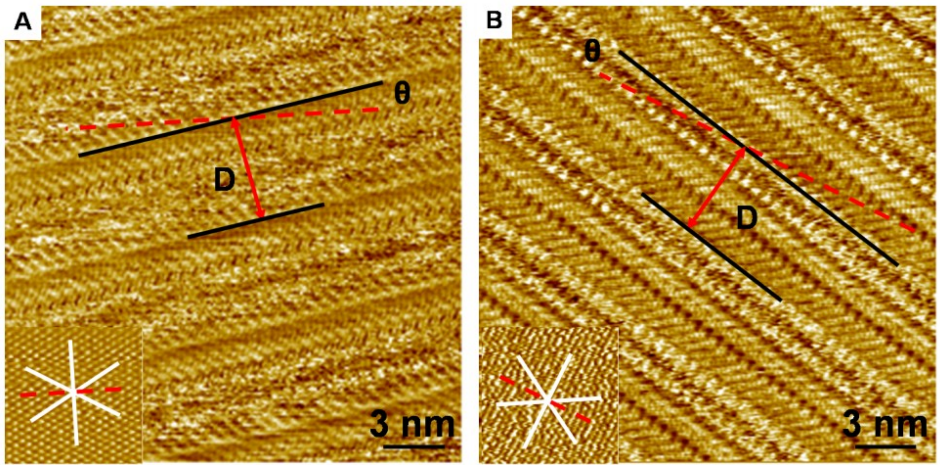

Figure 6.4 *STM images of monolayers formed upon premixing **1** and **2** at the 1-phenyloctane - HOPG interface. A) R-**1**+(R,R)-**2**+(S,S)-**2** (4:1:1) (I_{set} = 0.20 nA; V_{set} = 0.80 V), B) S-**1**+(R,R)-**2**+(S,S)-**2** (4:1:1) (I_{set} = 0.20 nA; V_{set} = 0.80 V). The insets show STM images of graphite (not to scale) corresponding with sites underneath the monolayer (I_{set} = 0.20 nA; V_{set} = 0.001 V). White solid lines indicate graphite main symmetry axes. Red dashed lines indicate the selected graphite reference axis running perpendicular to one of the main symmetry axes. Black solid lines indicate the direction of molecular rows. Double-headed red arrows show the width (D) of the bi-component rows.*

combinations. The structural details of the monolayers formed are listed in Table 6.2.

On the other hand, adding both enantiomers of **2** to one of the enantiomers of **1** (e.g. *R*-**1**) leads to the anticipated bicomponent pattern consisting of *R*-**1** and (*R*,*R*)-**2** and domains of the uncomplexed resorcinol derivative R-1. There is no indication of adsorption of the non-matching enantiomer of **2** ((*S,S*)-**2**). These experiments clearly show the molecular recognition events at the liquid-solid interface.

Table 6.1 *Structural characteristics of the monolayers. Width of adjacent rows (D), angle of row propagation direction with respect to the graphite reference axis (θ), domain composition [compound **1**/compound **2**] and numbers of domains investigated of different combinations of **1** and **2** at the 1-phenyloctane-graphite interface. *simplified notation of compounds, e.g. (R,R)-**2** → R-**2***

Solution composition*	D (nm)	θ (°)	Co-adsorption	Domain composition*	N
R-**1**	3.7±0.2	-4±2	No	*R*-**1**	13
S-**1**	3.7±0.1	+5±3	No	*S*-**1**	21
R-**1**+*S*-**1** (1:1)	3.8±0.1	-3±2	No	*R*-**1**	28
	3.8±0.1	+3±2	No	*S*-**1**	21
R-**1**+*S*-**2** (2:1)	3.7±0.1	-4±2	No	*R*-**1**	22
S-**1**+*R*-**2** (2:1)	3.5±0.2	+4±3	No	*S*-**1**	5
R-**1**+*R*-**2** (2:1)	5.3±0.4	-10±2	Yes	*R*-**1**/*R*-**2**	27
S-**1**+*S*-**2** (2:1)	5.4±0.3	+12±3	Yes	*S*-**1** /*S*-**2**	15
R-**1**+*R*-**2**+*S*-**2** (4:1:1)	5.3±0.1	-10±2	Yes	*R*-**1**/*R*-**2**	4
S-**1**+*R*-**2**+*S*-**2** (4:1:1)	5.1±0.2	+10±3	Yes	*S*-**1** /*S*-**2**	10
R-***1***+*S*-***1***+*R*-**2** *(1:1:1)*	3.7±0.1	+4±3	No	*S*-**1**	8
	5.4±0.2	-9±3	Yes	*R*-**1**/*R*-**2**	11
R-***1***+*S*-***1***+*S*-**2** *(1:1:1)*	4.1±0.1	-1±1	No	*R*-**1**	1
	5.4±0.2	+12±5	Yes	*S*-**1** /*S*-**2**	2

The experiments described above assumed the formation of a **1**-**2**-**1**

complex, which was reflected in the composition of the solutions used. At a 2:1 ratio of the resorcinol enantiomer with respect to the matching diaminocyclohexane, only bicomponent domains were observed.
To gain further insight into the importance of solution composition, i.e. the relative concentrations of the components, a number of additional experiments were carried out.

Table 6.2 *Width of adjacent rows (D), angle of row propagation direction with respect to the graphite reference axis (θ), domain composition [compound **1**/compound **2**] and numbers of domains investigated of different combinations of **1** and **2** at the 1-phenyloctane-graphite interface. *simplified notation of compounds, e.g. (R,R)-**2** → R-**2***

Solution composition*	D (nm)	θ (°)	Co-Adsorption	Domain composition*	n
R-**1**+*R*-**2** (66:1)	3.8±0.1	-2±1	No	*R*-**1**	12
	5.4±0.1	-12±3	Yes	*R*-**1**/*R*-**2**	4
R-**1**+*S*-**1**+*R*-**2** (33:33:1)	4.0±0.2	-4±3	No	*R*-**1**	2
	3.9±0.1	+1±1	No	*S*-**1**	3
	5.0±0.1	-15±1	Yes	*R*-**1**/*R*-**2**	1
R-**1**+*S*-**1**+*S*-**2** (33:33:1)	3.8±0.1	-4±2	No	*R*-**1**	2
	3.7±0.1	+2±1	No	*S*-**1**	1
	5.2±0.1	+11±1	Yes	*S*-**1**/*S*-**2**	2
R-**1**+*S*-**2** (2:10)	5.1±0.1	+19±2	Yes	*R*-**1**/*S*-**2**	10

In a first experiment, the concentration of *R*-**1** was kept constant and the concentration of molecule **2** varied. Upon mixing of *R*-**1** and (*R*,*R*)-**2** at a ratio of 66:1, in addition to bicomponent domains of co-adsorbed *R*-**1** and (*R*,*R*)-**2**, also pure *R*-**1** domains were observed. Surface area calculations indicate that the co-adsorbed structures are favored which indicates they are more stable. Indeed, the surface area covered by pure *R*-**1** domains is only a factor of 5.2 larger than the surface covered by domains of co-adsorbed *R*-**1** and (*R*,*R*)-**2**. On statistical grounds, a 30 times excess was expected for the *R*-**1** domains.
As described above, at a 2:1 ratio, a solution mixture of *R*-**1** and (*S*,*S*)-**2** only leads to *R*-**1** type domains. No (*S*,*S*)-**2** molecules are found on the

surface. However, if we increase the amount of (*S*,*S*)-**2** molecules 10 times (*R*-**1** : (*S*,*S*)-**2** = 1:5), there are strong indications that (*S*,*S*)-**2** molecules are involved in monolayer formation. A new pattern which is similar but not identical to the one formed by *S*-**1** and (*S*,*S*)-**2** is observed three hours after deposition (Figure 6.5A). So, at an excess of (*S,S*)-**2**, (*S*,*S*)-**2** molecules can be co-adsorbed. As the structural parameters of this monolayer show (D = 5.1 ± 0.1 nm, θ = +19±2°, Table 6.2) (*S*,*S*)-**2** dominates the molecular packing and chiral expression. The orientation of the *R*-**1** alkyl chains differs from the situation in bicomponent pattern of *S*-**1** and (*S*,*S*)-**2**. The angle between the alkyl chains and row propagation direction is about 10° larger than for the *S*-**1**+(*S*,*S*)-**2** system. In addition,

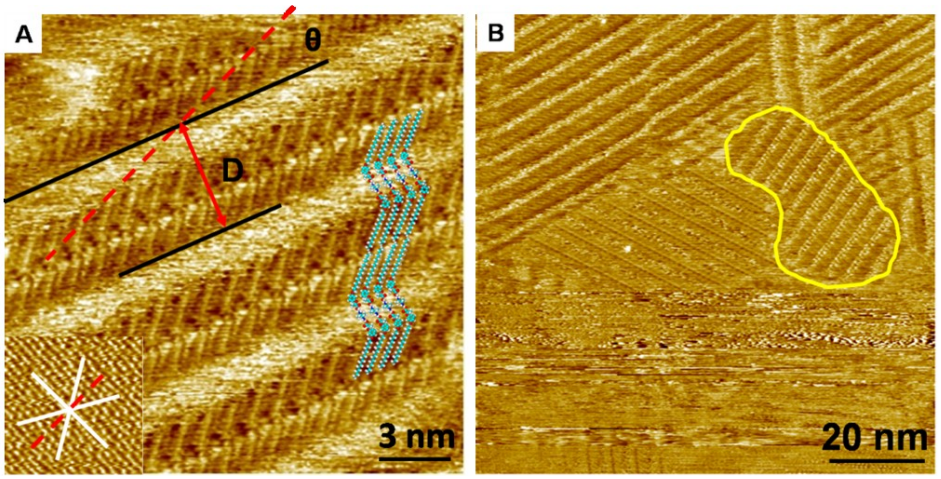

Figure 6.5 *STM images of monolayers formed upon premixing **1** and **2** at the 1-phenyloctane - HOPG interface. A) R-**1**+(S,S)-**2** (1:5) (I_{set} = 0.20 nA; V_{set} = 0.80 V), B) R-**1**+(S,S)-**2** (1:10) (I_{set} = 0.20 nA; V_{set} = 0.80 V), recorded 0.5 hour after deposition The insets show STM images of graphite (not to scale) corresponding with sites underneath the monolayer (I_{set} = 0.20 nA; V_{set} = 0.001 V). White solid lines indicate graphite main symmetry axes. Red dashed lines indicate the selected graphite reference axis running perpendicular to one of the main symmetry axes. Black solid lines indicate the direction of molecular rows. Double-headed red arrows show the width (D) of the bi-component rows. Domain marked in yellow in B) contains only R-**1**. In a tentative molecular model, resorcinol and diamine molecules are superimposed on the STM image to highlight their respective location.*

the angle between the propagation direction of the molecular rows and the HOPG reference axes <-1 1 0 0> increased to about 19°, which is about 10° larger than for *S*-**1** and (*S*,*S*)-**2**. The periodic contrast of alkyl chains in Figure 6.5A might be a Moiré pattern which is commonly observed in STM images. Upon further increasing the amount of (*S*,*S*)-**2**, the process of the co-adsorption on the surface became faster. At a ratio of 1:10, all initially formed *R*-**1** type domains disappeared in 1 hour (Figure 6.5B).

At this stage, no conclusions can be drawn concerning the exact structure of the complexes on the surface. Advanced molecular modeling should bring insight. Neither is it clear yet if complexes are preformed in solution or not. However, the ratio dependent data indicate that homochiral interactions (e.g. between *R*-**1** and (*R*,*R*)-**2**) are stronger than heterochiral interactions, at least upon physisorption. When adopting a homochiral combination of **1** and **2**, two -NH_2 groups on **2** interact with –OH groups of two resorcinol molecules **1**. The **1**-**2**-**1** trimers are densely packed and don't afford enough space for the phenyl group of **1** to be adsorbed parallel to the surface. The resorcinol groups are most likely tilted.
Without experimental evidence for complex formation in solution, it is not straightforward to conclude if the complex formation is directed by the surface or promoted upon adsorption or not. Both solution complex formation equilibrium and adsorption equilibrium processes can be involved.

6.4 Conclusions

In summary, chiral resolution is achieved by using two chiral components at the liquid-solid interface. Chiral resorcinol compound **1** can self-assemble on the surface and transfer its molecular chirality to supramolecular level. Chiral diamino compound **2** co-adsorbs with **1** in an enantioselective way. At a 2:1 molar ratio, the **1**-**2**-**1** trimer structures only appear for the homochiral combination. At higher ratios though, also heterocomplex **1**-**2**-**1** trimer structures are formed. Most importantly, we show that the resorcinol derivative can resolve in an enantioselective way

a racemic mixture of chiral diamino cyclohexanes. Upon premixing the resolving agent (the resorcinol derivative) with the racemic mixture (the diamino cyclohexane) under appropriate concentration conditions, exclusively one of the diaminocyclohexane enantiomers is adsorbed on the achiral graphite substrate as a diastereomeric complex. The other enantiomer is left in solution.

6.5 References

1 Yablon, D. G.; Giancarlo, L. C. and Flynn, G. W. *J. Phys. Chem. B* **2000**, *104*, 7627.

2 Yablon, D. G.; Wintgens, D. and Flynn, G. W. *J. Phys. Chem. B* ***2002***, *106*, 5470.

3 De Feyter, S.; Grim, P. C. M.; Rücker, M.; Vanoppen, P.; Meiners, C.; Sieffert, M.; Valiyaveettil, S.; Müllen K. and De Schryver, F. C. *Angew. Chem. Int. Ed.* **1998**, *37*, 1223.

4 Qian, P.; Nanjo, H.; Yokoyama, T.; Suzuki, T. M.; Akasaka K. and Orhui, H. *Chem. Commun.* **2000**, *20*, 2021.

5 Dressler, D. H. and Mastai, Y. *Chirality* **2007**, *19*, 358.

6 Dressler, D. H. and Mastai, Y. *J. Colloid Interface Sci.* **2007**, *310*, 653.

7 Fernández, A. I.; Fraile, J. M.; García, J. I.; Herrerías, C. I.; Mayoral, J. A. and Salvatella, L. *Catal. Commun.* **2001**, *2*, 165.

Conclusions and Perspectives

Conclusions

Most molecules, both chiral and achiral, which are able to self-assemble into monolayers at the liquid-solid interface, form chiral surface-confined assemblies. Two-dimensional chirality can be expressed by the fact that molecules self-assemble into one of the five chiral plane groups. Alternatively, or in addition, any offset of a unit cell vector of the monolayer with respect to a symmetry axes of the substrate underneath, reflects the chiral nature of the assembly. While enantiopure molecules form typically only one pattern of a couple of mirror-image domains, i.e. the surface is globally chiral, achiral molecules self-assemble into right-handed and left-handed domains, and therefore the surface-monolayer "composite" remains achiral at the macroscopic scale. Scanning tunneling microscopy is an ideal tool to unravel structural and dynamic aspects of self-assembly at the liquid-solid interface. In the self-assembly process, molecule-molecule, molecule-substrate, molecule-solvent, and solvent-substrate interactions are important. It was a major objective of this thesis to gain a deeper insight in a number of these aspects as far as expression of chirality in two dimensions is concerned. A constant factor in all experiments is the substrate: highly oriented pyrolytic graphite. Hence, the main focus was on the influence of molecular structure and solvent on the expression of chirality.

A first point which was addressed is the effect of the number of stereogenic centers on the expression of chirality. In chapter 2, the self-assembly of a set of achiral and chiral porphyrin molecules was characterized. The experimental data show that chirality on a surface is always expressed at the liquid-solid interface, irrespective of the number of chiral centers: one chiral center suffices for a 100% efficient transfer of chirality. The number of stereogenic centers influences only slightly the molecular packing: i.e. a slight deviation of the orientation of the molecular rows with respect to the HOPG substrate underneath.

In chapter 3, another aspect of molecular self-assembly on surfaces was

highlighted: dynamics. An enantiopure molecular hexapod turned out to be an ideal probe to follow dynamics (conformational, orientational and translational) at the single molecule level at the liquid-solid interface. Not surprisingly, the highest degree of conformational dynamics was observed in disordered areas. Cooperative phenomena were also revealed.

By varying the chemical structure of oligo(*p*-phenylene vinylene) derivatives (type of functional terminal groups, the length of backbones, the length of alkyl chains and the presence or absence of stereogenic centers), molecule-molecule and molecule-substrate interactions are tuned and lead to monolayers with different ordering, orientation and expression of chirality (chapter 4). The effect of solvent on the self-assembly was investigated. The choice of solvent clearly influences the dynamics and the pattern formation.

The effect of solvent was further explored in chapter 5. By using a chiral solvent which has the potential to interact with achiral oligo(*p*-phenylene vinylene) derivatives, the self-assembly of the achiral compound was biased towards the formation of only one type of mirror-image domain. With this method, symmetry breaking is achieved in the case of achiral molecules which self-assemble on an achiral substrate. The chiral solvent did not overrule though the intrinsic chiral expression of enantiomers upon self-assembly.

Finally, in chapter 6, chiral resolution was achieved in multicomponent systems at the liquid-solid interface. A resorcinol derivative can resolve in an enantioselective way a racemic mixture of chiral diaminocyclohexanes. In presence of the resorcinol enantiomer, only one of the diaminocyclohexane enantiomers was co-adsorbed as a diastereomeric complex on the substrate. So, the successful separation of enantiomers was achieved.

Perspectives

There are still many open topics in this area. For instance, the effect of solvent on the pattern formation and solvent induced symmetry breaking were clearly proven by STM, but the role of solvent is still not

well-understood. Since the solvent molecules didn't co-adsorb in the monolayer, they couldn't be observed by STM. More systems and different techniques should be considered to get a better understanding of these solvent induced phenomena.

Amplification of chirality effects is another key topic since the symmetry breaking at the liquid-solid interface may have an impact on the separation techniques used in the pharmaceutical industry. The effect of a minor amount of an enantiomer on the self-assembly of an achiral compound ("sergeant-soldier"), or of a minor excess of one enantiomer in a mixture of enantiomers ("majority rules"), is not addressed yet at the liquid-solid interface. Such experiments should be explored in the future.

In many cases, a racemic mixture leads to a conglomerate. By adding a second component (a chiral handle), the expression of chirality and the packing of the monolayer may change. Resolution experiments should be studied in detail for a larger set of compounds to explore the requirements to achieve successful resolution. It would also be worth to establish "upscaling" experiments, in other words to evaluate if the principles established for the resolution in one drop on a one-square centimeter surface can also be transferred to more practical situations.

Another aspect which could be explored in more detail is the role and influence of the substrate. By tuning molecule-molecule versus molecule-substrate interactions, the relative importance of the substrate in affecting different aspects of the expression of molecular chirality could be tuned.

As mentioned previously, scanning tunneling microscopy is a very versatile tool to explore structural and dynamic aspects at the liquid-solid interface. However, typically images which are a fraction of a square micrometer in size are recorded. The detailed information at the nanoscale comes at the expense of a reduced global view. Therefore, it would be ideal if scanning tunneling microscopy can be complemented by techniques which provide structural information at the microscopic scale. Under UHV conditions, low-energy electron diffraction has been successfully implemented to evaluate "chiral" aspects of monolayer formation. This technique cannot be used at the liquid-solid interface though. Non-linear optical techniques could proof to be very valuable at the liquid-solid interface.

Publications

1. Xu, H.; Minoia, A.; Tomović, Ž.; Lazzaroni, R. Meijer, E. W.; Schenning, A. P. H. J. and De Feyter S. “A Multivalent Hexapod: Conformational Dynamics of Six-Legged Molecules in Self-Assembled Monolayers at a Solid-Liquid Interface” *ACS NANO* **2009**, *3*, 1016.
2. Elemans, J. A. A. W.; De Cat, I.; Xu, H. and De Feyter, S. “Two-dimensional Chirality at Liquid–solid Interfaces” *Chem. Soc. Rev.* **2009**, *38*, 722.
3. De Feyter, S.; Iavicoli, P. and Xu, H. “Expression of Chirality in Physisorbed Monolayers Observed by Scanning Tunneling Microscopy” *Chirality at the Nanoscale (WILEY-VCH)*, *Chapter 7* **2009**, 215.
4. Katsonis, N.; Xu, H.; Haak, R. M.; Kudernac, T.; Tomović, Ž.; George, S.; Van der Auweraer, M.; Schenning, A. P. H. J.; Meijer, E. W.; Feringa, B. L. and De Feyter, S. “Emerging Solvent-induced Homochirality by the Confinement of Achiral Molecules Against a Solid Surface” *Angew. Chem. Int. Ed.* **2008**, *47*, 4997.
5. Amabilino, D. B.; De Feyter, S.; Lazzaroni, R.; Gomar-Nadal, E.; Veciana, J.; Rovira, C.; Abdel-Mottaleb, M. M.; Mamdouh, W.; Iavicoli, P.; Psychogyiopoulou, K.; Linares, M.; Minoia, A.; Xu, H. and Puigmartí-Luis, J. “Monolayer self-assembly at liquid–solid interfaces: chirality and electronic properties of molecules at surfaces” *J. Phys. Condens. Matter* **2008**, *20*, 184003.
6. Katsonis, N.; Minoia, A.; Kudernac, T.; Mutai, T.; Xu, H.; Uji-i, H.; Lazzaroni, R.; De Feyter, S. and Feringa, B. L. “Locking of Helicity and Shape Complementarity in Diarylethene Dimers on Graphite” *J. Am. Chem. Soc.* **2008**, *130*, 386.
7. Tomović, Ž.; van Dongen, J.; George, S.; Xu, H.; Pisula, W.; Leclère, P.; Smulders, M. M. J.; De Feyter, S.; Meijer, E. W. and Schenning, A. P. H. J. “Star-Shaped Oligo(p-phenylenevinylene) Substituted Hexaarylbenzene: Purity, Stability, and Chiral Self-assembly” *J. Am. Chem. Soc.* **2007**, *129*, 16190.